TOWARD THE CONSTRUCTION OF A KINETIC MODEL OF METHIONINE AND THREONINE BIOSYNTHESIS TO INCREASE SEED NUTRITIONAL VALUE: CHARACTERIZATION OF THREONINE SYNTHASE

By

Dominique Morneau, B.Sc.H

A thesis submitted to the Faculty of Graduate and Post-Doctoral Affairs in partial fulfillment of the the requirements for the degree of

Doctor of Philosophy

in

Biology

Department of Biology

Ottawa-Carleton Institute of Biology

Carleton University

Ottawa, Ontario

March 2014

ABSTRACT

Improving the nutritional quality of crop species, like *Cicer arietinum* and *Lens culinaris*, is of particular interest to agricultural biotechnology. These crops are deficient, from a human dietary perspective, in the essential amino acid L-methionine (L-Met). In plants, the biosynthesis of L-Met is initiated by the formation of L-cystathionine from *O*-phospho-L-homoserine (OPHS) catalyzed by cystathionine γ-synthase (CGS). OPHS occupies the branch-point between L-Met and L-threonine (L-Thr) biosynthesis, catalyzed by threonine synthase (TS), making these two enzymes targets for metabolic engineering studies to increase L-Met production. The construction of a kinetic model recreating the branch-point can facilitate the metabolic engineering of important crop species by providing a tool for anticipating disturbances in metabolic flux caused by manipulations to the branch-point. The focus of the research described in this thesis is to provide a starting point for the creation of a kinetic model of the OPHS branch-point in the target species. The characterization of plant TS requires a continuous spectrophotometric assay, which was developed using a non-allosteric variant of threonine deaminase from *Escherichia coli* (eTD_{L447F}) and hydroxyisocaproate dehydrogenase (HO-HxoDH) from *Lactobacillus delbrueckii*. The assay was verified for suitability for use under the various pH optima of TS across phyla. The functional coding sequences of TS from *C. arietinum* (CaTS) and *L. culinaris* (LcTS) share approximately 80% amino acid sequence identity with TS from *Glycine max*, and the residues of the allosteric site are conserved with those of TS from other plant species. The PLP-binding motif, which is conserved across plant and microbial species, is present in the active site of both enzymes. The kinetic parameters of CaTS, LcTS, and AtTS2 were measured with 100 μM of the

allosteric activator *S*-adenosyl-L-methionine (SAM), with the parameters of AtTS1 measured as a control. SAM increases the k_{cat}/K_m^{OPHS} of AtTS2, LcTS, CaTS, and AtTS1 by 10-, 20-, 25-, and 80-fold, respectively. Due to the varying flux control patterns of TS from *A. thaliana*, *C. arietinum*, and *L. culinaris*, the construction of a species-specific kinetic model of the branch-point is needed for future aimed at increasing L-Met biosynthesis to nutritionally significant levels.

PREFACE

This thesis follows the integrated thesis format and so the main chapters represent work that has already been published in a peer-reviewed journal (Chapters 2 and 3) at the time of submission of this thesis, or will soon be submitted for publication (Chapter 4).

Status of manuscripts corresponding to research Chapters at the time of thesis submission

Chapter 2:

D.K. Morneau, E. Abouassaf, J.E. Skanes, and S.M. Aitken. Development of a continuous assay and steady-state characterization of *Escherichia coli* threonine synthase, Analytical Biochemistry. 423 (2012) 78-85.

Chapter 3:

D.K. Morneau, A.F. Jaworski, and S.M. Aitken. Identification of Cystathionine γ-Synthase and Threonine Synthase from *Cicer arietinum* and *Lens culinaris*, Biochemistry and Cell Biology. 91 (2013) 95-101.

Chapter 4:

D.K. Morneau and S.M. Aitken. Measuring the steady-state kinetic parameters of Threonine Synthase from *A. thaliana*, *C. arietinum*, and *L. culinaris*. To be submitted to the journal Biochimica et Biophysica Acta.

Statement of contributions

My contributions to the research described in this thesis include:

1. development of research questions and experimental design, in partnership with Dr. S.M. Aitken,
2. collection and analysis of data,
3. the co-supervision, in collaboration with Dr. S.M. Aitken, of three undergraduate students: Seghen Woldai, who participated in the creation of the silent mutation in AtTS2 removing the internal *Nde*I site and the complementation described in Chapter 3; and Alexander Edwards and Jason Koppart, who assisted in the purification of eTD_{L447F}, HO-HxoDH, and eTS described in Chapters 2 and 4.

I formally acknowledge the contributions of the co-authors of the manuscripts that comprise the research chapters of this thesis. My supervisor, Dr. S.M. Aitken, contributed her expertise by guiding me in the formulation of the research questions and experimental design, and with the interpretation of data and the preparation of manuscripts for each of the three research chapters of my thesis. Edgar Abouassaf (Ph.D. candidate, Aitken lab, Dept. of Biology) and Jennifer E. Skanes (M.Sc. 2011) are co-authors of the published article corresponding to Chapter 2. Edgar constructed the 6-Histidine tagged constructs of *E. coli* threonine deaminase and *L. delbrueckii* Ho-HxoDH and completed the affinity purification and preliminary steady-state kinetic characterization of the two enzymes. Jennifer Skanes constructed the 6-Histidine tagged construct of *E. coli* threonine synthase. The contributions of undergraduate students is described above. Allison F. Jaworski (Ph.D. candidate, Aitken lab, Dept. of Biology) is a co-author of the published article corresponding to Chapter 3. Allison amplified the

coding sequences of CGS from *C. arietinum*, *L. culinaris*, and *A. thaliana*, completed the complementation studies for plant CGS, aided in the infiltration of GFP constructs into *N. tabacum*, and played a significant role in the writing of the manuscript.

I have obtained copyright permission from each publisher to reproduce published manuscripts and from each of my co-authors to use collaborative works in this thesis.

ACKNOWLEDGEMENTS

I would like to extend my deepest and sincerest gratitude to Dr. Susan Aitken, first for giving me the incredible opportunity to learn from her, and for providing a rich and challenging environment throughout the last six years. You encouraged me to work harder every day, and in doing so, helped me find a confidence I did not know I had. This experience, and the person I have grown into because of it, would not have been the same without your influence and your support, so thank you. I would also like to thank my thesis committee members, Drs. Owen Rowland and John Vierula. Both Owen and John have provided valuable advice, feedback, and ideas throughout the progression of my thesis. John always had a smile when I met him in the hallways of Nesbitt, and was always interested in my progress. Owen provided me with new ideas frequently, and gave me great opportunities through his professional contacts.

The boisterous environment of the Aitken lab has been an amazing place to complete my research. Duale Ahmed, Victoria Samaki, Emily Hopwood, Nikita Rayne, Justin Kicks, Jennifer Skanes, Colleen Woodhouse, Pratik Lodha, and Sorin Gustin were wonderful colleagues, and made each day a joy. Your advice on presentations, posters, research, and manuscripts was invaluable, and helped me grow both as a graduate student and as a scientist. Duale, thank you for being my companion on early mornings and weekends, for listening to me and giving me wise-beyond-your-years life advice, for laughing with/at me, and for your friendship. Undergraduate students of the Aitken lab, both past and present (Navya Kalidindi, Heidi Los, Ali Masoud, Lubna El-Sarji, Seghen Woldai, Rogeh Habashi, Winsfield Ling, Alexander Edwards, Jason Koppart, Amanda Foster, Nick Humphreys, Adrienne Manders, Sherwin Habibi, and Katrina Farrell) were

always willing to provide me with assistance in my work and helped create a wonderfully dynamic learning experience. I would also like to extend a huge thank you to Denise Chabot and Keith Hubbard from Agriculture and Agri-Food Canada, who manned the confocal microscope which enabled me to complete my localization studies. And finally, a big thanks to the administrative staff who keep the Department of Biology running. Lisa Chiarelli, for helping with my paperwork and endless questions about submission and scholarship application deadlines, and Laura Thomas and Michelle O'Farrell, for always being available for a mid-afternoon chat break.

Over the last six years, I have befriended some wonderful people, in the Department of Biology, the Institute of Health, and outside of Carleton. Thank you to Emilie Milroy, Jordan Miller, and Chris White for your friendship while I was completing my graduate diploma in the Institute of Health, and also to Siri Chunduri and Chandni Sondagar for being my CPHA cheering squad. And of course my sincerest gratitude to my lovely friends Eileen Conboy and Kim Bisson (and recently Eleanor Bisson) for their gracious, calming influence on my life.

I have had the unimaginable fortune of having the five very best friends that anyone could ever ask for in Valerie Hamelin, Chris Bisson, Sarah Edwards, Allison Jaworski, and Edgar Abouassaf. Over the years, each of you has contributed to this thesis in ways you may not be aware of. Valerie and Chris, you have been like family to me for 16-19 years, and I am so grateful to always have you to turn to when life gets overwhelming. Sarah, your friendship throughout our undergrad and grad degrees has been amazing. I love you and miss you so much more than I can say. Ally, you are a warrior-poet. If you had not been a part of this experience I would have left and gone to

live under a bridge ages ago. Your friendship means the world to me. Eddy, we had a rough start, but I'm glad we stuck with it. You've been a wonderful friend to me, thank you. I have had the most amazing time laughing, crying, and sharing with each of you, and your unwavering support throughout this process has been unbelievable. I don't think I could have made it here without each and every one of you.

And finally, none of this would have been possible without the unconditional love and support of my family. I love you guys with all of my heart. Ann, you are the best sister anyone could have (I mean that). You've been my friend, roommate, advocate, and therapist over the years, thank you for your love and for always having my back. Mom and dad, everything that I am and will ever be, I owe to your love, your confidence in me, and the sacrifices you have made in your dedication to seeing me succeed. I will never find the words to express to you how grateful I am for you in my life and the amazing opportunites that being your child has awarded me. Si vous n'étiez pas mes parents, je vous aurais voulu.

DEDICATION

For my parents, Michel and Nicole Morneau.
I owe you everything.

TABLE OF CONTENTS

LIST OF TABLES

LIST OF FIGURES

ABBREVIATIONS

α-KB	α-ketobutyrate
ADP	Adenosine diphosphate
AK	Aspartate kinase
ASDH	Aspartate semialdehyde dehydrogenase
A. thaliana	*Arabidopsis thaliana*
AtCGS	*Arabidopsis thaliana* cystathionine γ-synthase
ATP	Adenosine triphosphate
AtTS1	*Arabidopsis thaliana* threonine synthase homologue 1
AtTS2	*Arabidopsis thaliana* threonine synthase homologue 2
A. tumefaciens	*Agrobacterium tumefaciens*
C. arietinum	*Cicer arietinum*
CaCGS	*Cicer arietinum* cystathionine γ-synthase
CaMV	Cauliflower mosaic virus
CaTS	*Cicer arietinum* threonine synthase
CaTS-His	*Cicer arietinum* threonine synthase with C-terminal 6-His tag
CBL	Cystathionine β-lyase
CBS	Cystathionine β-synthase
CGL	Cystathionine γ-lyase
CGS	Cystathionine γ-synthase
CIAP	Calf intestinal alkaline phosphatase
CLSM	Confocal laser scanning microscopy
DEAE	Diethylethanolamine

DHDPS	Dihydrodipicolinate synthase
DNA	Deoxyribonucleic acid
DTT	Dithiothreitol
E. coli	*Escherichia coli*
EDTA	Ethylenediaminetetraacetic acid
eCGS	*Escherichia coli* cystathionine γ-synthase
eHSK	*Escherichia coli* homoserine kinase
eTD	*Escherichia coli* threonine deaminase
eTD_{L447F}	*Escherichia coli* threonine deaminase with Phe substitution at Leu447
eTS	*Escherichia coli* threonine synthase
FaCGS	*Fragaria ananassa* cystathionine γ-synthase
GFP	Green fluorescent protein
G. max	*Glycine max*
GmCGS	*Glycine max* cystathionine γ-synthase
GmTS	*Glycine max* threonine synthase
HEPES	(4-(2-hydroxyethyl)-1-piperazineethanesulfonic acid
HPLC	High performance liquid chromatography
HSDH	Homoserine dehydrogenase
HSK	Homoserine kinase
HO-HxoDH	D-2-Hydroxyisocaproate dehydrogenase
IPTG	Isopropyl-β-*D*-thiogalactopyranoside
L-Asp	L-Aspartate
L-Cys	L-Cysteine

LDH	L-Lactate dehydrogenase
L. culinaris	*Lens culinaris*
LcCGS	*Lens culinaris* cystathionine γ-synthase
LcTS	*Lens culinaris* threonine synthase
L-HSer	L-homoserine
L-Ile	L-isoleucine
L-Lys	L-lysine
L-Met	L-Methionine
L-Pro	L-Proline
L-Thr	L-Threonine
L-Val	L-Valine
LcTS	*Lens culinaris* threonine synthase
MBP	MOPS/Bicine/L-proline
M. sativa	*Medicago sativa*
M. truncatula	*Medicago truncatula*
MtTS	*Medicago truncatula* threonine synthase
MOPS	3-(N-morpholino)propanesulfonic acid
MS	L-Methionine synthase
mto	Methonine over-accumulating
NaCl	Sodium chloride
NAD^+	Nicotinamide adenine dinucleotide, oxidized form
NADH	Nicotinamide adenine dinucleotide, reduced form
Ni-NTA	Nickel-nitrilo triacetic acid

N. tabacum	*Nicotiana tabacum*
NtCGS	*Nicotiana tabacum* cystathionine γ-synthase
OPHS	*O*-phospho-L-homoserine
ORF	Open reading frame
PCR	Polymerase chain reaction
PEM	Protein energy malnutrition
PEP	Phospho(enol)pyruvate
PK	Pyruvate kinase
PLP	Pyridoxal 5'-phosphate
P. sativum	*Pisum sativum*
RNA	Ribonucleic acid
SAM	*S*-adenosyl-L-methionine
SAMS	*S*-adensosyl-L-methionine synthase
SDS-PAGE	Sodium dodecyl suflate polyacrylamide gel electrophoresis
S. tuberosum	*Solanum tuberosum*
StTS	*Solanum tuberosum* threonine synthase
TLC	Thin-layer chromatography
TS	Threonine synthase
TD	Threonine deaminase
UV	Ultraviolet
V. angularis	*Vigna angularis*
yTS	*Saccharomyces cerevisiae* threonine synthase

1. INTRODUCTION

1.1. Methionine and Pulse Species

Customizing crops to improve their nutritional quality for human and animal consumption is a primary goal of plant genetic and metabolic engineering. Humans and non-ruminant animals cannot produce *de novo* half of the 20 proteinogenic amino acids, relying on their food source to supply them. These are referred to as essential amino acids, and deficiency of one or more can lead to protein energy malnutrition (PEM), lowered disease resistance, decreased blood proteins, and retarded mental and physical development in children under the age of 4 (Hoorweg and Stanfield, 1976). PEM is estimated to affect one third of the children in developing countries, and accounts for up to 8% of all childhood deaths (de Onis, 1993; World Health Organization, 2006). While animal products generally contain a balance of amino acids aligned with human dietary requirements, plant proteins are often deficient in at least one of the essential amino acids (Hesse *et al.*, 2001). Methionine and lysine, for example, are two essential amino acids that are often limiting, from the perspective of human nutritional requirements, in legumes and cereals, respectively (Tabe and Higgins, 1998; Elango *et al.* 2009).

Grain legumes are crop plants of the Fabaceae family that develop pods and are cultivated for their protein-rich seeds. Pulse species are a subset of the grain legumes that are harvested for their dry seeds, and include *Cicer arietinum* (chickpea) and *Lens culinaris* (lentil). Pulses make up 10% of the world's supply of dietary protein and are an important source of Canadian agricultural revenue (Muntz *et al.* 1998). In 2009-2010, Canadian pulse exports exceeded 2 million tonnes, bringing in over $2 billion in revenue (Agriculture and Agri-Food Canada, 2011). These crops are also a dietary staple in areas

where vegetarian diets are predominant, with the majority of Canadian exports going to south-east Asian countries, such as India, Pakistan, and Bangladesh (Muntz *et al.* 1998; Agriculture and Agri-Food Canada, 2011).

In humans and non-ruminant animals, methionine is the precursor for the production of the amino acid cysteine, and so meeting the dietary requirements for these two sulfur-containing amino acids is dependent on the intake of sufficient amounts of methionine (Figure 1.1) (Mato *et al.* 2008; Elango *et al.* 2009). Humans and monogastric animals require a combined intake of methionine and cysteine of 3-5% of total dietary protein. In contrast, methionine and cysteine comprise 0.8-1.5% and 0.6-1%, of total protein, respectively, in the pulse species *Pisum sativum*, and the two sulfur-containing amino acids make up 1.3% of total protein in chickpeas (Tabe and Higgins, 1998; Elango *et al.* 2009). Increasing methionine content in the seeds of grain legumes has the potential to both increase the nutritional quality of these staple foods, as well as boost Canadian agricultural exports.

Increasing the level of methionine in legume seed proteins has previously been undertaken through the engineering of seed proteins with additional methionine residues, or through the expression of heterologous methionine-rich proteins. The former has generally been unsuccessful due to the inserted residues interfering with proper folding and accumulation of seed proteins, as exemplified by the degradation of mutated β-phaseolin from *Phaseolus vulgaris* containing a nine-methionine insertion in its variable region (Hoffman *et al.* 1988). The availability of the three-dimensional structure of

Figure 1.1. The transsulfuration pathway of plants and microorganisms and the reverse transsulfuration pathway of mammals. Abbreviations: CGS, cystathionine γ-synthase; CBL, cystathionine β-lyase; CGL, cystathionine γ-lyase; CBS, cystathionine β-synthase Figure adapted from Steegborn *et al.* (1999) and Farsi *et al.* (2009).

Plants and Microorganisms **Mammals**

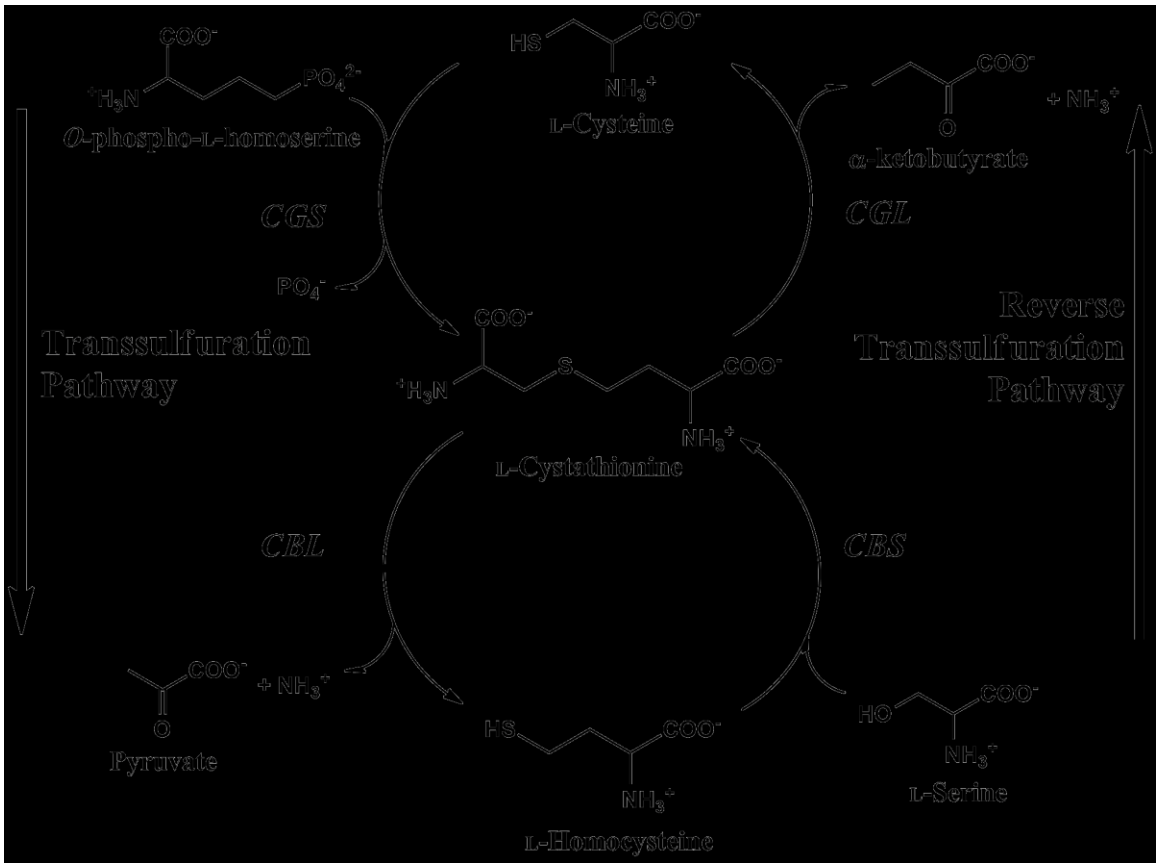

β-phaseolin later revealed that the insertion of nine residues at this site may have destabilized the formation of the quaternary structure of the seed protein (Sun *et al*. 2004). The expression of heterologous methionine-rich proteins has also been unsuccessful due to transferred allergenicity or the inability of transgenic plants to meet the increased demand for sulfur-containing amino acids. For example, the expression of some foreign methionine-rich proteins, such as 2s albumin from Brazil nut, has been shown to transfer allergenicity to transgenic *Glycine max* (Nordlee *et al.* 1996). Furthermore, in chickpea, the seed-specific expression of methionine-rich sunflower seed albumin increased methionine content in transgenic chickpea seeds, with an accompanying decrease in cysteine-containing proteins, resulting in no net gain in the seed sulfur amino acid content (Chiaiese *et al.* 2004). These results indicate that the rational engineering of endogenous seed storage proteins to increase the number of methionine residues may be preferable, to avoid the introduction of allergens, but must be complemented with enhanced methionine production to meet the increased demand for sulfur-containing amino acids (Hesse *et al.* 2004).

1.2. Methionine biosynthesis in plants

L-Methionine (L-Met) is a member of the L-aspartate (L-Asp)-derived family of amino acids. In plants, the carbon backbone of L-Met is supplied by the L-Asp-derivative *O*-phospho-L-homoserine (OPHS), which occupies the branch-point between the synthesis of L-Met and L-threonine (L-Thr) (Figure 1.2) (Jander and Joshi, 2010). In plants, the first step in L-Met biosynthesis is the condensation of OPHS with L-cysteine (L-Cys) by cystathionine γ-synthase (CGS), producing L-cystathionine; this enzyme

Figure 1.2. The biosynthesis of L-Met and L-Thr from L-Asp in plants. Abbreviations: AK, aspartate kinase; ASDH, aspartate semialdehyde dehydrogenase; HSDH, homoserine dehydrogenase; HK, homoserine kinase; CGS, cystathionine γ-synthase; TS, threonine synthase; SAMS, *S*-adenosyl-L-methionine synthase. Figure adapted from Morneau *et al.* (2013).

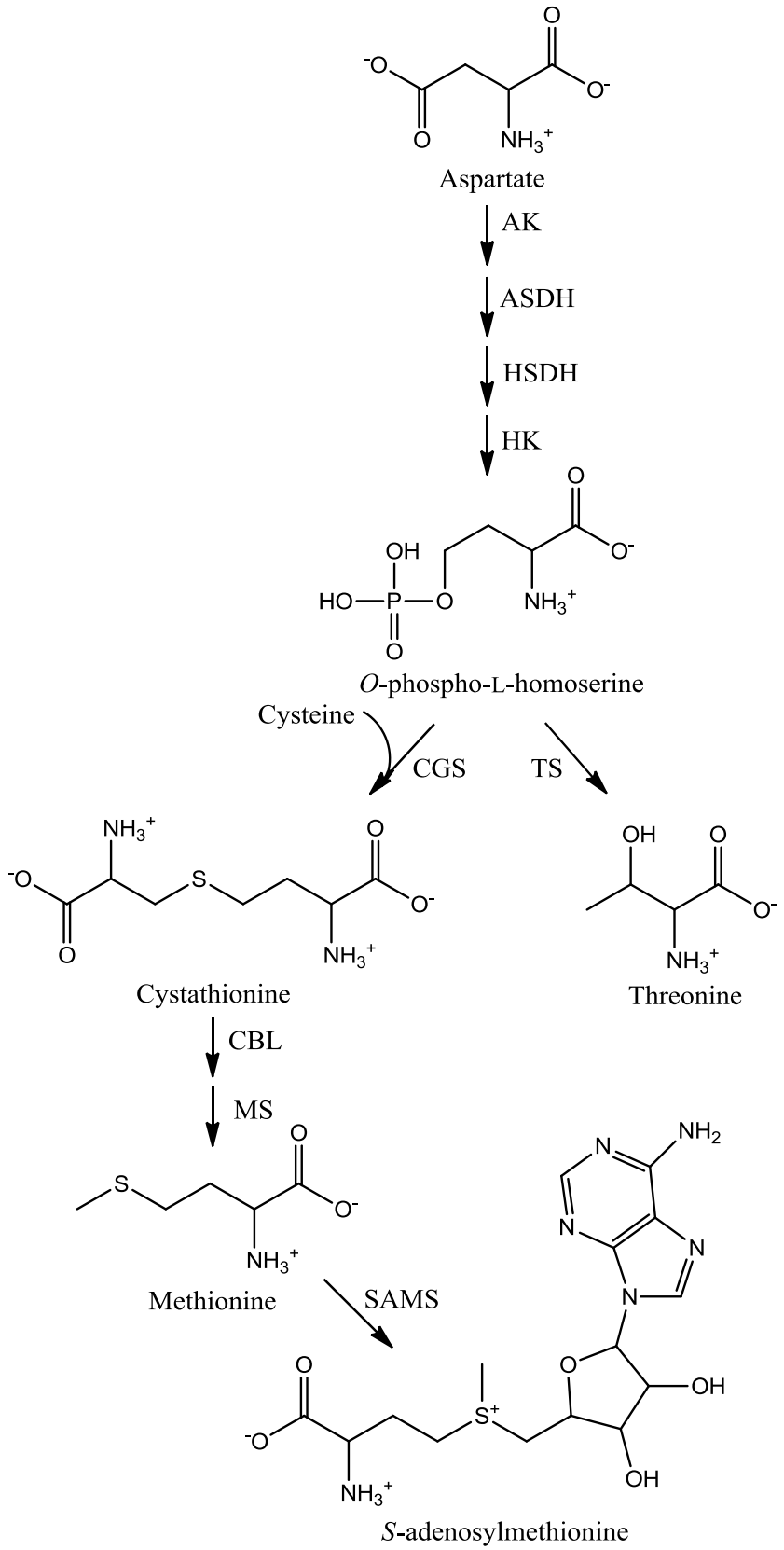
Aspartate
AK
ASDH
HSDH
HK
O-phospho-L-homoserine
Cysteine
CGS
TS
Cystathionine
Threonine
CBL
MS
Methionine
SAMS
S-adenosylmethionine

competes with threonine synthase (TS), which catalyzes the production of L-Thr from OPHS (Hesse *et al.* 2004). The metabolic flux of this pathway, or the flow of the substrate to L-Met or L-Thr biosynthesis, is determined by the activity of CGS and TS.

The synthesis of L-Met continues *via* the cleavage of L-cystathionine by cystathionine β-lyase (CBL), forming L-homocysteine. The reactions catalyzed by CGS and CBL make up the transsulfuration pathway of plants, which transfers the sulfur moiety from the β-carbon of L-Cys to the γ-carbon of L-homocysteine (Ravanel, 1997). Studies on transgenic *Solanum tuberosum* expressing antisense CBL constructs under the control of the CaMV-35S promoter revealed that CBL is necessary for L-Met synthesis and normal plant development, but that it is not involved in the regulation of OPHS partitioning between the competing L-Met and L-Thr pathways (Maimann *et al.* 2000; Maimann *et al.* 2001; Azavedo *et al.* 2006). The final step in L-Met synthesis is the methylation of L-homocysteine by methionine synthase (MS) (Eichel *et al.* 1995; Hesse *et al.* 2004). This step takes place in the cytosol, while the transsulfuration pathway, along with the biosynthetic pathways of the other L-Asp-derived amino acids, L-lysine (L-Lys), L-Thr, and L-isoleucine (L-Ile), are compartmentalized in the chloroplast (Eichel *et al.* 1995; Jander and Joshi, 2010).

The enzymes CGS and TS were identified as promising targets for the manipulation of OPHS flux to increase L-Met production following the discovery of the methionine over-accumulating (mto) mutant loci in *Arabidopsis thaliana*. The mto mutants comprise point mutations in the coding regions of *CGS* (*mto1*) or *TS* (*mto2*) (Inaba *et al.* 1994; Bartlem *et al.* 2000; Ominato *et al.* 2002). The *mto1* lines express *CGS* transcripts that are not susceptible to post-transcriptional regulation, and thus the

plants accumulate CGS protein, leading to 15- to 40-fold increases in free L-Met content in rosette leaves (Inaba *et al.* 1994; Ominato *et al.* 2002). The *mto2* line carries a leucine to arginine substitution in the TS active site, reducing the enzyme's capacity to bind OPHS, thereby reducing L-Thr synthesis 15-fold, and increasing L-Met levels 22-fold (Bartlem *et al.* 2000). The disruption of metabolic flux caused by impaired TS activity is associated with negative phenotypic effects including delayed growth, and reductions in fresh weight and root length (Bartlem *et al.* 2000; Kusano *et al.* 2010). This indicates that increasing L-Met synthesis in crop species can be achieved through manipulation of metabolic flux at the OPHS branch-point, but that the successful metabolic engineering of L-Met production without phenotypic side-effects requires a detailed understanding of the role of CGS and TS in OPHS partitioning in the target species.

1.3. Regulation of L-Met biosynthesis

Methionine is involved in the synthesis of proteins, initiation of translation, and is a precursor for a number of other biologically important compounds including *S*-adenosyl-L-methionine (SAM) (Inaba *et al.* 1994). SAM is the primary methyl-group donor for most methylation reactions occurring within the cell, and is also the precursor of polyamines and the phytohormone ethylene (Ravanel *et al.* 1998a; Roje, 2006). Amino acid biosynthetic pathways are commonly regulated by metabolic end-products, as exemplified by the L-Asp metabolic pathway, which is regulated through the feedback inhibition of aspartate kinase (AK) by both L-Thr, L-Lys, and SAM (Jander and Joshi, 2010). The partitioning of OPHS into the L-Met and L-Thr biosynthetic pathways is determined by intracellular SAM concentration.

In *A. thaliana*, SAM mediates the post-transcriptional regulation of *CGS* mRNA by binding to the regulatory region, designated the MTO region, which acts in *cis* to decrease *CGS* transcript stability. The *mto1* lines of *A. thaliana* contain point mutations in this region that inhibit regulation by SAM (Chiba *et al.* 2003). The regulation of CGS by SAM may vary across species. For example, *in vitro* transcription/translation studies of mRNA encoding *CGS* from *S. tuberosum* in the presence of varying concentrations of L-Met, with *A. thaliana CGS* as a control, found that *A. thaliana CGS* transcript stability was decreased when exposed to 0.1 mM L-Met, while *S. tuberosum CGS* transcripts were not affected (Kreft *et al.* 2003). At the time, the regulation of *A. thaliana CGS* was thought to be mediated by L-Met, hence its addition into the *in vitro* translation mixture; the L-Met was likely converted into SAM by SAM synthase (SAMS) in the wheat germ extract of the reaction mixture. These results indicate that the SAM-mediated regulation of CGS may be species-specific, illustrating the need to study the regulation of L-Met biosynthesis in the target species for future biotechnological endeavours.

The L-Met-derivative SAM also regulates TS activity, *via* allosteric activation, increasing its catalytic efficiency up to 87-fold (Laber *et al.* 1999). The post-transcriptional and allosteric regulation of CGS and TS, respectively, by SAM demonstrates the complexity of metabolic partitioning at the OPHS branch-point.

1.4. Threonine Synthase

In plants and bacteria, the last step in L-Thr biosynthesis is the TS-catalyzed β,γ-replacement of OPHS producing L-Thr, and inorganic phosphate (Curien *et al.* 1996). The newly formed L-Thr is either incorporated into protein, or used as a precursor for the

amino acids L-Ile and L-glycine (Jander and Joshi, 2010). The TS enzyme has been characterized from several plant species including *A. thaliana* (Curien *et al.* 1996; Curien *et al.* 1998; Laber *et al.* 1999), *Lemna paucicostata* (Giovanelli *et al.* 1984), and *S. tuberosum* (Casazza *et al.* 2000; Zeh *et al.* 2001). Plant TS, like other enzymes involved in amino acid synthesis, is a pyridoxal 5'-phosphate (PLP)-dependent enzyme (Curien *et al.* 1996; Casazza *et al.* 2000). PLP-dependent enzymes are categorized by their fold-type structure (Eliot and Kirsch, 2004). There are five evolutionary fold types of PLP-dependent enzymes and the homodimeric plant TS is a member of the fold-type II structural family (Curien *et al.* 1996; Mas-Droux *et al.* 2006). The enzymes of the fold-type II structural family generally possess at least one regulatory domain and active sites composed of residues from only one monomer despite being functional dimers (Eliot and Kirsch, 2004). Plant TS contains two regulatory SAM-binding sites at the dimer interface (Mas-Droux *et al.* 2006). In contrast, TS from microorganisms is not regulated by SAM and is a functional monomer (Garrido-Franco *et al.* 2002).

A. thaliana contains two forms of TS (AtTS1 and AtTS2). The purification of TS from *A. thaliana* leaves found AtTS1 (At4g29840) eluted in a single peak of activity, at a similar ionic strength to recombinantly expressed AtTS1, leading to the assumption that a single copy of TS is expressed in *A. thaliana* chloroplasts. However, the *A. thaliana* genome contains a gene encoding a second homologue of TS (AtTS2; At1g72810). Kinetic characterization of AtTS2 demonstrated that it is also subject to activation by SAM, but has a k_{cat} value that is 120-fold lower than that of AtTS1 in the presence of physiological concentrations of SAM (20 μM) (Curien *et al.* 2009).

1.4.1. Allosteric Regulation of TS

The crystal structure of AtTS1, solved with and without the allosteric effector, revealed the mechanism of activation of plant TS by SAM (Thomazeau *et al.* 2001; Mas-Droux *et al.* 2006). In its inactive form, the orientation of the PLP cofactor in the active site of AtTS1 prevents OPHS binding to the substrate site and acts as an inhibitor (Mas-Droux *et al.* 2006). AtTS1 binds SAM at the dimer interface; two SAM molecules associated with each monomer, with the functional dimer binding a total of four SAM molecules (Figure 1.3; Mas-Droux *et al.* 2006). Of these four SAM molecules, the two solvent exposed molecules, defined as SAM2 and SAM4, are mainly stabilized by forming stacking interactions with W101 of monomer A and B, respectively; however, the carboxylate group of SAM2 forms an electrostatic interaction with K141 and N147 of monomer B, whereas the methionine moiety of SAM4 interacts with only K141 of monomer A (Figure 1.4) (Mas-Droux *et al.* 2006). The interaction of SAM2 with both K141 and N147 contributes to the stabilization of residues 137-149 of monomer B, which does not occur in monomer A (Mas-Droux *et al.* 2006). This leads to the active site of monomer A undergoing a large rearrangement upon SAM-binding, consisting of a shift in loops 190-195, 260-264, and 294-299, resulting in a 150° rotation of the PLP molecule and leading to an active site conformation similar to that of TS from microorganisms (Figure 1.4) (Mas-Droux *et al.* 2006). The active site of monomer B remains unchanged, and it has been proposed that subsequent binding of OPHS to the active site of monomer A induces a rearrangement of the active site of monomer B (Mas-Droux *et al.* 2006). Thus, in the absence of OPHS, the PLP of monomer B remains in an inactive orientation (Figure 1.4) (Mas-Droux *et al.* 2006).

Figure 1.3. Crystal structure of *A. thaliana* TS1 in complex with PLP (yellow) and 2 molecules of SAM (green and blue) per monomer. Monomer A is shown in pink, and monomer B is shown in gray. (PDB: **2C2B**) (Mas-Droux *et al.* 2006).

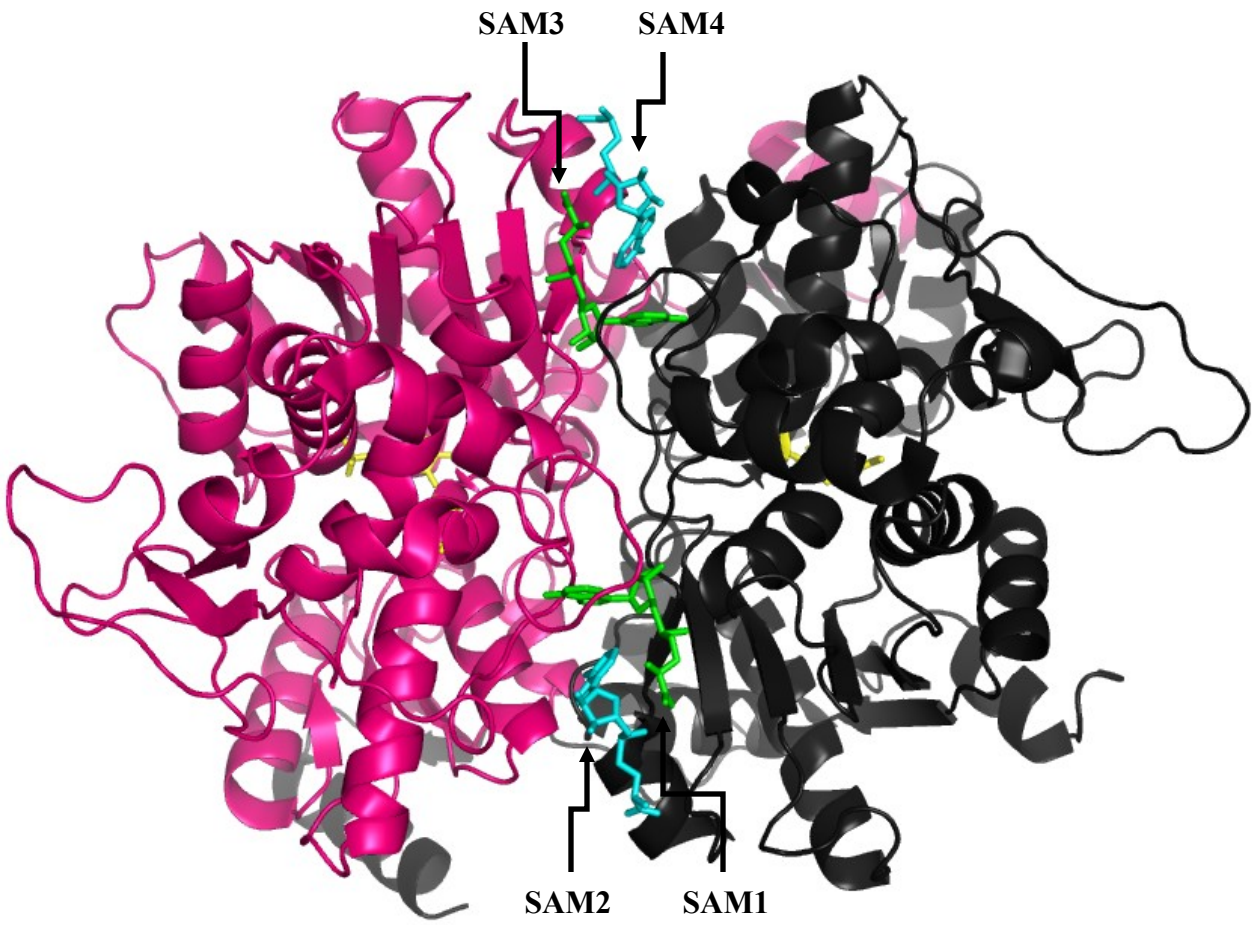
SAM3
SAM4
SAM2
SAM1

Figure 1.4. Cartoon and surface representations of the allosteric and active sites of *A. thaliana* TS1 (AtTS1) upon SAM binding. Monomers A and B are shown in pink and gray, respectively. SAM1 and SAM3 are in green, SAM2 and SAM4 are shown in blue. **(A)** Residues involved in the binding of SAM1 and SAM2 (i), and SAM3 and SAM4 (ii) are shown in the colors of their respective monomers. **(B)** Surface view of the active site and orientation of the PLP cofactor in the inactive form of monomer B (i) and the active form of monomer A (ii) upon SAM-binding. **(C)** Residues of loops 190-195 (green), 260-264 (pink), and 294-299 (blue) of the active sites of monomer B (i) and monomer A (ii) shown in stick format. (PDB: **2C2B**) (Mas-Droux *et al.* 2006).

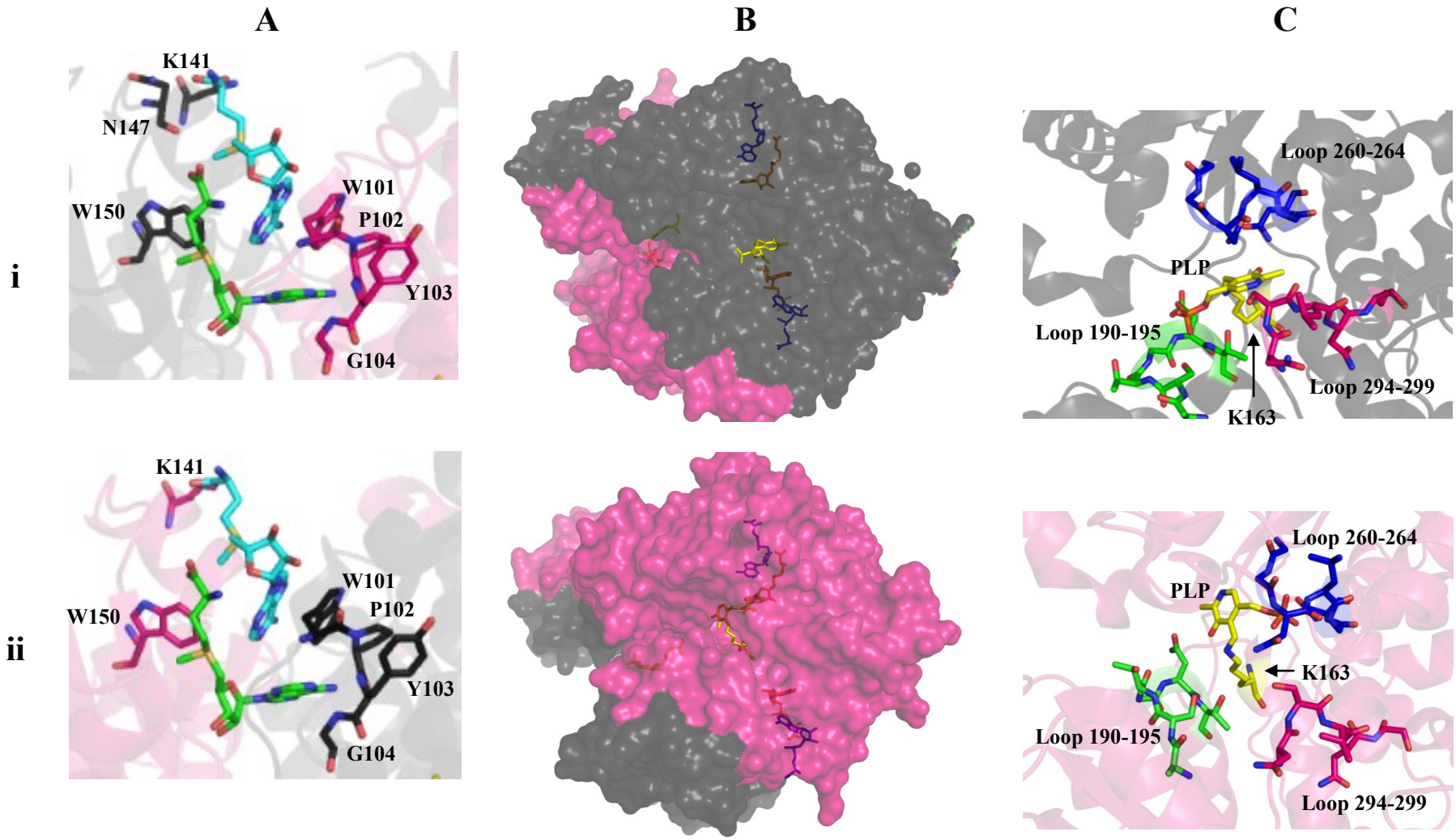
A
B
C
i
ii
K141
N147
W150
W101
P102
Y103
G104
PLP
Loop 260-264
Loop 190-195
Loop 294-299
K163

The presence of SAM increases the catalytic efficiency (k_{cat}/K_m) of TS by affecting both the K_m^{OPHS} and k_{cat} values, however this interaction is complex (Curien *et al.*1998; Laber *et al.* 1999). The k_{cat} of AtTS1 increases in a sigmoidal fashion at low SAM concentrations (<10 μM), suggesting cooperativity between the enzyme and activator (Curien *et al.* 1998). At SAM concentrations less than 2 μM, K_m^{OPHS} increases from 250 μM to 500 μM, then decreases at SAM concentrations >2 μM (Curien *et al.* 1998). While physiological SAM concentrations in the chloroplast are estimated at 20-40 μM, peak enzyme activity is reached at SAM concentrations of 100-250 μM (Laber *et al.*1999; Curien *et al.* 2003). At 100 μM SAM, the k_{cat} and K_m^{OPHS} of AtTS1 are reported at 0.86 s^{-1} and 30 μM, respectively, compared to 0.04 s^{-1} and 120 μM, respectively, in the absence of SAM (Laber *et al.* 1999).

1.5. Threonine synthase as a target for increasing L-Met biosynthesis

The activation of plant TS by SAM underlies the key role this enzyme plays in the partitioning of OPHS between the L-Met and L-Thr biosynthetic pathways. *In vitro* assessments of SAM-activated AtTS1 demonstrated a 83-fold lower K_m^{OPHS} than that of CGS from *A. thaliana* (AtCGS), such that under conditions of sufficient cellular L-Met and SAM, OPHS is channeled primarily to L-Thr synthesis (Ravanel *et al.* 1998b; Curien *et al.* 2009). Furthermore, the level of AtTS1 expressed in the chloroplast has been estimated to be 7-fold higher than that of CGS (Curien *et al.* 2003). As such, the L-Thr biosynthetic pathway accounts for 70-80% of OPHS flux under physiological conditions, and provides a good candidate for biotechnological manipulation to increase L-Met yield (Curien *et al.* 2003). In the *mto2* plant lines, the

arginine substitution in the TS active site impairs the synthesis of L-Thr, causing a 94% reduction in L-Thr synthesis, and resulting in a range of altered metabolic processes (Bartlem *et al.* 2000; Kusano *et al.* 2010). These plants are associated with a 3-fold accumulation of the upstream metabolites of L-Thr, along with a 3-fold increase in overall amino acid biosynthesis and in SAM concentration, which leads to a 3-fold increase in the synthesis of polyamines (Kusano *et al.* 2010). This illustrates the inter-connected nature of metabolic pathways and demonstrates that careful consideration must be given to the cellular role of TS when seeking to alter its effects on OPHS flux partitioning.

Manipulations of TS expression have had varying effects on cellular L-Met and L-Thr pools and plant phenotype in different species, as exemplified by studies in *A. thaliana* and *S. tuberosum* (Zeh *et al.* 2001; Avraham and Amir, 2005). For example, expression of *A. thaliana TS* in the antisense orientation downstream of the CaMV-35S promoter, thus reducing *TS* expression, led to a 17- to 47-fold accumulation of L-Met in transgenic *A. thaliana*. Similar expression of *S. tuberosum TS* in the antisense orientation in transgenic *S. tuberosum* plants led to up to 240-fold accumulation of L-Met (Zeh *et al.* 2001). These results highlight the necessity of characterizing TS and mapping metabolic flux in the target species prior to engaging in genetic engineering endeavours *in vivo*, since the degree to which TS affects OPHS flux distribution may vary across species.

1.6. Rational metabolic engineering through kinetic modeling

The pursuit of increased L-Met production has involved experiments using strong constitutive promoters, such as the CaMV-35S promoter, to increase expression of CGS or decrease expression of TS (Gakiere *et al.* 2002; Zeh *et al.* 2001). The resulting 15- to 240-fold increases in L-Met levels are higher than necessary to meet human dietary requirements, and are often associated with phenotypic effects, such as retarded growth, leaf chlorosis, and reduction in fresh weight (Zeh *et al.* 2001; Gakiere *et al.* 2002; Avraham and Amir, 2005). A 3-fold increase in seed L-Met is sufficient to achieve adequate nutritional quality, and is unlikely to cause perturbations to metabolic flux in other pathways, thus avoiding undesirable phenotypic effects. For example, the expression of a feed-back insensitive form of dihydrodipicolinate synthase (DHDPS), the first committed enzyme in the L-Lys metabolic pathway, under the control of the CaMV-35S promoter or a seed-specific promoter, led to a 5-fold and a 3-fold increase in L-Lys accumulation, respectively, in *Oryza sativa* (Shaver *et al.* 1996; Lee *et al.* 2001). The seeds expressing DHDPS under the strong constitutive promoter had poor germination rates and altered seed morphology, a trend that was proportional to DHDPS expression and L-Lys accumulation (Lee *et al.* 2001). The expression of a bacterial, feed-back insensitive form of DHDPS in *Zea mays* under the control of a maize seed promoter, successfully generated a high-lysine maize variety, with 2- to 3-fold elevations in L-Lys content, that was available commercially (LY038) but has since been withdrawn due to safety concerns raised by opponents of genetically modified foods (Dizigan *et al.* 2007; Galili and Amir, 2012). These results indicate

that modest increases in seed amino acid composition are possible, but require more subtle strategies that have been verified *in vitro* prior to engaging in metabolic engineering projects *in vivo*. This *in vitro* verification can be facilitated through the use of a mathematical model of metabolic flux (Rohwer, 2012).

Traditionally, the analysis of metabolism has been reductionist in nature, with the study of the enzymes of a given pathway occurring in isolation (Rohwer, 2012). Metabolic engineering causes changes in flux that affect the activities of other enzymes in the metabolic network, and so the assimilation of disparate kinetic data into a kinetic model can be used to recreate the dynamics of a metabolic pathway (Stitt *et al.* 2010; Rohwer, 2012). A kinetic model of the OPHS branch-point requires the integration of information about the activity and regulation of the component enzymes, TS and CGS for the OPHS branch-point, as well as the physiological conditions and metabolite concentrations in the relevant subcellular compartment (Rohwer, 2012).

Kinetic models increase our understanding of complex metabolic networks and enable the description of their behaviour and regulation in a quantitative manner (Rohwer and Botha, 2001). As such, these models can be used to predict the effect of manipulations on a given metabolic pathway prior to making these alterations *in vivo*. For example, the creation of kinetic models of sucrose metabolism have been used to identify the enzymes that regulate the energetically costly process of futile cycling of sucrose (Rohwer and Botha, 2001; Uys *et al.* 2007). The model was used to inform rational enhancement strategies for the improvement of sucrose accumulation by predicting the *in vivo* sucrose accumulation occurring when the expression of one of

the enzymes involved in futile cycling was decreased using RNA interference (Rossouw *et al.* 2007; Rohwer, 2012). Another model simulating the synthesis of aliphatic glucosinolates, an important secondary metabolite, in *A. thaliana* was used to understand interconnections in the regulation and expression of two homologues of one of the component enzymes, thus permitting the assessment of the relative flux contributions of each enzyme individually, which would not have been possible experimentally (Knoke *et al.* 2009).

1.7 Objective

Since methionine and cysteine make up 1.3% of the total protein content in *C. arietinum* seed proteins, and humans require a combined daily intake of 3-5% of total dietary protein for both amino acids (Elango *et al.* 2009), only a slight increase (approximately 3-fold) in seed L-Met is required to meet the daily nutritional needs of humans and non-ruminant animals. Many previous metabolic engineering projects aimed at increasing L-Met biosynthesis have employed strong constitutive promoters to increase the expression of *CGS* or decrease *TS* expression through anti-sense repression have yielded significant accumulation of free L-Met (Zeh *et al.* 2001; Kim *et al.* 2002). However, the use of a strong promoter like CaMV-35S is frequently associated with disruptions in flux accompanying the 8- to 240-fold increases in L-Met synthesis, leading to negative effects on plant phenotype, and thus making these strategies undesirable for use in crop species (Zeh *et al.* 2001; Kim *et al.* 2002; Nikiforova *et al.* 2002). To facilitate the engineering of the pulse species of interest with a modest increase in L-Met content, a detailed understanding of the flux at the

OPHS branch-point between the L-Met and L-Thr biosynthetic pathways is required. The construction of a metabolic model of the OPHS branch-point in important pulse species will provide the knowledge base required for manipulating flux to increase L-Met biosynthesis and meet the requirements for human nutrition.

Kinetic studies of TS of *C. arietinum* and *L. culinaris* under maximal activity conditions require the isolation of the enzymes and *in vitro* study using an efficient and reliable kinetic assay. The purpose of the research described in this thesis is to enhance our understanding of the role of TS from *C. arietinum* and *L. culinaris* through:

1. The development of a suitable continuous, coupled-coupled spectrophotometric assay for measuring TS activity, and a simplified and consistent method for the synthesis and purification of the OPHS substrate (Chapter 2);
2. The isolation of functional TS from the target species (Chapter 3); and
3. The measurement of the steady-state kinetic parameters of TS from *C. arietinum* and *L. culinaris* which, in combination with those of CGS, will provide the basis for modeling the partitioning of OPHS in these pulse species (Chapter 4).

Chapter 2: Development of a continuous assay and steady-state characterization of *Escherichia coli* threonine synthase

2.1. Abstract

Threonine synthase (TS) catalyzes the hydrolysis of *O*-phospho-L-homoserine (OPHS) to produce L-threonine (L-Thr) and inorganic phosphate. Here, we report a simplified purification protocol for the OPHS substrate and a continuous, coupled-coupled, spectrophotometric TS assay. The sequential actions of threonine deaminase (TD) and hydroxyisocaproate dehydrogenase (HO-HxoDH) convert the L-Thr product of TS to α-ketobutyrate (α-KB) and then to 2-hydroxybutyrate, respectively, and are monitored as the decrease in absorbance at 340 nm resulting from the concomitant oxidation of NADH to NAD^+ by HO-HxoDH. The effect of pH on the activities of *Escherichia coli* TD, and *Lactobacillus delbrueckii* HO-HxoDH was determined in order to establish this continuous assay as suitable for steady-state characterization and to facilitate the optimization of coupling enzyme concentrations under different assay conditions to enable studies of TS across phyla. To validate this assay, TS from *E. coli* was characterized. The kinetic parameters (k_{cat} = 4 s^{-1}, K_m^{OPHS} = 0.34 mM) and the pH optimum of 8.7, determined using the continuous assay, are consistent with the values reported for this enzyme based on the discontinuous malachite green assay. The k_{cat}/K_m^{OPHS} *versus* pH profile of eTS is bell-shaped and the apparent pK_a values for the acidic and basic limbs are 7.1 and 10.4, respectively.

2.2. Introduction

In plants and bacteria, threonine synthase (TS; E.C. 4.2.3.1) catalyzes the pyridoxal 5'-phosphate (PLP)-dependent hydrolysis of *O*-phospho-L-homoserine (OPHS) to produce L-threonine (L-Thr) and inorganic phosphate. The TS enzyme has been studied from a variety of species of microorganisms, including yeast, *Bacillus subtilis*, *Mycobacterium tuberculosis*, *Crytococcus neoformans*, *Thermus thermophilus*, and *Escherichia coli*, as well as from multiple plant species, including *Arabidopsis thaliana, Pisum sativum, Beta vulgaris* and *Lemna paucicostata* (Cohen and Hirsch, 1954; Watanabe and Shimura, 1955; Wormser and Pardee, 1958; Flavin and Slaughter, 1960; Madison and Thompson, 1976; Szczesiul and Wampler, 1976; Thoen *et al.* 1978; Giovanelli *et al.* 1984; Farrington *et al.* 1993; Laber *et al.* 1994a; Laber *et al.* 1994b; Ramos and Calderon, 1994; Curien *et al.* 1996; Curien *et al.* 1998; Laber *et al.* 1999; Chassagnole *et al.* 2001; Rais *et al.* 2001; Covarrubias *et al.* 2008; Kingsbury and McCusker, 2008; Murakawa *et al.* 2011). As an enzyme limited to plants and bacteria, TS is an attractive target for biotechnological applications, such as the development of anti-microbial and herbicidal compounds, and manipulation of amino acid biosynthesis (Thomazeau *et al.* 2001; Covarrubias *et al.* 2008). The OPHS substrate of TS is labile, and must be synthesized as it is not commercially available. The reliability of TS kinetic parameters is dependent on the purity and accurate quantification of the OPHS substrate and the variability in reported protocols for the synthesis and purification of OPHS complicates the comparison of reported kinetic values (Flavin and Slaughter, 1960; Datko *et al.* 1974; Madison and Thompson, 1976; Szczesiul and Wampler, 1976; Thoen *et al.* 1978;

Giovanelli *et al.*1984; Ramos and Calderon, 1994; Laber *et al.* 1994a; Laber *et al.* 1994b; Curien *et al.* 1996; Curien *et al.* 1998; Laber *et al.* 1999; Curien *et al.* 2003).

The discontinuous TS assays reported typically rely on quantification of the phosphate product, *via* reaction with malachite green, the use of [^{3}H]-labeled OPHS, or derivatization and detection of phenylthiocarbmoyl-L-threonine. The labour-intensive nature of these methods and the cost and difficulty of synthesizing a radioactive substrate illustrate the need for the development of a continuous TS assay. A continuous method for monitoring flux at the branch-point between the L-Met and L-Thr biosynthetic pathways of *A. thaliana,* reported by Curien *et al*., employed threonine deaminase (TD; E.C. 4.2.1.16) and lactate dehydrogenase (LDH) as coupling enzymes for TS (Curien *et al.* 2003). However, this method was not optimized for the steady-state characterization of TS and subsequent studies reporting TS kinetic parameters have continued to employ discontinuous assays (Lee *et al.* 2005; Covarrubias *et al.* 2008; Murakawa *et al.* 2011).

Although LDH can reduce the α-ketobutyrate (α-KB) product of TD, its catalytic efficiency for this reaction is an order of magnitude lower than that of the enzyme hydroxyisocaproate dehydrogenase (HO-HxoDH; E.C. 1.1.1.-) from *Lactobacillus delbrueckii* (Aitken *et al.* 2003). Therefore, the latter was selected for the design of a continuous, coupled-coupled assay to monitor TS activity (Figure 2.1). In order to validate this assay, *via* the characterization of *E. coli* TS, the TD enzyme from *E. coli* (eTD) was selected as a coupling enzyme. However, wild-type eTD is not an optimal coupling enzyme, as it displays cooperative substrate binding (Eisenstein, 1991). Therefore, the L447F site-directed variant of this enzyme, which

Figure 2.1. The continuous, coupled-coupled enzyme assay developed for TS. The TS-catalyzed β,γ-replacement of OPHS yields L-Thr and inorganic phosphate. The first coupling enzyme, TD, deaminates L-Thr, producing NH_3 and α-KB, which is subsequently reduced to 2-hydroxybutyrate by the second coupling enzyme, HO-HxoDH, with the concurrent oxidation of NADH (ε340 = 6200 $M^{-1}cm^{-1}$).

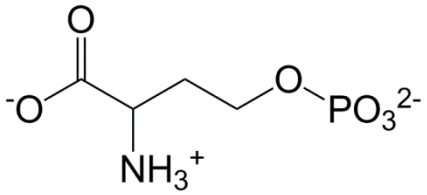

O-phospho-L-homoserine

Threonine Synthase

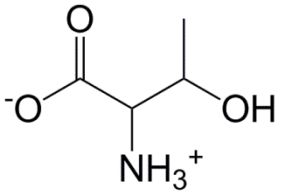

L-Threonine

NH3

Threonine Deaminase

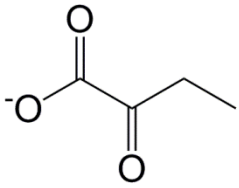

α-ketobutyrate

NADH

NAD+

Hydroxyisocaproate Dehydrogenase

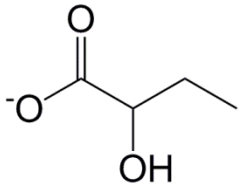

2-hydroxybutyrate

displays Michaelis-Menten kinetics, was selected for this system (Eisenstein *et al.* 1995). In this method the L-Thr product of TS is converted by eTD to α-KB, which is subsequently reduced by HO-HxoDH with the concomitant oxidation of NADH to NAD^+ (ε_{340} = 6200 $M^{-1}cm^{-1}$). The effect of pH on the catalytic efficiency of TD and HO-HxoDH was determined in order to establish this continuous, coupled-coupled assay as a method for studying TS activity from a variety of species, including plants, bacteria and other microorganisms, which have distinct pH optima (Sczcesiul and Wampler, 1976; Curien *et al.* 1998; Covarrubias *et al.* 2008).

2.3. Methods

2.3.1. Materials

L-Homoserine (L-HSer), adenosine-5'-triphosphate (ATP), α-ketobutyrate (α-KB), β-nicotinamide adenine dinucleotide (NADH), bicine, phospho(enol)pyruvate (PEP), pyruvate kinase (PK), L-lactate dehydrogenase (LDH), calf intestinal alkaline phosphatase (CIAP), ninhydrin, Triton x-100, and ammonium molybdate were obtained from Sigma-Aldrich. 4-(2-hydroxyethyl)-1-piperazineethanesulfonic acid (HEPES), 3-(N-morpholino)propanesulfonic acid (MOPS), L-proline (L-Pro), L-Thr, L-valine (L-Val) dithiothreitol (DTT), and isopropyl β-D-thiogalactopyranoside (IPTG) were Fisher Scientific products. Nickel-nitrilotriacetic acid (Ni-NTA) resin was purchased from Qiagen. Malachite green and diethylaminoethyl (DEAE) resin were obtained from BDH and GE Healthcare, respectively.

2.3.2. Construction of expression constructs and purification of eHSK, eTS, eTD and Ho-HxoDH

The coding regions of *E. coli* homoserine kinase (eHSK; *thrB*), threonine synthase (eTS; *thrC*) and eTD (*ilvA*) were amplified from the genomic DNA of strain DH10B (Table 2.1). The 3' primers for eHSK and eTS were designed to introduce a 6-Histidine (6-His), affinity tag at the C-terminal end of the recombinantly expressed proteins. Farsi *et al.* (2009) replaced the *Nco*I site of the pTrc-99a expression vector with a *Nde*I site, to produce pTrc-99a2, and subsequently introduced the sequence encoding a N-terminal, 6-His tag and linker containing a Factor Xa cleavage site, yielding the pTrc-99aAF expression vector (Farsi *et al.* 2009). The eHSK, eTS and eTD amplicons were inserted at the *Nco*I and *Xba*I, *Nde*I and *Sac*I, and the *Nde*I and *Xba*I sites of the pTrc99a (GE Healthcare), pTrc-99a2 and pTrc-99aAF plasmids, respectively. The coding region of HO-HxoDH (*hdhA*; Genbank accession X65222) was amplified from pTrc-99a and inserted between the *Nde*I and *Xba*I restriction sites of pTrc-99aAF (Aitken *et al.* 2003). Therefore, the 6-His, affinity tags of the expressed eTD and HO-HxoDH proteins are at the N-terminus, while those of eTS and eHSK are C-terminal. Overlap-extension, site-directed mutagenesis was employed to construct the L447F variant of eTD (eTD_{L447F}). All constructs were sequenced prior to expression and purification of the gene products. The genes encoding eHSK, eTD, eTD_{L447F}, eTS and HO-HxoDH were expressed in *E. coli* strain DH10B and purified *via* Ni-NTA affinity chromatography, as described by Farsi *et al.* (2009). Following the addition of glycerol, to a final concentration of 30% (v/v), the purified enzymes were aliquoted and stored at -80°C. Protein concentrations were

Table 2.1. Primers employed for the eHSK, eTS, eTD, eTD_{L447F}, and HO-HxoDH expression constructs.

Primer	Primer
eHK Fc-*Nco*I	5'-gagtctgccatggttaaagtttatgcc
eHK-6His Rc-*Xba*I	5'-gctctagattaatggtggtgatggtggtggttttccagtactcgtgcgc
eTS-Start-*Nde*I	5'-gacatatgaaactctacaatctgaaagatca
eTS-Stop-*Sac*I	5'-ggagctcttaatgatggtgatgatgatgctgatgattcatcatcaaattacgca
TD 5'c-f-*Nde*I	5'-tctcatatggctgactcgcaacccctgtc
TD 3'c-r-*Xba*I	5'-gcatctagactaacccgccaaaaagaaacctgaacgc
TD-L447F-F[a]	5'-tcaccgggcgcgttcctgcgcttcctc
TD-L447F-R[a]	5'-gaggaagcgcaggaacgcgcccggtga
HO-HxoDHfc-*Nde*I	5'-gactcatatgactaaattgccatgtataatgtc
HO-HxoDHrc-*Xba*I	5'-gacttctagattacaggttaacgatgcttcttgg

[a]Primers employed for site-directed mutagenesis of eTD.

determined *via* the Bradford assay (Bio-Rad) using bovine serum albumin as the standard (Bradford, 1976).

2.3.3. Synthesis of O-phospho-L-homoserine

The reaction conditions for the phosphorylation of L-HSer were modified from those reported by Laber and colleagues, by reducing the ATP in solution from 5 mM to 1 mM, to facilitate quantification using malachite green hydrochloride (Laber *et al.* 1994a; Laber *et al.* 1994b). The 3-mL reaction mixture was comprised of 25 mM Tris-HCl (pH 7.8), 10 mM $MgCl_2$, 1 mM ATP, 100 mM L-HSer and 100 mM PEP and the reaction was initiated by the addition of 0.2 μM PK and 1.2 μM eHSK. An identical aliquot of both enzymes was added after 2 hours and the reaction was incubated at 25°C for a further 22 hours before being applied to a 20-mL column (2.5 cm x 10 cm) of DEAE anion exchange resin. The column was subsequently washed with 100 mL of water and the OPHS was eluted with a 100 mL linear gradient of 0-200 mM NaCl and collected in 3.5-mL fractions, with the OPHS generally eluting between fractions 15-23. The amino acid content of the fractions was determined by reaction with ninhydrin, following separation by thin layer chromatography using 70% isopropanol. Fractions containing OPHS were tested for residual pyruvate by reaction with 20 μM HO-HxoDH and 1.5 mM NADH, as the presence of pyruvate, produced from PEP, will increase background in the eTS coupled assay. Fractions containing OPHS and pyruvate were pooled, reapplied to the DEAE column and separated under the same conditions. All fractions containing OPHS, but not pyruvate, generally fractions 20-25, were pooled and concentrated by rotary

evaporation. The concentration of OPHS was determined *via* the malachite green assay, following treatment with CIAP (1 mg/mL) for 5-6 hours at room temperature to release the phosphate moiety of OPHS (Lanzetta *et al.* 1979; van Veldhoven and Mannaerts, 1987). Ammonium molybdate was added, to a final concentration of 0.6% (v/v), and samples were incubated at room temperature for 10 minutes. Malachite green was subsequently added to a final concentration of 0.006% (v/v), and samples were incubated at room temperature for a further 10 minutes. Absorbance was measured at 620 nm, and the concentration of released phosphate was determined by comparison to a standard curve of 0-50 μM inorganic phosphate.

2.3.4. Enzyme Assays

All enzyme assays were performed in a total volume of 100 μL at 25ºC and monitored at 340 nm using a SpectraMax spectrophotometer. Unless otherwise stated, the assay solution was comprised of 50 mM HEPES (pH 8.0) and 1.5 mM NADH. Pyridoxal 5'-phosphate (PLP) was added to a final concentration of 20 μM for assays involving the PLP-dependent enzymes eTD and eTS. All reactions were equilibrated with coupling enzyme(s) at 25ºC and a background rate was recorded prior to initiation of the reaction by the addition of the enzyme being assayed. The reduction of α-KB (0.35-60 mM) to 2-hydroxybutyrate by HO-HxoDH (0.14 μM) was detected by the concomitant conversion of NADH to NAD^+ (ε_{340} = 6,200 $M^{-1}s^{-1}$). The deamination of L-Thr (0.2-80 mM) by eTD and eTD_{L447F} (0.07 μM) was similarly monitored, using HO-HxoDH (5.1 μM) as the coupling enzyme, both in the presence and absence of 0.5 mM L-Val, an allosteric activator of wild-type eTD (Eisenstein,

1991). The production of L-Thr from OPHS (0.05-8 mM) by eTS (0.14 μM) was also detected as the conversion of NADH to NAD^+, using the continuous assay employing eTD_{L447F} (2.6 μM) and HO-HxoDH (8.2 μM) as coupling enzymes (Figure 2.1). Homoserine kinase activity was monitored using the PK/LDH coupled assay (Theze *et al.* 1974). The eHSK assay mixture contained 25 mM Tris-HCl (pH 7.8), 10 mM $MgCl_2$, 4.8 mM PEP, 1.5 mM NADH, 2.5 mM ATP and 0.03-4.8 mM L-HSer, or 0.03-4.8 mM ATP and 1.5 mM L-HSer, 0.96 μM PK and 1.2 μM LDH. Reactions were initiated by the addition of 1 μM eHSK and the production of OPHS from L-HSer was detected *via* the recycling of ADP to ATP by PK, coupled with the reduction of pyruvate to lactate by LDH, with the concomitant conversion of NADH to NAD^+.

The k_{cat} and K_m of HO-HxoDH, eTD_{L447F}, and eTS were determined by fitting the data to the Michaelis-Menten equation, and the k_{cat}/K_m values were obtained independently from equation 2.1.

$$\frac{v}{[E]} = \frac{k_{cat}/K_m[S]}{1+[S]/K_m} \tag{2.1}$$

Values for k_{cat} and $K_m^{\text{L-Thr}}$ of eTD, which exhibits cooperative binding at low L-Thr concentrations, were obtained by fitting the data to equation 2.2.

$$\frac{v}{[E]} = \frac{k_{cat}[S]^n}{K_m{}^n + [S]^n} \tag{2.2}$$

The k_{cat} and K_m^{ATP} values of eHSK were obtained by fitting the data to the Michaelis-Menten equation, while $K_m^{L\text{-}HSer}$ was determined from equation 2.3, which incorporates the $K_i^{L\text{-}HSer}$ term for substrate inhibition of eHSK by L-HSer.

$$\frac{v}{[E]} = \frac{k_{cat}[S]}{K_m + [S](1 + [S]/K_i^{L-Hser})} \tag{2.3}$$

2.3.5. Evaluation of the pH dependence of HO-HxoDH, eTD$_{L447F}$, and eTS

The pH dependence of the reactions catalyzed by HO-HxoDH, eTD$_{L447F}$ and eTS was determined in the three-component MBP buffer (50 mM MOPS, pK_a = 7.2; 50 mM bicine, pK_a = 8.3; 50 mM L-Pro, pK_a = 10.7) (Perrachi *et al.* 1996). The activity of HO-HxoDH (0.83-26.6 μM) was measured between pH 6.2-10.6 in MBP assay buffer containing 0.22-55 mM α-KB and 1.5 mM NADH. The pH dependence of eTD$_{L447F}$ was determined between pH 7.2-10.6 in a reaction mixture comprising 0.6-90 mM L-Thr, 1.5 mM NADH, 20 μM PLP, 15-20 μM HO-HxoDH, and 0.07 μM eTD$_{L447F}$. The effect of pH on the catalytic efficiency of eTS was determined between pH 6.8-10.5 in a reaction mixture comprising 0.1-8 mM OPHS, 1.5 mM NADH, 20 μM PLP, 8.2-16.3 μM HO-HxoDH, 1.3-2.6 μM eTD$_{L447F}$, and 0.14 μM eTS. The concentration of the HO-HxoDH and eTD$_{L447F}$ coupling enzymes were optimized and the measured activity was shown to be linearly dependent on eTS concentration across the pH range investigated. The k_{cat}/K_m *versus* pH data for eTD$_{L447F}$ and eTS were fitted to the bell-shaped curve described by equation 2.4, and the pH dependence of the k_{cat}/K_m of HO-HxoDH was fitted to the curve described by equation 2.5 (Aitken *et al.* 2003).

$$\frac{k_{cat}}{K_m} = \frac{(k_{cat}/K_m)_{\max}}{1+10^{pK_{a1}-pH}+10^{pH-pK_{a2}}} \quad (2.4)$$

$$\frac{k_{cat}}{K_m} = \frac{(k_{cat}/K_m)_{\max}}{1+10^{pH-pK_{a2}}} \quad (2.5)$$

2.4. Results

All enzymes were recombinantly expressed in fusion with a 6-His tag, to enable purification *via* Ni-NTA affinity chromatography, and their purity was verified by SDS-PAGE (Figure 2.2). The yields of eHSK, HO-HxoDH, eTD, eTD_{L447F}, and eTS were 19, 24, 33, 16 and 23 mg per 1L of *E. coli* culture, respectively.

2.4.1. Synthesis and separation of OPHS:

The K_m^{ATP} (0.19 mM), $K_m^{L\text{-}HSer}$ (0.8 mM) and $K_i^{L\text{-}HSer}$ (3.5 mM) values determined for eHSK are within 2.5-fold of those previously reported, demonstrating that the C-terminal, 6-His affinity tag has negligible effect on the enzyme (Theze *et al.* 1974; Shames and Wedler 1984). The use of the malachite green assay for quantification of OPHS requires treatment with CIAP to release the phosphate moiety. Separation of OPHS from residual pyruvate, produced from PEP by PK, is not required for the malachite green or [^{1}H]-OPHS endpoint assays, but is essential for the continuous TD/HO-HxoDH assay as pyruvate is converted to lactate by HO-HxoDH, thereby resulting in increased background and the possibility of overestimating TS activity. Therefore, the OPHS synthesis method reported by Laber

Figure 2.2. SDS-PAGE of the purified recombinant enzymes. Lane 1 – *E. coli* HSK (MW = 30 kDa) (Burr *et al.* 1976); Lane 2 – *E. coli* TS (MW 47 kDa) (Parsot *et al.* 1983); Lane 3 – *E. coli* TD (MW = 56 kDa) (Eisenstein, 1991); Lane 4 – *E. coli* TD_{L447F} (MW = 56 kDa) (Eisenstein, 1991); Lane 5 – *L. delbrueckii* HO-HxoDH (MW = 36 kDa) (Bernard *et al.* 1994); Lane 6 – Benchmark protein ladder (Invitrogen). Molecular markers are indicated at 50 kDa and 20 kDa.

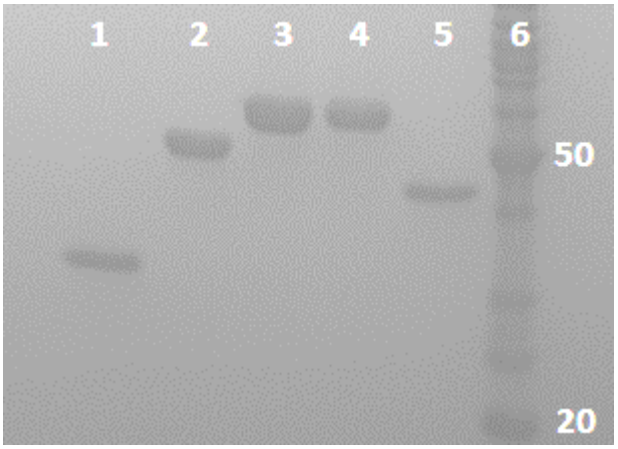
1
2
3
4
5
6
50
20

and colleagues was modified to reduce the ATP concentration from 5 mM to 1 mM to minimize the effect of the α and β phosphates of ADP, also released by CIAP treatment, on the accuracy of OPHS quantification, and the OPHS purification procedure was optimized to ensure the separation of OPHS from pyruvate (Laber *et al.* 1994a; Laber *et al.* 1994b). The presence of OPHS following separation, *via* anion exchange chromatography, was confirmed by TLC analysis, and by reaction with eTS, and fractions were tested with HO-HxoDH to ensure pyruvate was not present (Figure 2.3). Rotary evaporation was employed to concentrate the purified OPHS to ~25-30 mM, for use in eTS enzyme assays.

2.4.2. Optimization of Assay Parameters

The steady-state kinetic parameters of eTD, eTD_{L447F}, and HO-HxoDH were determined under eTS assay conditions (Table 2.2) and the effect of 0.5 mM L-Val on eTD activity was investigated (eTD_{Val}). The $K_m^{L\text{-}Thr}$ values of eTD (10.6 mM) and eTD_{Val} (11.7 mM) are within 2-fold of the reported $K_m^{L\text{-}Thr}$ values of 8 mM and 5.7 mM, respectively (Eisenstein, 1991). The $K_m^{L\text{-}Thr}$ value of eTD_{L447F} (5.7 mM), which displays Michaelis-Menten behavior and is not allosterically activated by L-Val, is identical to the reported value for this site-directed variant (Eisenstein *et al.* 1995). The $k_{cat}/K_m^{\alpha\text{-}KB}$ for the reduction of α-KB to 2-hydroxybutyrate by the N-terminally, 6-His tagged HO-HxoDH at pH 8.0 is 1.2×10^4 $M^{-1}s^{-1}$, which is in agreement with the reported values of 2.6×10^4 $M^{-1}s^{-1}$, for the wild-type enzyme (Bernard *et al.* 1994), and 1.6×10^4 $M^{-1}s^{-1}$ (Aitken *et al.* 2003), for the C-terminally 6-His tagged enzyme, both assayed at pH 7.5.

Figure 2.3. Verification of OPHS production by eHSK by thin-layer chromatography. Lane 1 – 10 mM L-homoserine standard (R_f = 0.62); Lane 2 – OPHS, product of eHSK reaction, (R_f = 0.36); Lane 3 – OPHS sample treated with CIAP for 6 hrs, to produce L-HSer and inorganic phosphate, (R_f = 0.62); Lane 4 – 10 mM L-Thr standard (R_f = 0.62); Lane 5 – OPHS sample following reaction with eTS, to produce L-Thr, (R_f = 0.62). Chromatography was performed using 70% isopropanol.

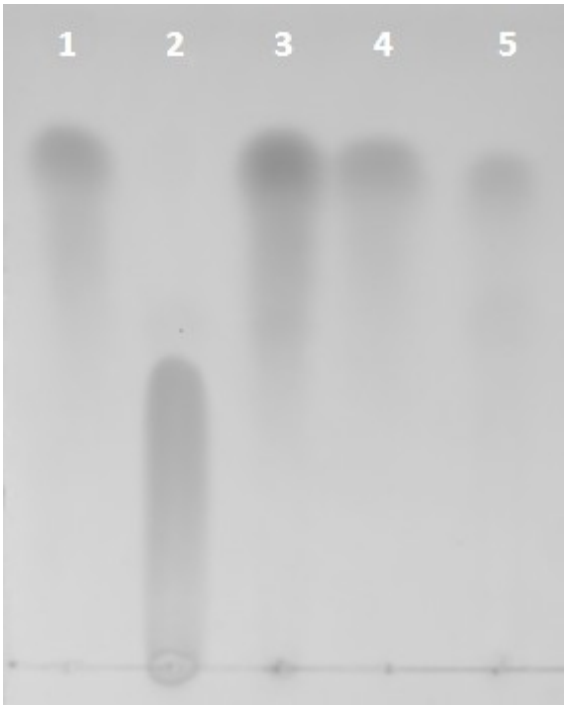
1
2
3
4
5

Table 2.2. Kinetic parameters of *E. coli* threonine synthase (eTS), homoserine kinase (eHSK), threonine deaminase (eTD) and the site-directed variant eTD_{L447F}, and *L. delbrueckii* hydroxyisocaproate dehydrogenase (HO-HxoDH).[a]

Enzyme	K_M (mM)	k_{cat} (s^{-1})	k_{cat}/K_M ($M^{-1}\ s^{-1}$)
eHSK	0.19±0.01 (ATP)	4.3±0.06	(2.3±0.13) x 10^4 (ATP)
	0.8±0.1 (L-HSer)	8.8±0.6	(1.1±0.05) x 10^4 (L-HSer)
HO-HxoDH	3.6±0.2 (α-kb)	42.4±0.7	(1.2±0.7) x 10^4 (α-kb)
eTD	10.6±0.4 (L-Thr)	51.6±1.4	4.9 x 10^3 (L-Thr)
eTD_{Val}[b]	11.7±0.7 (L-Thr)	66.1±1.3	(5.6±0.2) x 10^3 (L-Thr)
eTD_{L447F}	5.7±0.4 (L-Thr)	42.1±0.8	(7.3±0.4) x 10^3 (L-Thr)
eTS	0.34±0.04 (OPHS)	4.0±0.1	(1.2±0.1) x 10^4 (OPHS)

[a]The 6-His, affinity tag of eHSK and eTS are C-terminal, while those of HO-HxoDH, eTD and eTD_{L447F} are N-terminal. The assay solution for HO-HxoDH, eTS, eTD and eTD_{L447F} was comprised of 50 mM HEPES (pH 8.0) and 1.5 mM NADH and 20 μM PLP, for eTD and eTS enzymes. The substrate and enzyme concentrations for HO-HxoDH and eTD assays were 0.35-60 mM α-KB and 0.14 μM HO-HxoDH, and 0.2-80 mM L-Thr and 0.07 μM eTD or eTD_{L447F}, with 5.1 μM HO-HxoDH coupling enzyme, respectively. The substrate and enzyme concentrations for the eTS assay were 0.05-8 mM OPHS and 0.14 μM eTS with 2.6 μM eTD_{L447F} and 8.2 μM HO-HxoDH. Homoserine kinase (1 μM) activity was monitored in 25 mM Tris-HCl (pH 7.8), 10 mM $MgCl_2$, 4.8 mM PEP, 1.5 mM NADH, 2.5 mM ATP and 0.03-4.8 mM L-HSer, or 0.03-4.8 mM ATP and 1.5 mM L-HSer, 0.96 μM PK and 1.2 μM LDH.

[b]Kinetic parameters determined in the presence of 0.5mM of the allosteric activator L-Val.

The concentration of HO-HxoDH required in the continuous eTD_{L447F} assay, assuming a short lag period (τ = 4 s), was calculated to be 13 μM (equation 2.6) (Aitken *et al.* 2003).

$$[HO-HxoDH] = \frac{K_m^{\alpha-KB}}{k_{cat}^{HO-HxoDH}\tau} \tag{2.6}$$

This value was employed to determine that an eTD_{L447F} concentration of 11.3 μM is required for the eTS assay to give an overall lag of 12 s, using eq. 2.7 (Aitken *et al.* 2003).

$$[eTD_{L447F}] = \frac{K_m^{Thr}/k_{cat}^{eTD}}{\tau - (K_m^{\alpha-KB}/k_{cat}^{HO-HxoDH})[HO-HxoDH]} \tag{2.7}$$

The calculated HO-HxoDH and eTD_{L447F} concentrations were subsequently optimized experimentally to 8.2 and 2.6 μM, respectively, by independently varying the concentration of each enzyme, and the reaction was demonstrated to be linear at eTS concentrations between 0.03-1.6 μM (Figure 2.4). The steady-state kinetic parameters of eTS (k_{cat} = 4 s^{-1} and K_m^{OPHS} = 0.34 mM) were subsequently determined using the eTD_{L447F}/HO-HxoDH assay (Table 2.2). The eTS-catalyzed deamination of OPHS was also investigated to determine whether this would be a factor in monitoring the β,γ-replacement activity of this enzyme. However, no conversion of NADH to NAD^+ was detected when 7.5 μM eTS was incubated with 20 mM OPHS, thereby demonstrating that α-ketobutyrate is not produced, under assay conditions, by eTS.

Figure 2.4. Dependence of the rate of NADH oxidation on eTS, (inset A) eTD_{L447F}, and (inset B) HO-HxoDH concentration in the coupled eTD_{L447F}/HO-HxoDH assay. Reactions were carried out in a volume of 100 μL at 25°C. Reaction conditions: 50 mM HEPES (pH 8.0), 1.5 mM NADH, 20 μM PLP and 5 mM OPHS, with (main panel) 0.03-7.4 μM eTS, 2.6 μM eTD_{L447F}, and 8.2 μM HO-HxoDH, with (inset A) 1.4μM eTS, 0.04-5.25 μM eTD_{L447F}, and 8.2 μM HO-HxoDH, or with (inset B) 1.4 μM eTS, 2.6 μM eTD_{L447F}, and 0.12-16.3 μM HO-HxoDH.

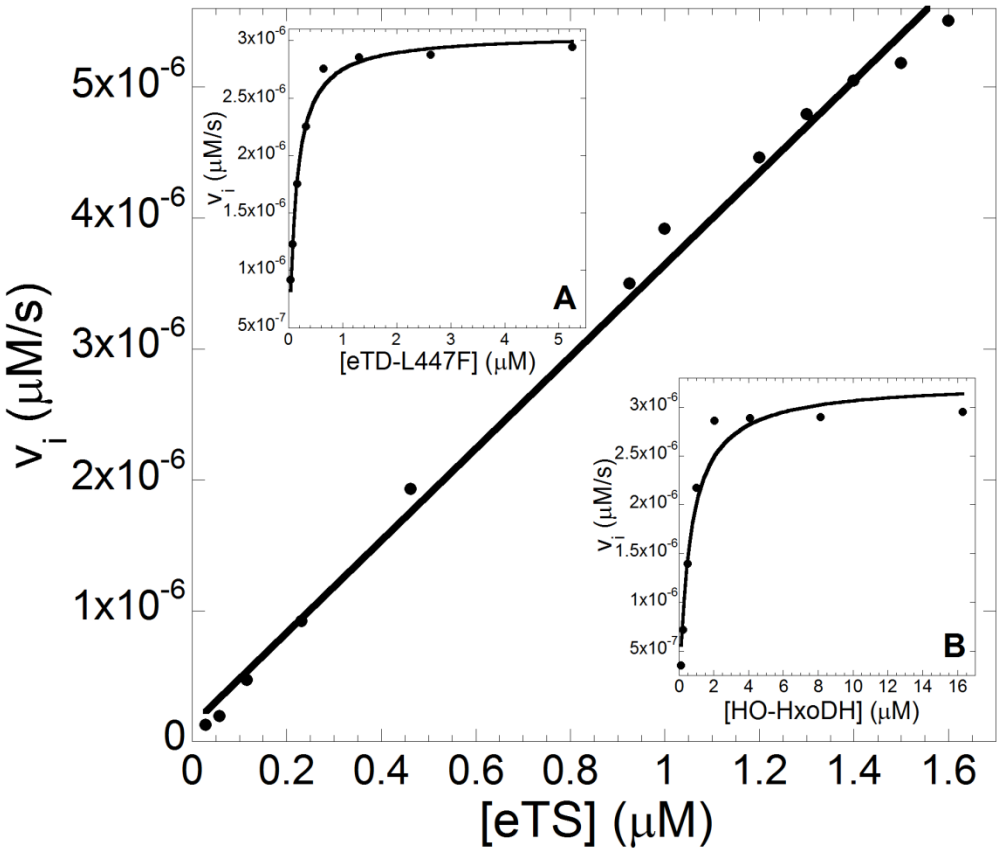
v_i (μM/s)
[eTS] (μM)
A
[eTD-L447F] (μM)
B
[HO-HxoDH] (μM)

2.4.3. The pH Dependence of eTS, eTD_{L447F}, and HO-HxoDH Activity

The effect of pH on the catalytic activity of HO-HxoDH and eTD_{L447F} was investigated to assess the suitability of the coupled assay for the steady-state characterization of TS from diverse species, which may have distinct pH optima, and for investigation of the effect of pH on the kinetic parameters of eTS (Figure 2.5). The k_{cat}/K_m *versus* pH profiles of eTD_{L447F} (pK_{a1} = 8.6 and pK_{a2} = 9.1) and HO-HxoDH (pK_a = 7.2) demonstrate that the pH optimum of eTD_{L447F} (pH 8.8) is similar to that of eTS (pH 8.7), while that of HO-HxoDH is ≤6.5. The latter illustrates the importance of optimizing the concentration of coupling enzymes at each pH in order to reliably determine the effect of pH on eTS activity. Therefore, the kinetic parameters of the coupling enzymes were employed to calculate their optimal concentration at each pH, using equations 2.6 and 2.7, and this was subsequently verified experimentally. The k_{cat}/K_m *versus* pH data for eTS was fit to eq. 2.4, and pH optimum, pK_{a1} and pK_{a2} values of 8.7, 7.1 and 10.4 were determined (Figure 2.6).

Figure 2.5. The pH dependencies of k_{cat}/K_m of *L. delbrueckii* HO-HxoDH and *E. coli* TD_{L447F} (eTD_{L447F}). Reaction conditions: Bicine-MOPS-Proline buffer (50 mM bicine, 50 mM MOPS, 50 mM L-Pro), 1.5 mM NADH. For HO-HxoDH (closed circles), 0.22-55 mM α-ketobutyrate, and 0.83-26.6 μM enzyme were added to the reaction mixture. For eTD_{L447F} (open circles), 20 μM PLP, 0.6-90 mM L-Thr, 15-20 μM HO-HxoDH, and 0.07 μM eTD_{L447F} were added to the reaction mixture.

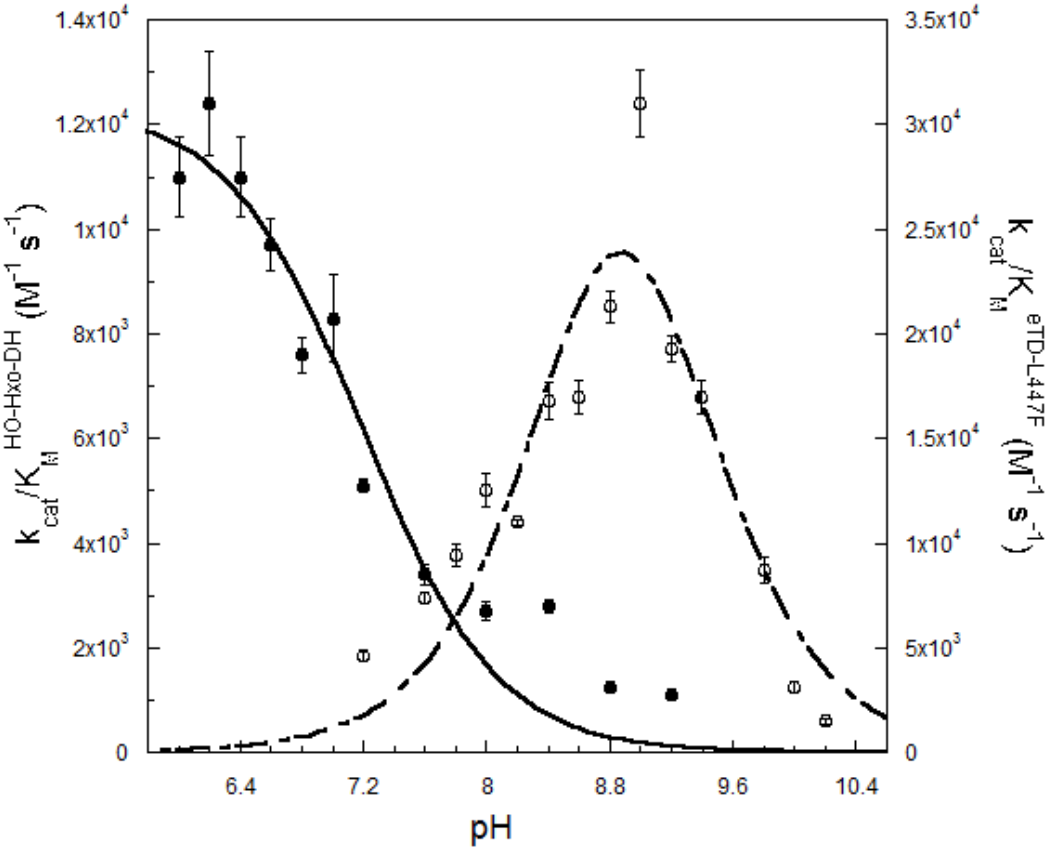
1.4x10^4
1.2x10^4
1x10^4
8x10^3
6x10^3
4x10^3
2x10^3
0
3.5x10^4
3x10^4
2.5x10^4
2x10^4
1.5x10^4
1x10^4
5x10^3
0
6.4
7.2
8
8.8
9.6
10.4
pH
k_cat/K_M HO-Hxo-DH (M^-1 s^-1)
k_cat/K_M eTD-L447F (M^-1 s^-1)

Figure 2.6. The pH dependence of k_{cat}/K_m^{OPHS} of eTS. Reaction conditions: Bicine-MOPS-Proline buffer (50 mM bicine, 50 mM MOPS, 50 mM L-Pro), 1.5 mM NADH, 20 μM PLP, 0.1-8 mM OPHS, 8.2-16.3 μM HO-HxoDH, 1.3-2.6 μM eTD_{L447F} and 1.4 μM eTS.

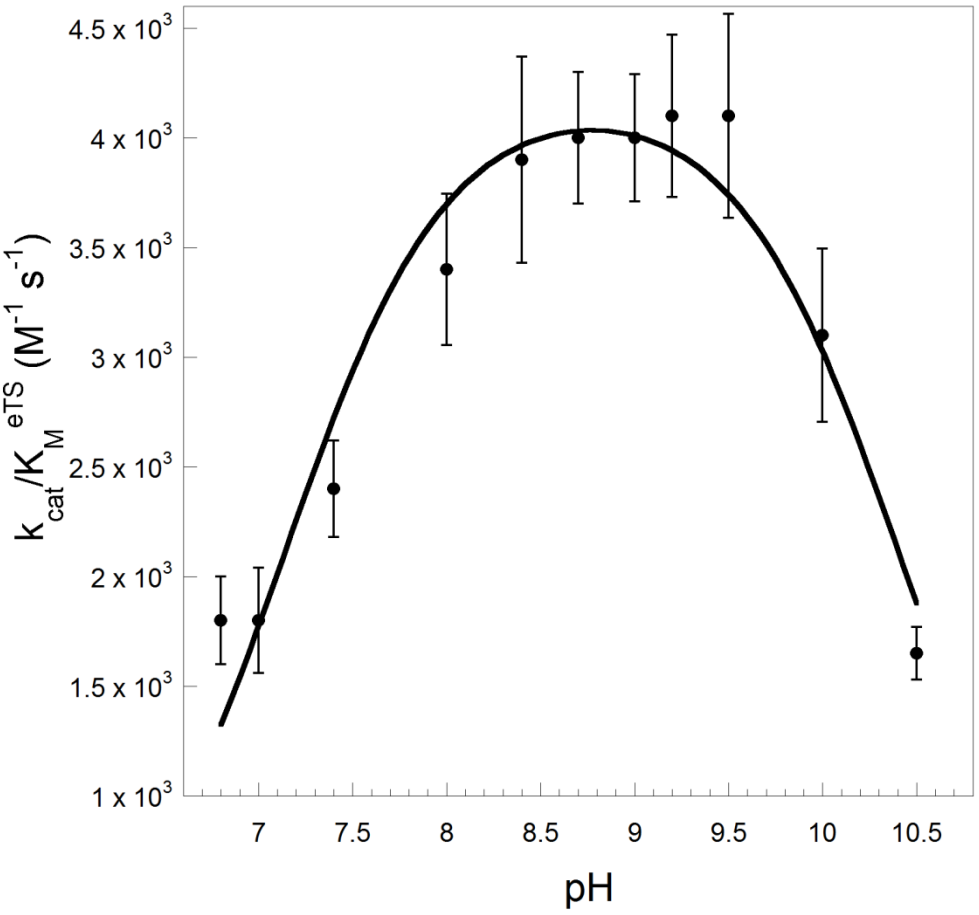
4.5 x 10^3
4 x 10^3
3.5 x 10^3
3 x 10^3
2.5 x 10^3
2 x 10^3
1.5 x 10^3
1 x 10^3
k_cat/K_M^eTS (M^-1 s^-1)
7
7.5
8
8.5
9
9.5
10
10.5
pH

2.5. Discussion

The restriction of TS to plants and microorganisms, which synthesize L-Thr *de novo*, provides a suitable target for many biotechnological applications, including the development of antibiotics and herbicides and metabolic engineering to produce crop varieties with increased nutritional value (Thomazeau *et al.* 2001; Covarrubias *et al.* 2008). In plants, OPHS occupies the branch point between the L-Thr and L-Met biosynthetic pathways (Ravanel *et al.* 1998b). Manipulation of the metabolic flux of either pathway, suggested as a strategy to increase the L-Met content of crop species deficient in this essential amino acid, requires an in-depth knowledge of the kinetic and regulatory properties of the enzymes involved (Curien *et al.* 2003). Therefore, an efficient, reliable, and robust continuous assay for the measurement of TS activity is necessary to enhance our understanding of this enzyme, and to provide a starting point for biotechnological applications.

A continuous, spectrophotometric TS assay was developed in this study with the goal of providing a rapid and rigorous method to investigate TS kinetic parameters. The proposed mechanism of the β,γ-replacement reaction catalyzed by TS has been described by Laber and coworkers (Figure 2.7) (Laber *et al.* 1994a). An enzymatic method for the synthesis of the OPHS substrate was optimized for compatibility with this assay. Chemical and enzymatic methods for the synthesis of OPHS have been reported (Watanabe and Shimura, 1955; Wormser and Pardee, 1958; Flavin and Slaughter, 1960; Schildkraut and Greer, 1973; Skarstedt and Greer, 1973; Datko *et al.* 1974; Schnyder and Rottenberg, 1975; Madison and Thompson,

Figure 2.7. The proposed mechanism of the β,γ-replacement reaction catalyzed by threonine synthase (Laber *et al.* 1994a). **1**, PLP in Schiff base linkage with the active site lysine of AtTS1 (internal aldimine); **2**, transaldimination of PLP with OPHS forming the external aldimine; **3**, quinonoid intermediate of OPHS and PLP; **4**, γ-elimination of phosphate group; **5**, PLP-quinonoid intermediate gains a proton at Cγ; and **6**, formation of L-threonine through the addition of a hydroxyl group at Cβ, and release through reverse transaldimination reaction.

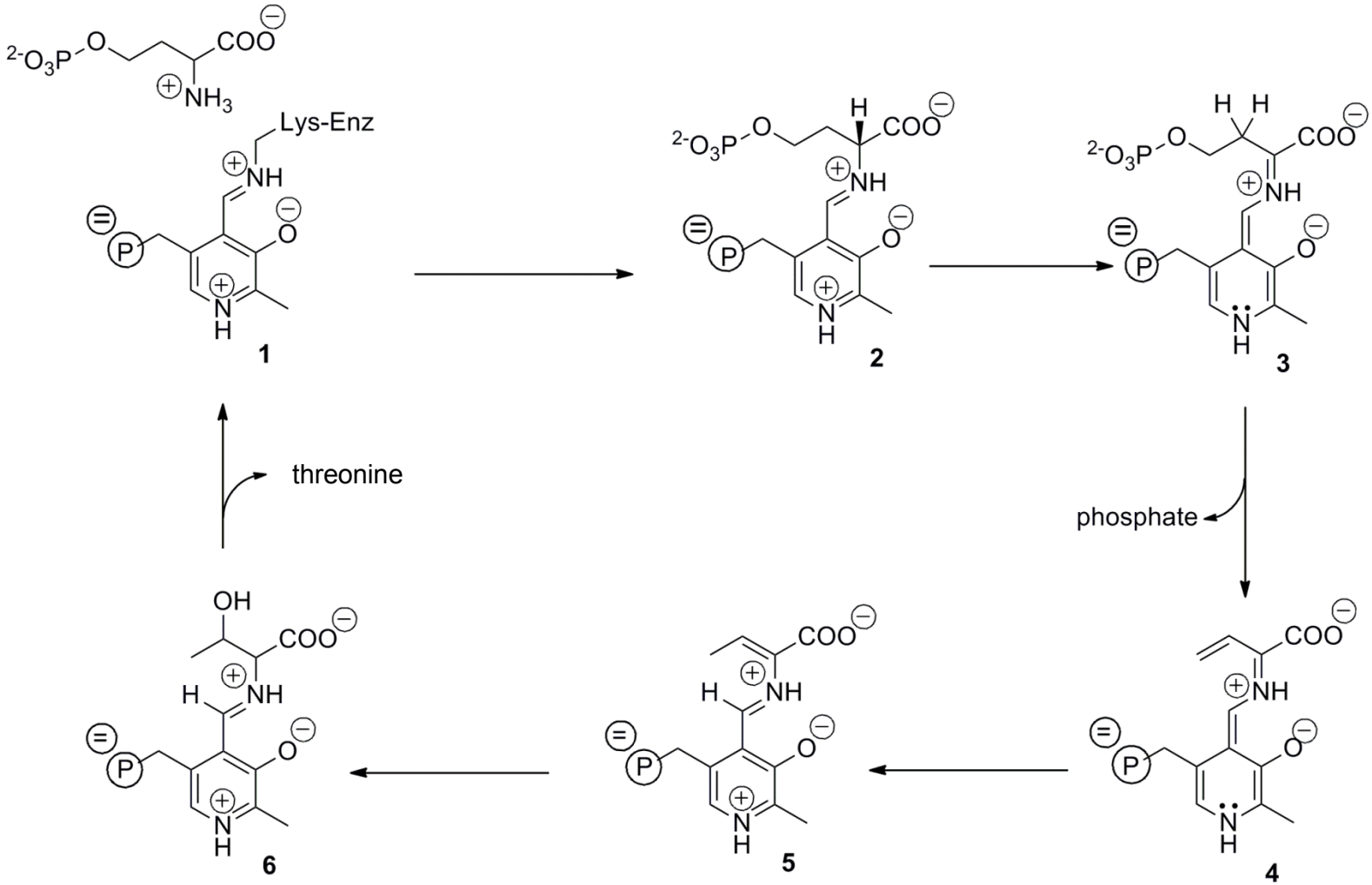
Lys-Enz
threonine
phosphate
1
2
3
4
5
6

1976; Szczesiul and Wampler, 1976; Thoen *et al.* 1978; Giovanelli *et al.* 1984; Farrington *et al.* 1993; Laber *et al.* 1994a; Laber *et al.* 1994b; Ramos and Calderon, 1994; Ravanel *et al.* 1995; Chassagnole *et al.* 2001; Rais *et al.* 2001; Covarrubias *et al.* 2008). The commercial availability of the L-HSer and ATP substrates, combined with the simplicity of the single-step synthesis catalyzed by HSK, provides a method that is accessible to researchers investigating the properties of TS from a biological perspective. Enzymatic synthesis also has the advantage of allowing small amounts of substrate, sufficient for immediate experimental requirements, to be produced quickly, thereby reducing the need for assessment of substrate stability and purity following storage. However, the reported methods for the enzymatic synthesis, and subsequent purification, of OPHS vary and the necessity to accurately quantify the OPHS produced, as well as the type of TS assay to be employed, must be considered when selecting the appropriate synthetic method. The two primary variables in reported methods are the use of crude cell extracts *versus* purified HSK, and the addition of PEP and PK to recycle the ATP substrate of HSK (Watanabe and Shimura, 1955; Wormser and Pardee, 1958; Flavin and Slaughter, 1960; Schildkraut and Greer, 1973; Skarstedt and Greer, 1973; Datko *et al.* 1974; Madison and Thompson, 1976; Szczesiul and Wampler, 1976; Thoen *et al.* 1978; Giovanelli *et al.* 1984; Farrington *et al.* 1993; Laber *et al.* 1994a; Laber *et al.* 1994b; Ramos and Calderon, 1994; Ravanel *et al.* 1995; Chassagnole *et al.* 2001; Rais *et al.* 2001). Modern recombinant methods now enable the use of affinity tags, thereby obviating the need for complex purifications and increasing the accessibility of enzymes for the synthesis of a variety of compounds, including substrates. The addition of a carboxy-

terminal, 6-His, affinity tag to eHSK was shown to have negligible effect on the kinetic parameters of the enzyme, demonstrating that it is suitable for use in the preparation of the OPHS substrate of TS. Although synthesis of OPHS from equimolar amounts of L-HSer and ATP is the simplest enzymatic method, requiring only HSK, the difficulty of separating the ADP and OPHS products can result in overestimation of the concentration of the latter when using the malachite green assay, commonly employed for this purpose, which measures free phosphate and requires that the sample be treated with CIAP to release the phosphate moiety. To circumvent this problem PEP and PK were added to the HSK reaction mixture, as described by Laber and colleagues, to recycle the ADP product to ATP, and the ATP concentration was further reduced from 5 to 1 mM (Laber *et al.* 1994a; Laber *et al.* 1994b). The OPHS product was subsequently purified by ion exchange chromatography, to separate it from the pyruvate product of PK and concentrated to 25-30 mM for use in eTS assays.

Previous investigations of plant and bacterial TS have relied on four end-point assays: (1) detection of the phosphate product *via* a colorimetric method, such as malachite green (Watanabe and Shimura, 1955; Wormser and Pardee, 1958; Szczesiul and Wampler, 1976; Farrington *et al.* 1993; Laber *et al.* 1994a; Laber *et al.* 1994b; Laber *et al.* 1999; Chassagnole *et al.* 2001; Rais *et al.* 2001; Covarrubias *et al.* 2008); (2) separation and quantification of the L-Thr product *via* HPLC (Ramos and Calderon, 1994; Curien *et al.* 1998; Murakawa *et al.* 2011); (3) use of a radioactive tracer with subsequent separation of the OPHS substrate and L-Thr product by TLC and quantification of the latter by scintillation counting (Madison and Thompson,

1976; Thoen *et al.* 1978) and (4) measurement of the L-Thr product *via* periodate oxidation (Flavin and Slaughter, 1960; Schildkraut and Greer, 1973). The eTD_{L447F}/HO-HxoDH continuous assay described here will facilitate the study of TS by reducing sample handling and eliminating the need for separation of substrates and products or for the use of radioactive tracers in routine applications. A continuous assay also enhances data quality by allowing the collection of larger data sets and ensuring that measurements of initial velocity are not underestimated, thereby resulting in a reduced k_{cat} value, by mis-selection of sampling time points in endpoint assays. A further advantage is that L-Thr is processed by the coupling enzymes, thereby mimicking steady-state cellular conditions and preventing the overestimation of K_m^{OPHS}, as the OPHS substrate and L-Thr product of TS bind to the same enzyme form.

The continuous TS assay described in the current study employs two coupling enzymes, eTD_{L447F} and HO-HxoDH, and monitors the production of L-Thr *via* a decrease in absorbance at 340 nm as α-KB, the product of L-Thr deamination by eTD_{L447F}, is reduced by HO-HxoDH with the concomitant oxidation of NADH. A continuous method for studying the flux of OPHS, the branch-point metabolite between the L-Thr and L-Met biosynthetic pathways of *A. thaliana,* has been described, in which TS was coupled with TD and LDH (Curien *et al.* 2003). However, the TD/LDH system employed to simulate and monitor metabolic flux was not optimized for the determination of TS kinetic parameters and although these enzymes provided a useful method to mimic metabolic flux, they are not optimal for the development of a continuous TS assay. The enzyme HO-HxoDH is a more

appropriate selection than LDH for this purpose because the catalytic efficiency of the latter for α-KB ($k_{cat}/K_m^{\alpha\text{-KB}}$ = 1.8 x 10^3 M^{-1} s^{-1}) is an order of magnitude lower than that of HO-HxoDH (Table 2.2) (Aitken *et al.* 2003). Additionally, the wild-type eTD enzyme is not suitable because it displays a sigmoidal response to substrate at L-Thr concentrations in the micromolar to low-millimolar range, a factor that limits its usefulness as a coupling enzyme, as maximal responsiveness to the product of the target enzyme, L-Thr in the case of TS, is required for an effective continuous assay. In contrast, the L447F site-directed variant of this enzyme exhibits Michaelis-Menten behavior (Eisenstein *et al.* 1995). Therefore, the eTD_{L447F}/HO-HxoDH assay described in this paper is well suited to the measurement of TS activity. The close agreement between the kinetic parameters of both coupling enzymes (Table 2.2) and the reported values demonstrate that the addition of a 6-His, affinity tag, to facilitate purification of the coupling enzymes, is well tolerated and does not affect their use for the continuous TS assay. In order to validate this assay, the kinetic parameters of eTS obtained (Table 2.2) were compared to those previously reported. The K_m^{OPHS} of 0.34 mM and the k_{cat} of 4 s^{-1} determined are within 2-fold of the reported values of 0.5 mM and 7.3 s^{-1}, respectively, and the k_{cat}/K_m^{OPHS} of 1.2 x 10^4 M^{-1} s^{-1} is almost within experimental error of the value of 1.5 x 10^4 M^{-1} s^{-1}, obtained using the standard malachite green assay (Laber *et al.* 1994a). This comparison demonstrates the effectiveness of the eTD_{L447F}/HO-HxoDH assay and that the addition of the C-terminal 6-His tag does not alter the kinetic parameters of eTS. The slight reduction in the K_m^{OPHS} value of eTS reported here may result from the relief of product inhibition by the eTD_{L447F}/HO-HxoDH coupled assay.

The eTD_{L447F}/HO-HxoDH assay was optimized at pH 8 to enable comparison to reported kinetic parameters for eTS, as this enzyme has been found to display maximal activity between pH 8-8.5 (Sczcesiul and Wampler, 1976; Laber *et al.* 1994a; Laber *et al.* 1994b). The effect of pH on the kinetic parameters of eTD_{L447F} and HO-HxoDH was also determined in order to estimate the concentration of each enzyme required under a range of TS assay conditions. The concentrations of the coupling enzymes determined using equations 2.6 and 2.7 were within 5-fold of the experimentally determined values, thereby facilitating the optimization of TS assay conditions (Figure 2.4). The pH profiles of the coupling enzymes determined in this study will facilitate the optimization of this assay to study TS from other species, which may have distinct pH optima. The effect of pH on the activity of HO-HxoDH has not been previously reported. However, the pH optimum of $\leq$6.5 determined for HO-HxoDH is consistent with the observation that many enzymes from *L. delbrueckii* display optimal activity in the pH range of 5.5-6.8 (Laloi *et al.* 1991; Bockelmann *et al.* 1995; Bourniquel *et al.* 2002).

The continuous, coupled-coupled eTS assay and optimized method for synthesis of the OPHS substrate described in this study provide tools for the investigation of TS, a significant target for biotechnological applications. The kinetic parameters determined using this continuous assay are in agreement with those previously reported using the malachite green end-point assay (Laber *et al.* 1994a), demonstrating the effectiveness of the continuous assay. Furthermore, the effect of pH on each of the enzymes was observed in order to establish this assay as suitable for studying TS from a variety of plant and microbial species. The use of this assay

in measuring plant TS activity will provide the in-depth knowledge of kinetic and regulatory properties of the enzyme necessary for manipulation of the threonine and methionine biosynthetic pathways.

Chapter 3: Identification of Cystathionine γ-Synthase and Threonine Synthase from *Cicer arietinum* and *Lens culinaris*

3.1. Abstract

In plants, cystathionine γ-synthase (CGS) and threonine synthase (TS) compete for the branch-point metabolite *O*-phospho-L-homoserine (OPHS). These enzymes are potential targets for metabolic engineering studies, aiming to alter the flux through the competing methionine and threonine biosynthetic pathways, with the goal of increasing methionine production. Although CGS and TS have been characterized in the model organisms *Escherichia coli* and *Arabidopsis thaliana*, little information is available on these enzymes in other, particularly plant, species. The functional CGS and TS coding sequences from the grain legumes *Cicer arietinum* (chickpea) and *Lens culinaris* (lentil) identified in this study share approximately 80% amino acid sequence identity with the corresponding sequences from *Glycine max*. At least seven active-site residues of grain legume CGS and TS are conserved in the model bacterial enzymes, including the catalytic base. Putative processing sites that remove the targeting sequence and result in functional TS were identified in the target species.

3.2. Introduction

Grain legumes, such as chickpea (*Cicer arietinum*) and lentil (*Lens culinaris*), provide approximately 10% of the world's supply of dietary protein (Alliance grain traders 2011). However, chickpea and lentil are deficient in the essential amino acid methionine, according to the requirements for human nutrition, containing 1.3% and 0.8% methionine, respectively, rather than the 3-5% recommended for daily intake (Galili and Hofgen 2002; Mandal and Mandal 2000; Tabe and Higgins 1998). Since these crops are major contributors to vegetarian diets, and with current trends in population growth, improving the nutritional quality of grain legumes is an area of active research in crop biotechnology.

Plants and bacteria synthesize methionine *de novo*. In plants, the amino acid backbone, the sulfur atom and the ε-methyl group of methionine (L-Met) are derived from aspartate (L-Asp), *via* *O*-phospho-L-homoserine (OPHS), the thiol group of cysteine, *via* the transsulfuration pathway, and the β-carbon of serine, *via* methionine synthase, respectively (Ravanel *et al.* 1998b). The branch-point between the L-Met and threonine (L-Thr) biosynthetic pathways is occupied by OPHS in plants. The first committed step of L-Met biosynthesis is catalyzed by cystathionine γ-synthase (CGS), which condenses OPHS and cysteine (L-Cys) to form cystathionine, *via* a γ-replacement mechanism, displacing the phosphate group of OPHS by the thiol of L-Cys. Threonine synthase (TS) catalyzes the β,γ-rearrangement of OPHS, with the release of phosphate, to produce L-Thr. *S*-adenosyl-L-methionine (SAM), a direct metabolite of L-Met, regulates the flux of OPHS between the L-Met and L-Thr biosynthetic pathways by diminishing the translation of the CGS transcript and

allosterically activating TS (Hacham *et al.* 2002; Chiba *et al.* 2003; Curien *et al.* 1998; Mas-Droux *et al.* 2006).

Altering the flux at the OPHS branch-point is an attractive strategy to increase the level of L-Met in grain legumes. However, the available research indicates the results of altering the expression, activity and/or regulation of CGS and TS can vary from species to species, making it essential to study these enzymes in the targeted species. For example, expression of *A. thaliana* CGS (AtCGS) under the CaMV-35S promoter in *A. thaliana* led to an 8- to 15-fold increase in L-Met accumulation, but expression of *Solanum tuberosum* (potato) CGS, under the control of the same promoter, did not alter L-Met accumulation in potato (Gakiere *et al.* 2002; Kreft *et al.* 2003). Similarly, although the anti-sense expression of *A. thaliana* TS (AtTS) under the CaMV-35S promoter in *A. thaliana* resulted in 17- to 47-fold increase in L-Met, the transgenic plants produced infertile seeds, while the same strategy resulted in 2- to 240-fold increase in L-Met in potato that was correlated with a reduction in the above-ground biomass (Avraham and Amir 2005; Zeh *et al.* 2001).

This study reports the isolation and sequence characteristics of functional chickpea and lentil CGS and TS. Subsequent studies on these enzymes will complement the available research on the flux through the OPHS branch-point by expanding the number of plant species for which CGS and TS have been characterized.

3.3. Methods and Materials

3.3.1. Materials

Isopropyl-β-D-thiogalactopyranoside (IPTG), rifampicin, kanamycin, and gentamicin were purchased from BioShop; ampicillin, L-Met, and L-Thr from Fisher Scientific; and spectinomycin from Sigma-Aldrich. All enzymes were obtained from New England Biolabs, oligonucleotide primers were synthesized by Integrated DNA Technologies and coding sequences were sequenced by BioBasic. The Δ*thrC*724(del)::kan *E. coli* strain JW0003-2 was obtained from The Coli Genetic Stock Center.

3.3.2. Amplification of CGS and TS coding sequences.

Total RNA was extracted from *A. thaliana*, chickpea and lentil young leaf tissue using the RNeasy mini kit (Qiagen), with the DNaseI treatment, and cDNA was synthesized from 1 μg of RNA using an oligo(dT_{18}) primer and 200 U M-MuLV reverse transcriptase (NEB). Degenerate oligonucleotide primers were employed to amplify portions of the coding regions of *CGS* and *TS* from the chickpea and lentil cDNA. Degenerate primers for *CGS* and *TS* amplification were designed within conserved regions, based on multiple sequence alignments of the coding sequences of *Glycine max* (*GmCGS*; Accession number AF141602), *A. thaliana* (*AtCGS*; Acc. no. AF039206), and *Fragaria ananassa* (*FaCGS*; Acc. no. FVAJ1451) for *CGS*, and *G. max* (*GmTS*; Acc. no. DQ275353), *Medicago truncatula* (*MtTS*; Acc. no. AY560919), *S. tuberosum* (*StTS*; Acc. no. AF082894), and *A. thaliana* (*AtTS1*; Acc. no. AB027151) for *TS*. The sequences of the resulting amplicons were used to design

species-specific primers to amplify the 5' end of the coding sequence *via* the GenomeWalker Universal kit (Clontech), and the 3'-end of the coding sequence *via* an oligo-dT_{18} adapter primer (GTC GGA TCC ACC TCC AGA TCG TTT TTT TTT TTT TTT TTT). Genomic DNA for genome walking was isolated from chickpea and lentil leaf tissue using the DNeasy mini kit (Qiagen), and was digested with *EcoR*V, *Hpa*I, *Dra*I, and *Sca*I (NEB).

Sequences encoding the full length and mature (lacking the plastid targeting sequence) transcripts of *A. thaliana*, chickpea and lentil *CGS* and *TS* were amplified from cDNA and inserted into the pTrc-99a2 expression vector (Farsi *et al.* 2009) using the primers in Table 3.1. A silent mutation was introduced into *AtTS2* to remove the internal *Nde*I site, facilitating insertion into pTrc-99a2.

3.3.3. Complementation of L-Met and L-Thr auxotrophic E. coli strains

The functional identity of the putative *CGS* and *TS* coding sequences was confirmed by complementation of L-Met and L-Thr auxotrophic *E. coli* strains lacking the *metB* and *thrC* coding sequences, respectively. The plant sequences were placed under the control of the IPTG-inducible *trc* promoter in the pTrc-99a2 vector. Full-length and mature CGS and TS coding sequences from *A. thaliana,* chickpea and lentil were transformed into *ΔmetB* (*metB*::*aadA*, ER1821) and *ΔthrC* (thrC724(del)::kan, JW0003-2) strains of *E. coli*, respectively (Farsi *et al.* 2009; Baba *et al.* 2006). Cultures (10 mL) grown at 37^{o}C for 16 h were harvested, washed three times with 1 mL of sterile 0.85% NaCl, and plated on M9 minimal media (20% dextrose, M9 salts, 1 mM $MgCl_2$) containing 1.5% agar (w/v), 100 μg/ml of

Table 3.1. Primers used to amplify full-length and mature CGS and TS[a]

Primer name	Primer sequence (5' – 3')
*CaCGS*F	ATGGCCGTTTCAAGTTTCCACCGC
*Ca*mat*CGS*F	ATGCAACTCAGCACCAAAGCTCGTCGT
*CaCGS*R	CTATATGGCTTCGAGAGCTTGCAGG
*LcCGS*F	ATGGCCGTTTCAAGCCTCCACCGTG
*Lc*mat*CGS*F	ATGCAGCGTCAGCTAAGCACTAAAGCTCG
*LcCGS*R	CTATATGACTTCCAGTGCCTGCACG
*CaTS*F	ATGGCGGTGTCTTCTCTGT
*Ca*mat*TS*F	ATGGACAACATCAAAGATAAAGC
*CaTS*R	CTACTTTGGGGTCTTACTC
*LcTS*F	ATGTCTTCTTCAACAACAAC
*Lc*mat*TS*F	ATGGAAAACATCCGCGACGAAG
*LcTS*R	CTAATGATACTTGGGTGCCT
*At*mat*TS1*F	ATGGATAACATTCGAGATGAGGC
*AtTS1*R	CTAAAAGTTTTCAAA
*At*mat*TS2*F	ATGATTCGAGACGAAGCTC
*AtTS2*R	TTATTTATCATTGCTCTTC
AtTS2-H339H-F[b]	CAAAGGGTTTCACATGTGTAAAGAG
AtTS2-H339H-R[b]	CTCTTTACACATGTGAAACCCTTTG

[a]Primers used to amplify the full-length and mature (mat) *CGS* and *TS* coding sequences from *A. thaliana* (*At*), *C arietinum* (*Ca*) and *L. culinaris* (*Lc*).
[b]Primers used in the site-directed mutagenesis of AtTS2 to remove the internal *Nde*I site.

ampicillin, 50 μg/ml of kanamycin and 1 mg/mL uracil (*thrC*724(del)::kan strain) or 50 μg/ml spectinomycin and 1 mg/mL thiamine (*metB*::*aadA* strain), in the presence of 1 mM IPTG, 75 μg/mL L-Met, or 75 μg/mL L-Thr (*thrC*724(del)::kan only). Cells were incubated at 30°C for 48 hrs.

3.3.4. Binary plasmid construction and intracellular localization

The plastid targeting sequences of *TS* from *A. thaliana*, chickpea and lentil were transferred from the pTrC-99a2 expression constructs to the pVKH18 vector, immediately 5' of the coding sequence of green fluorescent protein (GFP), expressed under the control of the CaMV-35S promoter (Sparkes *et al.* 2006). Constructs were transformed into *Agrobacterium tumefaciens* (C58C GV3101 pMP90 RK) by electroporation (2.5 kV, 25 μF, and 400 Ω for 9 secs) and, following incubation at 28°C for 3 hrs, were plated on LB media containing 1.5% agar, 50 μg/mL kanamycin, 100 μg/mL rifampicin, and 40 μg/mL gentamicin. Transient expression of GFP, and the transit peptide-GFP fusion constructs, in *Nicotiana tabacum* epidermal cells was completed as described by Sparkes *et al.* (2006). Three days after infiltration, *N. tabacum* leaf samples were excised and GFP expression was imaged using confocal laser scanning microscopy (CLSM) with a Zeiss LSM 510 Meta using a Plan Apochromat 63x objective (Carl Zeiss MicroImaging, Inc.). Samples were excited with a 488 nm argon laser and emission was recorded at 505 nm for GFP and 650 nm for chlorophyll autofluorescence.

3.4. Results

One strategy to alleviate the dietary deficiency of L-Met in grain legumes is to alter the flux through the OPHS branch-point, between the competing L-Met and L-Thr biosynthetic pathways, by manipulating the expression of the competing enzymes, CGS and TS. Available research demonstrates that the result of modifying the expression of these key enzymes of primary metabolism is species dependent, thereby suggesting that additional knowledge of CGS and TS from a range of plant species is required to understand the regulation of flux at the OPHS branch-point, particularly in the target grain legumes. This study describes the isolation of functional CGS and TS coding sequences from the grain legumes chickpea and lentil, as a necessary step to provide the starting point for research in these important crop species.

3.4.1. CGS

The *CaCGS* and *LcCGS* transcripts have open reading frames (ORF) of approximately 1600 bp and encode proteins of approximately 58 kDa that share 85% and 81% amino acid sequence identity, respectively, with GmCGS (Acc. no. AF141602). Both CGS amino acid sequences contain the pyridoxal 5'-phosphate (PLP) binding motif, including the active-site lysine residue (CaCGS-K350 and LcCGS-K351). Characteristic of the plant CGS enzymes studied to date, both CaCGS and LcCGS possess an N-terminal extension that is not present in bacterial CGS. This segment includes a plastid targeting peptide and the regulatory MTO region (Chiba *et al.* 1999; Ominato *et al*, 2002; Ravanel *et al*, 1998b). The MTO

region consists of 11 residues (R77-V89 in AtCGS) and is common to CGS from plant species. The MTO regions of CaCGS (R66-V78) and LcCGS (R68-V80) share 100% identity with that of AtCGS and GmCGS.

The ability of CaCGS and LcCGS to complement the methionine auxotrophy of the ER1821Δ*metB* *E. coli* strain, deficient in *E. coli* CGS (eCGS), was investigated. The Δ*metB* strain containing the empty pTrc-99a2 vector produced colonies only on media supplemented with L-Met (Table 3.2). The wild-type eCGS coding sequence, under the control of the *trc* promoter of pTrc-99a2, complemented the ER1821Δ*metB* cells only in the absence of IPTG (Table 3.2), an observation also reported by Farsi *et al.* (2009). In contrast, complementation of the Δ*metB* strain was observed for both the full-length and mature forms of CaCGS, LcCGS, and AtCGS only in the presence of IPTG (Table 3.2).

3.4.2. TS

The *AtTS2, CaTS* and *LcTS* transcripts contain ORFs of 1551, 1569 and 1614 bp, encoding 57, 57 and 59-kDa proteins, respectively. The resulting protein sequences share 75%, 82% and 77% amino acid sequence identity, respectively, with GmTS (Acc. no. DQ275353) (Figure 3.1). Analysis of the amino acid sequences reveals the signature PLP-binding motif, including the characteristic active-site lysine residue AtTS2-K194, CaTS-K200 and LcTS-K212. The SAM-binding region identified in AtTS1 is also present in the N-terminal region of the TS enzymes examined in this study (AtTS2: V127-G185, CaTS: V133-G192, and LcTS: V145-

Table 3.2. Complementation of L-Met and L-Thr auxotrophic *E. coli* strains by full-length and mature CGS and TS, respectively, from *A. thaliana*, *C. arietinum*, *L. culinaris*, and *E. coli*.[a]

	With IPTG			No IPTG	
	M9			M9 + Met	M9
AtCGS	●			●	○
matAtCGS	●			●	○
CaCGS	●			●	○
matCaCGS	●			●	○
LcCGS	●			●	○
matLcCGS	●			●	○
eCGS	○			●	●
Δ*metB* cells	○			●	○
pTrc-99a2 vector	○			●	○
	M9 + Thr	M9 + Met (-Thr)	M9	M9 + Thr	M9
AtTS1	●	●	●	●	○
matAtTS1	●	●	●	●	○
AtTS2	●	●	○	●	○
matAtTS2	●	●	●	●	○
CaTS	●	●	●	●	○
matCaTS	●	●	●	●	○
LcTS	●	●	●	●	○
matLcTS	●	●	●	●	○
eTS	○	○	○	●	●
Δ*thrC* cells	●	○	○	●	○
pTrc-99a2 vector	●	○	○	●	○

[a]Closed (●) and opened circles (○) indicate strong growth and no growth, respectively. Δ*metB*::aadA, ER1821 (Farsi *et al.* 2009) cells were grown at 30°C for 48 hrs on M9 minimal media containing 100 μg/mL ampicillin, 50 μg/mL spectinomycin, 100 μg/mL thiamine, and supplemented with 1 mM IPTG or 75 μg/mL L-Met. *thrC*724(del)::kan, JW0003-2 cells were grown at 30°C for 48 hrs on M9 minimal media containing 100 μg/mL ampicillin, 50 μg/mL kanamycin, 100 μg/mL uracil, and supplemented with 1 mM IPTG, 75 μg/mL L-Thr or 75 μg/mL L-Met.

Figure 3.1. Amino acid sequence alignment of AtTS1 (AB027151), AtTS2 (NM_105939), CaTS, LcTS, and GmTS (DQ275353.1). The residues responsible for interactions with SAM and PLP are shown in white font in the black and gray boxes, respectively. Leu204, responsible for the *mto2-1* methionine overaccumulating mutant, is underlined. Markings below the amino acid sequences denote fully conserved (*), strongly conserved (**:**), and weakly conserved (**.**) residues.

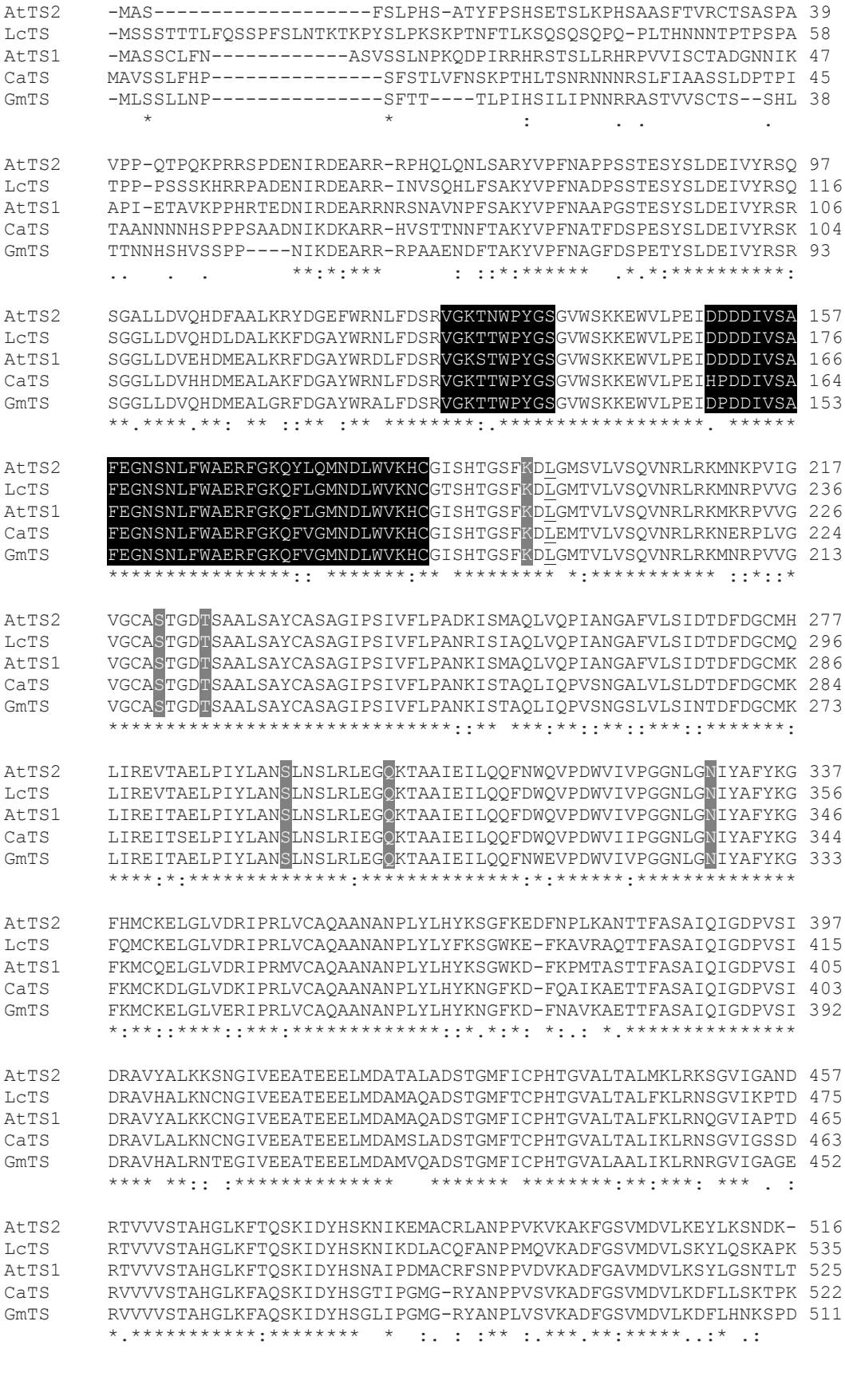
AtTS2 -MAS----------FSLPHS-ATYFPSHSETSLKPHSAASFTVRCTSASPA 39
LcTS -MSSSTTTLFQSSPFSLNTKTKPYSLPKSKPTNFTLKSQSQSQPQ-PLTHNNNTPTPSPA 58
AtTS1 -MASSCLFN----------ASVSSLNPKQDPIRRHRSTSLLRHRPVVISCTADGNNIK 47
CaTS MAVSSLFHP----------SFSTLVFNSKPTHLTSNRNNNRSLFIAASSLDPTPI 45
GmTS -MLSSLLNP----------SFTT----TLPIHSILIPNNRRASTVVSCTS--SHL 38
AtTS2 VPP-QTPQKPRRSPDENIRDEARR-RPHQLQNLSARYVPFNAPPSSTESYSLDEIVYRSQ 97
LcTS TPP-PSSSKHRRPADENIRDEARR-INVSQHLFSAKYVPFNADPSSTESYSLDEIVYRSQ 116
AtTS1 API-ETAVKPPHRTEDNIRDEARRNRSNAVNPFSAKYVPFNAAPGSTESYSLDEIVYRSR 106
CaTS TAANNNNHSPPPSAADNIKDKARR-HVSTTNNFTAKYVPFNATFDSPESYSLDEIVYRSK 104
GmTS TTNNHSHVSSPP----NIKDEARR-RPAAENDFTAKYVPFNAGFDSPETYSLDEIVYRSR 93
AtTS2 SGALLDVQHDFAALKRYDGEFWRNLFDSRVGKTNWPYGSGVWSKKEWVLPEIDDDDIVSA 157
LcTS SGGLLDVQHDLDALKKFDGAYWRNLFDSRVGKTTWPYGSGVWSKKEWVLPEIDDDDIVSA 176
AtTS1 SGGLLDVEHDMEALKRFDGAYWRDLFDSRVGKSTWPYGSGVWSKKEWVLPEIDDDDIVSA 166
CaTS SGGLLDVHHDMEALAKFDGAYWRNLFDSRVGKTTWPYGSGVWSKKEWVLPEIHPDDIVSA 164
GmTS SGGLLDVQHDMEALGRFDGAYWRALFDSRVGKTTWPYGSGVWSKKEWVLPEIDPDDIVSA 153
AtTS2 FEGNSNLFWAERFGKQYLQMNDLWVKHCGISHTGSFKDLGMSVLVSQVNRLRKMNKPVIG 217
LcTS FEGNSNLFWAERFGKQFLGMNDLWVKNCGTSHTGSFKDLGMTVLVSQVNRLRKMNRPVVG 236
AtTS1 FEGNSNLFWAERFGKQFLGMNDLWVKHCGISHTGSFKDLGMTVLVSQVNRLRKMKRPVVG 226
CaTS FEGNSNLFWAERFGKQFVGMNDLWVKHCGISHTGSFKDLEMTVLVSQVNRLRKNERPLVG 224
GmTS FEGNSNLFWAERFGKQFVGMNDLWVKHCGISHTGSFKDLGMTVLVSQVNRLRKMNRPVVG 213
AtTS2 VGCASTGDTSAALSAYCASAGIPSIVFLPADKISMAQLVQPIANGAFVLSIDTDFDGCMH 277
LcTS VGCASTGDTSAALSAYCASAGIPSIVFLPANRISIAQLVQPIANGAFVLSIDTDFDGCMQ 296
AtTS1 VGCASTGDTSAALSAYCASAGIPSIVFLPANKISMAQLVQPIANGAFVLSIDTDFDGCMK 286
CaTS VGCASTGDTSAALSAYCASAGIPSIVFLPANKISTAQLIQPVSNGALVLSLDTDFDGCMK 284
GmTS VGCASTGDTSAALSAYCASAGIPSIVFLPANKISTAQLIQPVSNGSLVLSINTDFDGCMK 273
AtTS2 LIREVTAELPIYLANSLNSLRLEGQKTAAIEILQQFNWQVPDWVIVPGGNLGNIYAFYKG 337
LcTS LIREVTAELPIYLANSLNSLRLEGQKTAAIEILQQFDWQVPDWVIVPGGNLGNIYAFYKG 356
AtTS1 LIREITAELPIYLANSLNSLRLEGQKTAAIEILQQFDWQVPDWVIVPGGNLGNIYAFYKG 346
CaTS LIREITSELPIYLANSLNSLRIEGQKTAAIEILQQFDWQVPDWVIIPGGNLGNIYAFYKG 344
GmTS LIREITAELPIYLANSLNSLRLEGQKTAAIEILQQFNWEVPDWVIVPGGNLGNIYAFYKG 333
AtTS2 FHMCKELGLVDRIPRLVCAQAANANPLYLHYKSGFKEDFNPLKANTTFASAIQIGDPVSI 397
LcTS FQMCKELGLVDRIPRLVCAQAANANPLYLYFKSGWKE-FKAVRAQTTFASAIQIGDPVSI 415
AtTS1 FKMCQELGLVDRIPRMVCAQAANANPLYLHYKSGWKD-FKPMTASTTFASAIQIGDPVSI 405
CaTS FKMCKDLGLVDKIPRLVCAQAANANPLYLHYKNGFKD-FQAIKAETTFASAIQIGDPVSI 403
GmTS FKMCKELGLVERIPRLVCAQAANANPLYLHYKNGFKD-FNAVKAETTFASAIQIGDPVSI 392
AtTS2 DRAVYALKKSNGIVEEATEEELMDATALADSTGMFICPHTGVALTALMKLRKSGVIGAND 457
LcTS DRAVHALKNCNGIVEEATEEELMDAMAQADSTGMFTCPHTGVALTALFKLRNSGVIKPTD 475
AtTS1 DRAVYALKKCNGIVEEATEEELMDAMAQADSTGMFICPHTGVALTALFKLRNQGVIAPTD 465
CaTS DRAVLALKNCNGIVEEATEEELMDAMSLADSTGMFTCPHTGVALTALIKLRNSGVIGSSD 463
GmTS DRAVHALRNTEGIVEEATEEELMDAMVQADSTGMFICPHTGVALAALIKLRNRGVIGAGE 452
AtTS2 RTVVVSTAHGLKFTQSKIDYHSKNIKEMACRLANPPVKVKAKFGSVMDVLKEYLKSNDK- 516
LcTS RTVVVSTAHGLKFTQSKIDYHSKNIKDLACQFANPPMQVKADFGSVMDVLSKYLQSKAPK 535
AtTS1 RTVVVSTAHGLKFTQSKIDYHSNAIPDMACRFSNPPVDVKADFGAVMDVLKSYLGSNTLT 525
CaTS RVVVVSTAHGLKFAQSKIDYHSGTIPGMG-RYANPPVSVKADFGSVMDVLKDFLLSKTPK 522
GmTS RVVVVSTAHGLKFAQSKIDYHSGLIPGMG-RYANPLVSVKADFGSVMDVLKDFLHNKSPD 511

G204). In AtTS1, W101 and W150 are responsible for forming a stacking interaction with the adenine ring and stabilizing the L-Met moiety of SAM, respectively (Mas-Droux *et al.* 2006). These two tryptophan residues are conserved in AtTS2 (W132 and W181), CaTS (W139 and W188) and LcTS (W104 and W153).

The junction of the plastid targeting sequence and the mature form of the enzyme is conserved in CGS, but not TS. Therefore, to investigate the plastid-transit capability of the N-terminal region and identify functional truncated TS enzymes, lacking the transit peptide, the putative TS plastid targeting sequences were fused in-frame to GFP in the pVKH18 vector and transiently expressed by infiltration of transformed *A. tumefaciens* (C58C GV3101 pMP90 RK) into tobacco epidermal cells (Sparkes *et al.* 2006). Imaging of the transient expression of GFP by CLSM demonstrated that the N-terminal regions of AtTS2 (M1-N55), CaTS (M1-D61) and LcTS (M1-E73) are sufficient to direct GFP into the chloroplast, as demonstrated by the overlap of the GFP signal in green (λ_{em} = 505 nm) and the autofluorescence of the chloroplast in red (λ_{em} = 650 nm) in Figure 3.2.

The threonine-auxotrophic JW0003-2 *thrC*724(del)::kan strain, deficient in TS activity, was complemented by the full-length and mature coding sequences of AtTS1, AtTS2, CaTS, LcTS and *E. coli* TS (eTS), but not the pTrc-99a2 plasmid (Table 3.2). Growth of the Δ*thrC* cells was observed for eTS only in the absence of IPTG, a trend consistent with eCGS complementation (Farsi *et al.* 2009). In contrast, IPTG enabled complementation by the full-length and mature forms of AtTS1, CaTS and LcTS and the mature form of AtTS2. A unique feature of the full-length AtTS2

Figure 3.2. Expression of fluorescent fusion proteins in epidermal cells of *Nicotiana tabacum*. (A) empty pVKH18 vector and (B) pVKH18 vector containing RUBISCO-GFP fusion construct, respectively, provide controls for the pVKH18 vector containing the GFP-fusions with the signal peptides of (C) AtTS1 (M1-D61), (D) AtTS2 (M1-N55), and (E) CaTS (M1-D61). Photographs were taken in a dark field showing (i) the autofluorescence of chloroplasts (650 nm, red), (ii) GFP (505 nm, green), and (iii) the overlap showing localization of GFP fusion constructs to chloroplasts. CLSM was done with a Zeiss LSM 510 Meta using a Plan Apochromat 63x objective. The scale bars shown in panel (iii) represent 50 μm.

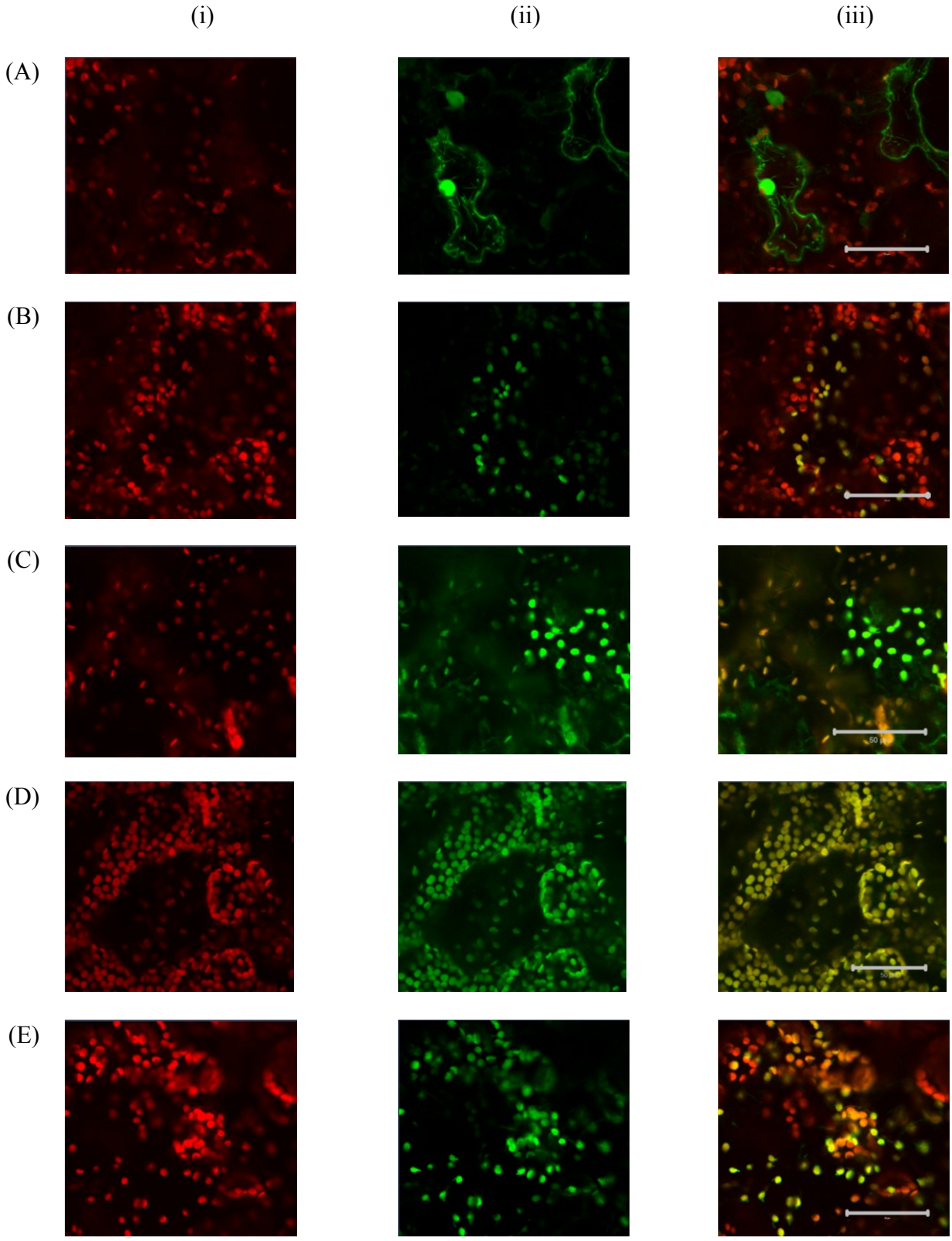
(i)
(ii)
(iii)
(A)
(B)
(C)
(D)
(E)

sequence is the requirement for L-Met supplementation in the growth media for complementation of the *E. coli* Δ*thrC* strain (Table 3.2).

3.5. Discussion

A 3-fold increase in accumulation would be sufficient to alleviate the dietary L-Met deficiency of the seeds of grain legumes such as *C. arietinum* (chickpea) and *L. culinaris* (lentil) (Tabe and Higgins 1998). The enzymes at the OPHS metabolic branch-point, CGS and TS, are targets to improve the nutritional quality of these crop species by increasing the accumulation of L-Met. However, results from previous studies indicate that, as enzymes of primary metabolism, manipulation of CGS and TS expression may produce deleterious phenotypes and/or species-specific changes in L-Met accumulation (Gakiere *et al.* 2002; Kim *et al.* 2002; Kreft *et al.* 2003). For example, transgenic *Medicago sativa* (alfalfa) expressing AtCGS downstream of the rubisco small subunit promoter accumulated up to 32-fold more L-Met than wild-type plants while expressing the same gene under the CaMV-35S promoter in potato did not alter L-Met accumulation (Kim *et al.* 2002; Gakiere *et al.* 2002). Reduction in the expression of TS in *A. thaliana* and potato resulted in a wide range of increased L-Met accumulation, 17- to 47-fold and 2- to 240-fold, respectively, beyond the required 3-fold increase (Avraham and Amir 2005; Zeh *et al.* 2001). Deleterious phenotypes, including reduced growth and yield, have also been reported, particularly when employing the CaMV-35S promoter, as reported for the transgenic *A. thaliana* and potato with reduced TS expression (Avraham and Amir 2005; Zeh *et al.* 2001). Results from previous studies that manipulated the flux of metabolites through the

OPHS branch-point to increase the accumulation of L-Met illustrate the need to study CGS and TS in target plant species to get an acceptable increase in L-Met content.

The *CGS* transcripts amplified from *C. arietinum* (*CaCGS*) and *L. culinaris* (*LcCGS*) encode functional CGS enzymes (Table 3.2) of approximately 58 kDa, consistent with the characterized *A. thaliana* (60 kDa) and *G. max* (58 kDa) CGS (Hughes *et al.* 1999; Ravanel *et al.* 1998a). Both CaCGS and LcCGS contain the PLP-binding motif LGADLXXHSXTKY (Ravanel *et al.* 1998a; Hughes *et al.*1999). Their first exon encodes the conserved chloroplast transit peptide cleavage site (CaCGS-Q58 and LcCGS-Q60) and the MTO region that includes the core RRNCSNIGVAQ sequence that is linked to the post-transcriptional regulation of plant CGS by SAM (Ominato *et al.* 2002; Ravanel *et al.* 1998a). The crystal structure of *N. tabacum* CGS in complex with inhibitors identified three active site residues responsible for binding the distal phosphate group of the OPHS substrate (E107, Y111 and K165) (Steegborn *et al.* 2001). These residues are conserved in plant CGS, including CaCGS (E196, Y200 and K255) and LcCGS (E197, Y201 and K256), but not in bacterial CGS, for which the activated L-homoserine (L-HSer) substrate is *O*-succinyl-L-homoserine (OSHS) not OPHS. The difference in substrates between bacterial and plant CGS may explain the requirement for IPTG in plant CGS complementation studies, as the branch-point between the L-Met and L-Thr biosynthetic pathways is OPHS and L-HSer in plants and bacteria, respectively. The CaCGS and LcCGS sequences share eight conserved active site residues with the structures of NtCGS and *E. coli* CGS (eCGS: D45, Y46, R48, Y101, R106, K198, S326 and R361), including the catalytic base (eCGS-K198, CaCGS-K350 and

LcCGS-K351), which tethers the PLP cofactor by Schiff base linkage, and the serine residue (eCGS-S326, CaCGS-S447 and LcCGS-S478) that guides the ε-amino group of the catalytic base (Clausen *et al.* 1998; Steegborn *et al.* 2001; Jaworski *et al.* 2012). The arginine residues in eCGS (R48, R106 and R361) that are responsible for tethering the distal and α-carboxylate of OSHS are conserved in the active sites of CaCGS (R199, R256, and R512) and LcCGS (R200, R257, and R512) and are likely involved in positioning the corresponding distal phosphate and α-carboxylate groups of the OPHS substrate (Clausen *et al.* 1998; Jaworski *et al.* 2012).

Threonine synthase transcripts amplified from *C. arietinum* (CaTS) and *L. culinaris* (LcTS) encode functional TS enzymes (Table 3.2) of 57 and 59-kDa, respectively, consistent with the 57-kDa AtTS1 (Curien *et al.* 1998). Both sequences contain the allosteric SAM-binding site found in AtTS1 that is conserved in plant TS including CaTS and LcTS but not in *Saccharomyces cerevisiae* TS (yTS) or eTS, which are not allosterically regulated by SAM (Mas-Droux *et al.* 2006). The k_{cat}/K_m^{OPHS} of AtTS1 is increased approximately 87-fold by SAM-binding (Laber *et al.* 1999). Therefore, the requirement for allosteric activation by SAM of the plant TS enzymes and differences in the cellular pools of SAM between plants and *E. coli* may explain their requirement of IPTG for complementation of the Δ*thrC E. coli* cells. This distinguishes them from the native eTS enzyme for which the leaky expression of the *trc* promoter is sufficient. In contrast, the threonine auxotrophic *E. coli* strain is not complemented by eTS in the presence of IPTG, suggesting that the presence of excess functional TS disrupts primary metabolism. The PLP-binding motif , including the active-site lysine residue responsible for Schiff base linkage (CaTS-K200; LcTS-

K212) and the residues that form hydrogen bonds with the phosphate group (CaTS-S229 and CaTS-T233; LcTS-S242 and LcTS-T246), N1 (CaTS-S299; LcTS-S313) and O3' (CaTS-Q308 and CaTS-N337; LcTS-Q321 and LcTS-N350) of PLP are conserved in fungal, bacterial and plant TS including CaTS and LcTS (Mas-Droux *et al.* 2006). Plant TS has an N-terminal extension of approximately 50-60 residues compared to yTS and eTS, which contains the transit peptide and mature start site of the enzyme.

There is little conservation among plant TS sequences at the identified cleavage site, T39, of AtTS1 (Curien *et al.* 1996). The first conserved region in the plant TS, identified through amino acid sequence alignments of all available plant TS sequences begins at AtTS1-D61, AtTS2-N55, CaTS-D61, and LcTS-E73. These residues were used as the truncation sites in this study to confirm the function of both the amino-terminal transit peptide and the truncated enzymes. Complementation of the Δ*thrC E. coli* strain by the truncated coding sequences of AtTS1, AtTS2, CaTS, and LcTS (Table 3.2) demonstrates that these sequences encode functional TS enzymes, suggesting that truncation at this site does not interfere with TS activity. The N-terminal regions of AtTS2 (M1-N55), CaTS (M1-D61) and LcTS (M1-E73) directed GFP into the chloroplasts (Figure 3.1), indicating that this region is sufficient to for plastid targeting of the native enzymes.

AtTS2, identified from analysis of the *A. thaliana* genome, has not been as extensively studied as AtTS1 and has been excluded from L-Asp-derived amino acid branch-point models because it is 120-fold less active than AtTS1 at physiological SAM concentrations (Curien *et al.* 2009). Application of exogenous L-Met, which

may increase the intracellular concentration of SAM, was a unique requirement of full-length AtTS2 for complementation of the Δ*thrC E. coli* strain (Table 3.2), thereby supporting the reported lower activity of AtTS2 compared to AtTS1. However, the mature AtTS2 is functional (Table 3.2) and is likely localized to the chloroplast (Figure 3.1), where L-Thr and L-Met biosynthesis occurs. Therefore, a role in L-Thr biosynthesis for AtTS2 may exist, suggesting that this enzyme should be considered when modeling the OPHS branch-point.

Research focused on manipulating the flux of metabolites through the OPHS branch-point has shown that the effect of altering the expression or regulation of CGS and TS on L-Met accumulation varies depending on the target plant species. The same strategy, such as expressing AtCGS under the CaMV-35S promoter, employed in two different species may yield distinct results (Gakiere *et al.* 2002; Kreft *et al.* 2003). Therefore, characterization of CGS and TS from grain legumes is a necessary prelude to studies aiming to increase the nutritional value of these crops. This study provides a foundation for future research on the activity and regulation of CGS and TS in grain legumes, with the ultimate goal of increasing L-Met content in these important crop plants.

Chapter 4: The steady-state kinetic parameters of Threonine Synthase from *A. thaliana*, *C. arietinum*, and *L. culinaris*

4.1. Abstract

Threonine synthase (TS) catalyses the β,γ-replacement of *O*-phospho-L-homoserine (OPHS), forming L-threonine (L-Thr) and inorganic phosphate. In plants, OPHS occupies the branch-point between the biosynthetic pathways of L-methionine (L-Met) and L-Thr. In this study, TS from *Cicer arietinum* (CaTS) and *Lens culinaris* (LcTS), as well as the two homologues of TS from *Arabidopsis thaliana* (AtTS1 and AtTS2) was recombinantly expressed in *Escherichia coli* and purified. The kinetic parameters of TS were measured in the presence and absence of 100 μM *S*-adenosyl-L-methionine (SAM). The activator increases the k_{cat}/K_m^{OPHS} of CaTS, LcTS, AtTS1, and AtTS2 by 25-, 20-, 80-, and 8.5-fold, respectively. The k_{cat}/K_m^{OPHS} of AtTS2 in the presence of SAM ((1.7 ± 0.1) x 10^3 M^{-1} s^{-1}) is one order of magnitude lower than that of AtTS1. The analysis of AtTS2 flux control into the mathematical reconstruction of the OPHS branch-point model showed that this enzyme is responsible for 14% of the flux of OPHS, and that CGS accounts for 6% of the flux. Therefore AtTS2 should be integrated into the *A. thaliana* branch-point model. In the presence of SAM, the k_{cat}/K_m^{OPHS} of AtTS1 ((2.4 ± 0.30) x 10^4 M^{-1} s^{-1}), *C. arietinum* ((1.5 ± 0.3) x 10^4 M^{-1} s^{-1}) and *L. culinaris* ((1.4 ± 0.2) x 10^4 M^{-1} s^{-1}) are consistent with the reported value for AtTS1. Despite the consistency in the kinetic parameters of pulse and *A. thaliana* TS, the kinetic model of the *A. thaliana* OPHS branch-point may not be an appropriate model of flux in other species due to the difference in the proportion of flux control of AtTS1 (80%) and the estimated values of CaTS (91%) and LcTS (94%).

4.2. Introduction

In plants, the L-homocysteine precursor of the essential amino acid L-methionine (L-Met) is derived from the carbon backbone of L-aspartate (L-Asp), *via* *O*-phospho-L-homoserine (OPHS), and the sulfur moiety of L-cysteine (L-Cys). The first committed step of L-Met biosynthesis is the cystathionine γ-synthase (CGS)-catalyzed condensation of OPHS and L-Cys to form L-cystathionine (Kreft *et al.* 1994). This reaction competes with β,γ-rearrangement of OPHS, to produce threonine (L-Thr), catalyzed by threonine synthase (TS) (Laber *et al.* 1994a). The competition between TS and CGS for OPHS is unique to plants as L-Met is derived from *O*-succinyl-L-homoserine in bacteria. The partitioning of OPHS is regulated by the L-Met-metabolite, *S*-adenosyl-L-methionine (SAM), which post-transcriptionally modulates the stability of the *CGS* mRNA transcript, and allosterically activates the TS enzyme (Curien *et al.* 1996; Chiba *et al.* 1999). The catalytic efficiency of the predominant *A. thaliana* TS isoform (AtTS1) is increased 87-fold in the presence of 100 μM SAM (Laber *et al.* 1999).

L-Met is an essential amino acid used in the synthesis of proteins and for the biosynthesis of L-Cys in animals. Important crop plants such as legumes are deficient in the sulfur-containing amino acids, from the perspective of human nutritional requirement (Tabe and Higgins, 1998). Increasing the production of L-Met, to improve nutritional quality, requires a detailed understanding of the flux between the competing pathways at the OPHS branch-point. Kinetic models reconstruct a metabolic pathway or branch-point based on network, kinetic, and regulatory information (Schallau and Junker, 2010). Therefore, determination of the kinetic

parameters of the relevant enzyme(s), CGS and TS in the case of L-Met, is required to model the effect of genetic engineering on metabolic flux through the competing pathways. This is exemplified by the kinetic model of the L-Asp metabolic pathway from *A. thaliana* created by Curien and coworkers (Curien *et al.* 2009). This model was employed to simulate the effects of increasing SAM concentration from 2-30 μM on the flux of OPHS, as a representation of a similar increase in L-Met levels (Curien *et al.* 2009). The result was a 10-fold reduction in L-Met synthesis, and an approximately 50% reduction in the activity of L-Asp kinase (AK), which is feed-back inhibited by SAM, leading to an overall reduction in L-Asp-derived amino acids (Curien *et al.* 2009). A model of this kind can thus be used to predict how other alterations, such as a 3-fold increase in L-Met flux would affect the overall L-Asp metabolic pathway *in vivo*. The *A. thaliana* model took into consideration different homologues for several enzymes, including L-Asp kinase (AK), dihydrodipicolinate synthase (DHDPS), and homoserine dehydrogenase (HSDH) (Curien *et al.* 2009). The authors recognized that these homologues have distinct effects on metabolic flux due to their different kinetic parameters, and so each homologue must be represented in the model. However, the second homologue of *A. thaliana* TS, AtTS2, was not included in the model because its measured k_{cat} is 120-fold lower than that of AtTS1 at physiological SAM concentrations (20μM), and it was assumed not to be co-located in the chloroplast with AtTS1 and CGS (Curien *et al.* 1996; Curien *et al.* 2009). We have subsequently shown that AtTS2 possesses a functional plastid targeting sequence, suggesting that it should be further characterized and considered in a model of OPHS partitioning in *A. thaliana* (Chapter 3).

The biochemical characterization of TS from a variety of plant species, including *A. thaliana*, *Lemna paucicostata*, *Pisum sativum*, and *Beta vulgaris*, has been reported and inter-species variation is apparent (Madison and Thompson, 1976; Giovanelli *et al.* 1984; Thoen *et al.* 1978; Curien *et al.* 1998; Laber *et al.* 1999). For example, K_m^{OPHS} values of 2.2 mM and 0.67 mM have been reported for *P. sativum* TS in the absence and presence, respectively, of 400 μM SAM, while the corresponding K_m^{OPHS} values of AtTS1, of *A. thaliana*, are 120 μM and 30 μM (Thoen *et al.* 1978; Laber *et al.* 1999). In contrast, the K_m^{OPHS} of CGS from *A. thaliana* and *Spinacia oleraceae* is reported at 2.5 mM and 1.4 mM, respectively, more than one order of magnitude higher than the intraplastidial OPHS concentration of 50-100 μM (Ravanel *et al.* 1995; Ravanel *et al.* 1998b). This indicates the importance of TS in OPHS distribution, and for studies attempting to increase the free L-Met pool *in vivo*, as it accounts for 70-80% of the flux of OPHS under physiological conditions (Curien *et al.* 2003). The inter-species variation in the kinetic parameters of TS and CGS also illustrates the need to develop kinetic models of the OPHS branch point in the species of interest prior to engaging in genetic engineering studies. The creation of a kinetic model of the OPHS branch-point for both *C. arietinum* and *L. culinaris* will enable prediction of effect of interventions on the partitioning of OPHS, and focus *in vivo* studies on those changes less likely to result in a deleterious phenotype.

4.3. Methods

4.3.1. Materials

Pyruvate kinase (PK), L-homoserine (L-HSer), phospho(enol) pyruvate (PEP), adenosine-5'-triphosphate (ATP), ammonium sulfate, β-nicotinamide adenine dinucleotide (NADH), calf intestinal alkaline phosphatase (CIAP), ninhydrin, ammonium molybdate, and Triton X-100 were obtained from Sigma-Aldrich. 4-(2-Hydroxyethyl)-1-piperazineethanesulfonic acid (Hepes), dithiothreitol (DTT), ethylenediaminetetraacetic acid (EDTA), and isopropyl-β-D-thiogalactopyranoside (IPTG) were Fisher Scientific products. Nickel-nitrilotriacetic acid (Ni-NTA) resin was purchased from Qiagen. Toyopearl butyl-650M resin was from TosoHaas. Malachite green and diethylaminoethyl (DEAE)-Sepharose resin were from BDH and GE Healthcare, respectively. The Δ*thrC*724(del)::kan *E. coli* strain JW0003-2 was obtained from The *Escherichia coli* Genetic Stock Center. Synthesis of OPHS and expression and purification of 6-Histidine (6-His) tagged eTD_{L447F} and HO-HxoDH were completed as described in Chapter 3 (Morneau *et al.* 2012).

4.3.2. Purification of wild-type plant TS

Cells of *E. coli* strain JW0003-2 *thrC*724(del)::kan; (Δ*thrC*; Baba *et al.* 2006), expressing wild-type TS from *A. thaliana* (AtTS1 and AtTS2), *C. arietinum* (CaTS), and *L. culinaris* (LcTS), under the *trc* promoter of the pTrc-99a2 expression vector were grown in 4 L Luria-Burtani (LB) broth at 37°C and 200 rpm to mid-log phase (OD_{600} = 0.5) (Farsi *et al.* 2009). The cultures were induced with 150 μM IPTG and incubated for a further 14 h prior to harvesting, *via* centrifugation at 5000 rpm and

4°C. Harvested cells were washed with 0.85% NaCl and resuspended in 35 mL buffer A (50 mM Hepes, pH 7.5, 20μM PLP). The cells were lysed by incubation with 1 mg/mL lysozyme on ice for 20 min followed by repeated (8 x 30 s) cycles of sonication (Vibra Cell sonicator, Sonic and Material, Inc.).

The lysates were centrifuged at 15 000 rpm for 60 min at 4°C (Sorvall RC 6+ centrifuge, Thermo Scientific). Ammonium sulfate was added to the supernatant to 30% saturation (164 g/L) and centrifuged at 17 500 rpm for 75 min. The resulting supernatant was applied to a 2.5 x 10 cm column of Toyopearl butyl-650M resin equilibrated with buffer A containing 30% ammonium sulfate. The column was washed with 250 mL of the same buffer, and the enzyme was eluted with a 500 mL linear gradient of 30% to 0% ammonium sulfate in buffer A. Fractions were tested for TS activity, using the continuous assay described in Chapter 3 (Morneau *et al.* 2012), and for purity, *via* sodium dodecyl sulfate-polyacrylamide gel electrophoresis (SDS-PAGE). The fractions containing TS activity and minimal contaminating proteins were pooled, concentrated, dialyzed against 3 L of buffer A for 16 h, and loaded onto a 2.5 x 10 cm column of DEAE-Sepharose resin. The column was washed with 250 mL buffer A, and the enzyme was eluted with a 500 mL linear gradient of 0 to 500 mM NaCl in buffer A. Fractions were analyzed for activity and purity as described above, and those containing >90% pure TS protein, as assessed by SDS-PAGE, were concentrated and dialyzed against buffer A containing 1 mM EDTA for 16 h prior to the addition of 20% glycerol (v/v) and storage at -80°C.

4.3.3. Construction of expression construct and purification of affinity tagged CaTS

The coding sequence of TS from *C. arietinum* (CaTS) was amplified with CaTS-specific primers to introduce a C-terminal, hexahistidine (6-His) affinity tag: 5' GC CAT *ATG* GCG GTG TCT TCT CTG TT and 5' GCT CTA GAC TAG TGG TGG TGG TGG TGG TGC TTT GGG GTC TTA CTC AAC (restriction sites are underlined, and the ATG start codon is in italics). The 6-His tagged CaTS (CaTS-His) was introduced between the *Nde*I and *Xba*I site of the pTrc99a2 expression vector (Farsi *et al.* 2009) and transformed into *E. coli* strain JW0003-2 *thrC*724(del)::kan (Δ*thrC*; Baba *et al.* 2006).

Cells expressing CaTS-His were grown and harvested as described above. Harvested cells were washed with 0.85% NaCl and resuspended in 35 mL buffer B (50 mM potassium phosphate, pH 7.5, 20 μM PLP). The cells were disrupted by incubation with 1 mg/mL lysozyme on ice for 20 min, followed by sonication (8 cycles, 30 s each). The lysate was loaded onto a 1 x 5 cm column of Ni-NTA resin equilibrated with buffer B. The column was washed in 100 mL buffer B, and the enzyme was eluted with a 200 mL gradient of 0-200 mM imidazole. Fractions containing CaTS-His were analyzed as described above. Fractions were pooled, concentrated, and dialyzed overnight in buffer B containing 1 mM EDTA prior to the addition of 20% glycerol (v/v) and storage at -80°C.

4.3.4. Enzyme Assays

All enzyme assays were performed in a total volume of 200 μL at 25°C and monitored at 340 nm using an Agilent 8453 UV-visible spectrophotometer. The

assay solution was composed of 50 mM Hepes (pH 7.5) containing 20 μM PLP, 0.02-5 mM OPHS, 1.5 mM NADH, eTD_{L447F} (2.5 μM), HO-HxoDH (5.4 μM). The requisite concentrations of the coupling enzymes HO-HxoDH and eTD_{L447F} at pH 7.5 were calculated using equations (2.6) and (2.7), respectively, and were determined to be 13.3 μM and 12.9 μM, respectively. The calculated concentrations were optimized experimentally to 5.4 μM for Ho-HxoDH and 2.5 μM for eTD_{L447F} by independently varying the concentration of each enzyme. The reaction was demonstrated to be linear at TS concentrations ranging from 0.25-2 μM.

A background rate was recorded, and reactions were initiated with the addition of AtTS1 (0.25-0.5 μM), AtTS2 (1 μM), CaTS (0.5 μM), CaTS-His (0.25-0.5 μM), or LcTS (0.25-0.5 μM). For assays containing SAM, the TS enzyme was incubated with 100 μM SAM on ice for 5 min prior to initiation of the reaction. The k_{cat} and K_m^{OPHS} of AtTS1, AtTS2, CaTS, CaTS-His, and LcTS in the presence and absence of SAM were determined by fitting the data to the Michaelis-Menten equation. The k_{cat}/K_m^{OPHS} values were obtained independently using equation (2.1).

4.4. Results

Wild-type TS from *A. thaliana* (AtTS1 and AtTS2), *C. arietinum* (CaTS), *L. culinaris* (LcTS), and CaTS-His were recombinantly expressed in *E. coli*. The wild-type enzymes were purified *via* hydrophobic interaction and anion-exchange chromatography and the 6-His tagged CaTS protein was purified by Ni-NTA affinity chromatography. Their purity was assessed to be >90% by SDS-PAGE (Figure 4.1). The yields of recombinant AtTS1, AtTS2, CaTS, CaTS-His, and LcTS were 39.9, 2.6, 6.4, 8.5, and 6.3 mg per liter of *E. coli* culture, respectively.

Figure 4.1. SDS polyacrylamide gel showing purified recombinant plant TS enzymes. Lanes: **1**, protein molecular weight ladder (Benchmark, Invitrogen); **2**, AtTS1; **3**, AtTS2; **4**, CaTS; **5**, CaTS-His; **6**, LcTS. The 10% polyacrylamide gel was loaded with 2 μg protein per lane and stained with Coomassie brilliant blue.

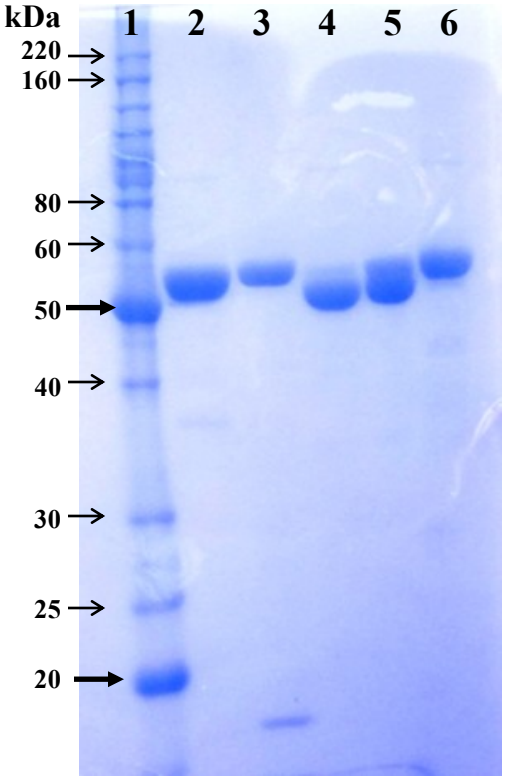
kDa
1
2
3
4
5
6
220
160
80
60
50
40
30
25
20

4.4.1. Kinetic Parameters

The kinetic parameters of AtTS1 were measured in the presence and absence of 100 μM SAM (Figure 4.2; Table 4.1). The presence of 100 μM SAM in the reaction results in an 8.5-fold increase in the k_{cat} of AtTS1, from 0.20 ± 0.04 s^{-1} to 1.7 ± 0.1 s^{-1}. The measured k_{cat}/K_m^{OPHS} of AtTS1 increases 80-fold in the presence of SAM, from (3 ± 1) x 10^2 M^{-1} s^{-1} to (2.4 ± 0.3) x 10^4 M^{-1} s^{-1} (Table 4.1). For CaTS and LcTS, the presence of 100 μM SAM results in a 2.5-fold and 4-fold increase in k_{cat}, respectively, and a 11-fold and 5-fold decrease in K_m^{OPHS}, respectively (Table 4.1; Figure 4.3 A and B). The k_{cat}/K_m^{OPHS} of CaTS increases 25-fold in the presence of SAM, from (6 ± 1) x 10^2 M^{-1} s^{-1} to (1.5 ± 0.3) x 10^4 M^{-1} s^{-1} (Table 4.1). Similarly, the k_{cat}/K_m^{OPHS} of LcTS increases 20-fold, from (7 ± 3) x 10^2 M^{-1} s^{-1} to (1.4 ± 0.2) x 10^4 M^{-1} s^{-1} in the presence of SAM (Table 4.1). The addition of the 6-His tag on the C-terminus of CaTS results in 5-fold and 3-fold increases in K_m^{OPHS} and k_{cat}, respectively, thereby lowering k_{cat}/K_m^{OPHS} 1.4-fold in the presence of 100 μM SAM, compared to wild-type CaTS (Figure 4.4).

The k_{cat} of AtTS2 increases 7-fold with a 1.5-fold decrease in K_m^{OPHS} in the presence of 100 μM SAM (Table 4.1; Figure 4.3C). These changes in kinetic parameters lead to an 8.5-fold increase in the k_{cat}/K_m^{OPHS} value of AtTS2 when 100 μM SAM is added to the reaction (Table 4.1).

Figure 4.2. The dependence of AtTS1 activity on OPHS concentration in the presence (●) and absence (○) of 100 μM SAM. The kinetic parameters are given in Table 4.1. Reaction conditions: 50 mM Hepes (pH 7.5), 1.5 mM NADH, 20 μM PLP, 2.5 μM eTD_{L447F}, 5.4 μM HO-HxoDH, 0.25-0.5 μM AtTS1, and 0.02-5 mM OPHS.

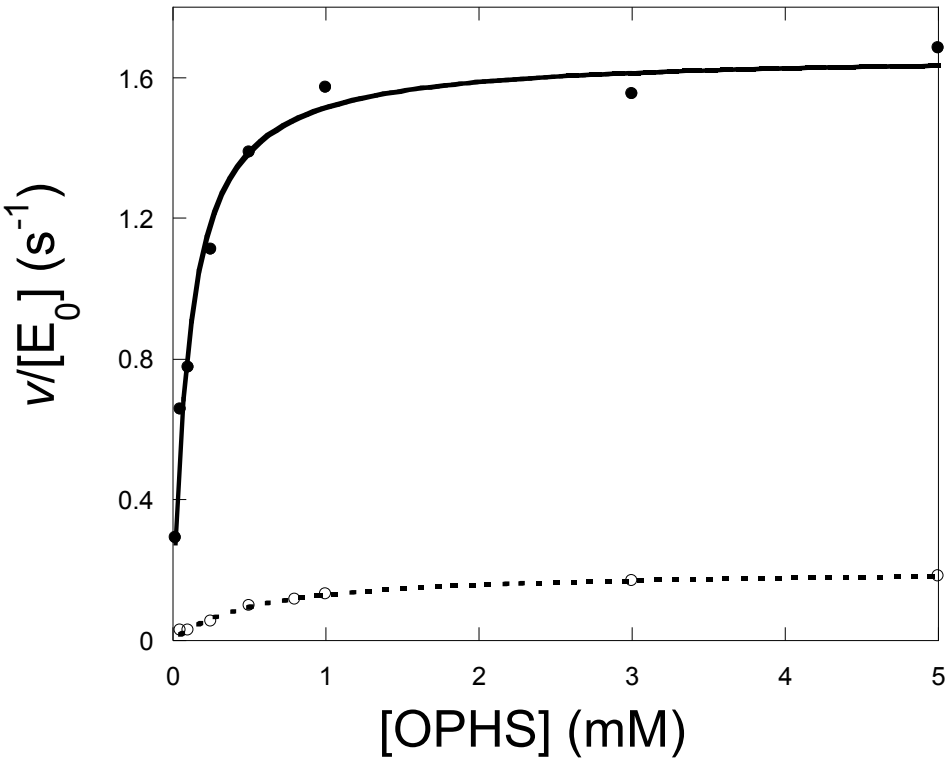
1.6
1.2
0.8
0.4
0
0
1
2
3
4
5
v/[E0] (s-1)
[OPHS] (mM)

Table 4.1. Kinetic parameters of wild-type TS from *A. thaliana*, *C. arietinum* and *L. culinaris* and C-terminally 6-His tagged TS from *C. arietinum* (CaTS-His), in the presence and absence of 100 μM SAM.

TS Construct	K_m^{OPHS} (μM) (100 μM SAM)	K_m^{OPHS} (μM) (no SAM)	k_{cat} (s^{-1}) (100 μM SAM)	k_{cat} (s^{-1}) (no SAM)	k_{cat}/K_m^{OPHS} (M^{-1} s^{-1}) (100 μM SAM)	k_{cat}/K_m^{OPHS} (M^{-1} s^{-1}) (no SAM)
CaTS (WT)	70 ± 20	800 ± 200	1.00 ± 0.04	0.40 ± 0.03	(1.5 ± 0.3) x 10^4	(6 ± 1) x 10^2
CaTS-His	300 ± 30	500 ± 200	2.9 ± 0.1	1.5 ± 0.2	(1.1 ± 0.1) x 10^4	(3 ± 1) x 10^3
LcTS (WT)	100 ± 15	500 ± 250	1.50 ± 0.04	0.35 ± 0.05	(1.4 ± 0.2) x 10^4	(7 ± 3) x 10^2
AtTS2 (WT)	400 ± 30	600 ± 300	0.70 ± 0.01	0.10 ± 0.02	(1.7 ± 0.1) x 10^3	(2.0 ± 0.1) x 10^2
AtTS1 (WT)	70 ± 10	700 ± 500	1.7 ± 0.1	0.20 ± 0.04	(2.4 ± 0.3) x 10^4	(3 ± 1) x 10^2
Reported[a] AtTS1	30	120	0.86	0.04	2.9 x 10^4	3.3 x 10^2

[a]Laber *et al.* 1999

Figure 4.3. The dependence of the activity of CaTS (A), LcTS (B), and AtTS2 (C) on OPHS in the presence (●) and absence (○) of 100 μM SAM. Reaction conditions: 50 mM Hepes (pH 7.5), 1.5 mM NADH, 20 μM PLP, 2.5 μM eTD_{L447F}, 5.4 μM HO-HxoDH, and 0.02-5 mM OPHS. Reactions were initiated with the addition of 0.5 μM CaTS, 0.25-0.5 μM LcTS, or 1 μM AtTS2.

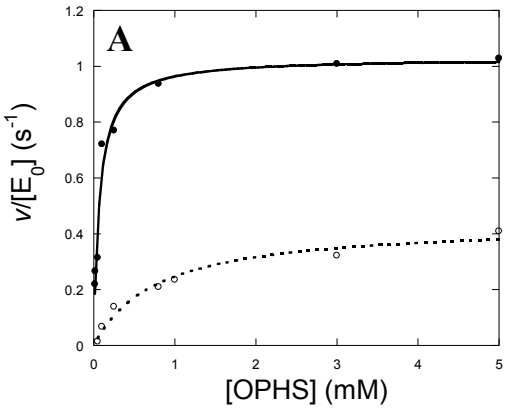
A
v/[E0] (s-1)
[OPHS] (mM)

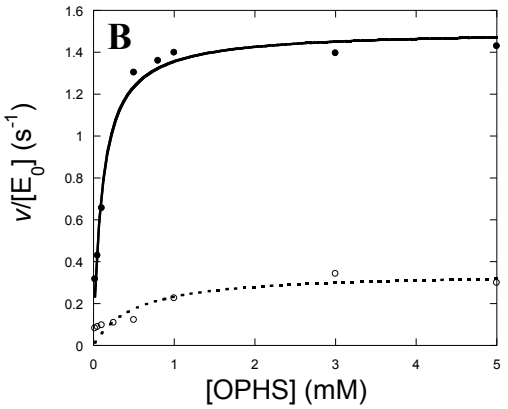
B
v/[E0] (s-1)
[OPHS] (mM)

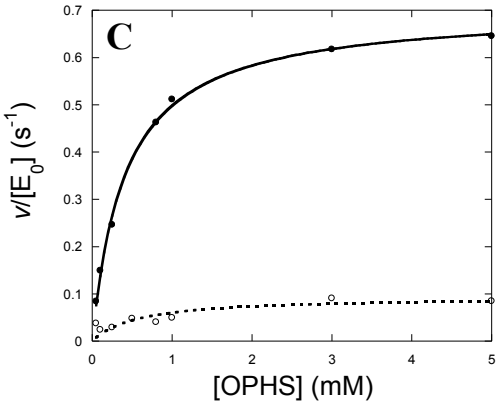
C
v/[E0] (s-1)
[OPHS] (mM)

Figure 4.4. The dependence of the activity of CaTS (●) and CaTS-His (○) on OPHS concentration in the presence (A) or absence (B) of 100 μM SAM. Reaction conditions were 50 mM Hepes (pH 7.5), 1.5 mM NADH, 20 μM PLP, 2.5 μM eTD_{L447F}, 5.4 μM HO-HxoDH, 0.02-5 mM OPHS, and 0.5-1 μM CaTS or 0.25-0.5 μM CaTS-His.

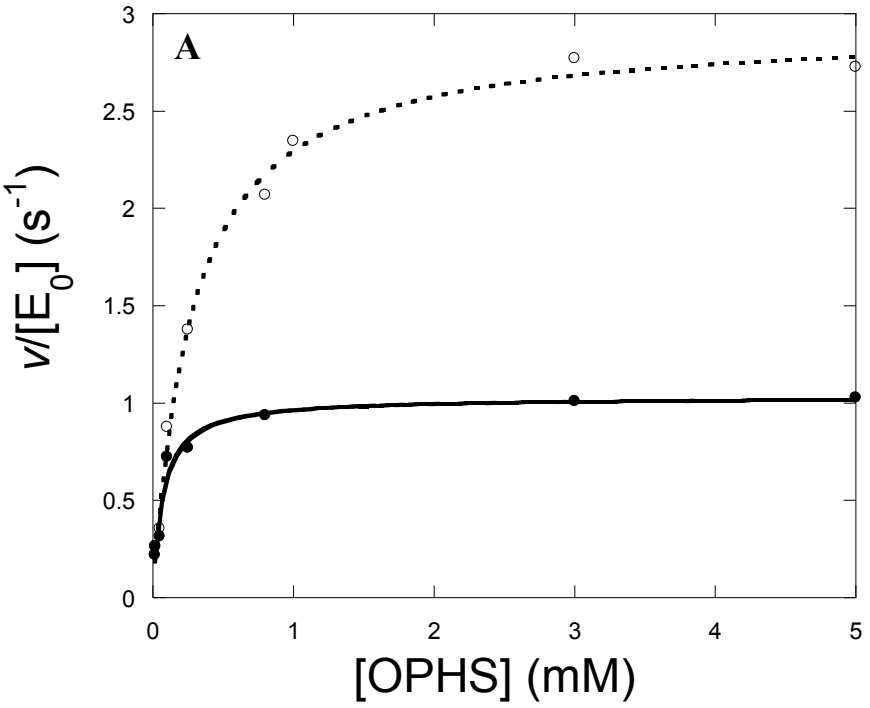
A
v/[E0] (s-1)
[OPHS] (mM)
0
0.5
1
1.5
2
2.5
3
0
1
2
3
4
5

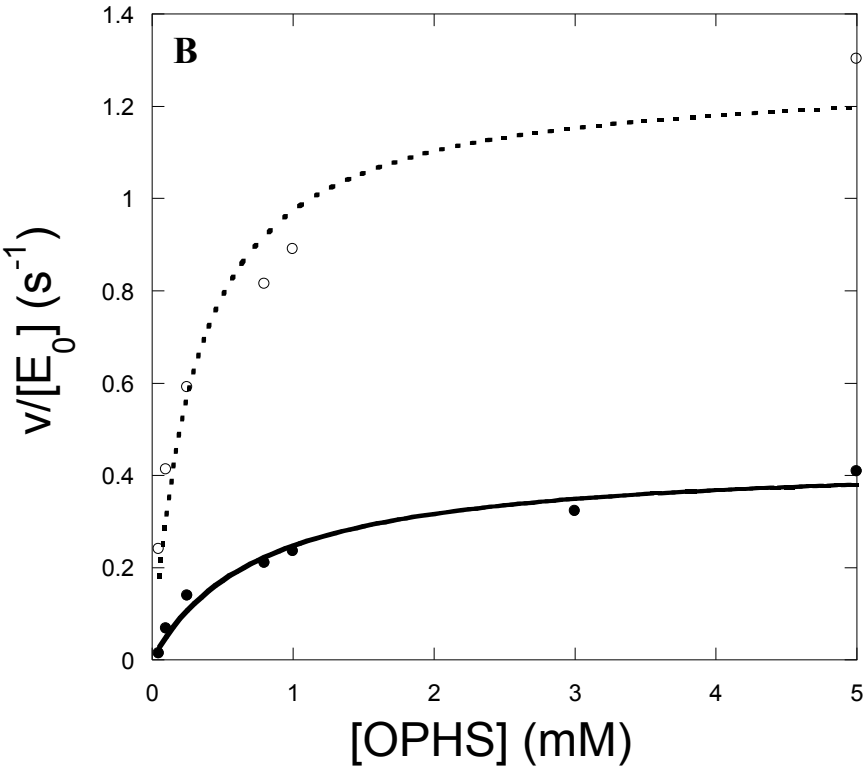
B
v/[E0] (s-1)
[OPHS] (mM)
0
0.2
0.4
0.6
0.8
1
1.2
1.4
0
1
2
3
4
5

4.5. Discussion

Increasing L-Met in staple crops such as *C. arietinum* and *L. culinaris* is of particular interest in the field of plant biotechnology, given their nutritional deficiency in this essential amino acid. In plants, OPHS occupies the branch-point between L-Met and L-Thr biosynthesis, and the metabolic flux between these two pathways is regulated by the L-Met-metabolite SAM. The complexity of the regulation of OPHS partitioning has confounded metabolic engineering endeavours, as exemplified in the systemic metabolic disruptions observed in previous attempts (Zeh *et al.* 2001; Gakiere *et al.* 2002; Avraham and Amir, 2005; Kusano *et al.*2010). The creation of a kinetic model of the OPHS branch-point in the target species will facilitate the pursuit of increased L-Met biosynthesis by providing a tool for predicting the effect of genetic engineering studies focusing on CGS and/or TS (Curien *et al.* 2009; Rohwer, 2012). This type of model first requires the kinetic parameters of the component enzymes under conditions of minimum and maximum activity (Rohwer, 2012).

The presence of 100 μM SAM results in an 8.5-fold increase in the k_{cat} of AtTS1 (from 0.20 ± 0.04 s^{-1} to 1.7 ± 0.1 s^{-1}) and a 10-fold decrease in K_m^{OPHS} (from 700 ± 500 μM to 70 ± 10 μM). The resulting k_{cat}/K_m^{OPHS} value of (2.4 ± 0.3) x 10^4 M^{-1} s^{-1}, in the presence of SAM, is consistent with the previously reported value of 2.9 x 10^4 M^{-1} s^{-1} at 100 μM SAM (Laber *et al.* 1999). The catalytic efficiency of AtTS1 in the absence of SAM (k_{cat}/K_m^{OPHS} = (3 ± 1) x 10^2 M^{-1} s^{-1}) is also consistent with the previously reported value of 3.3 x 10^2 M^{-1} s^{-1} (Laber *et al.* 1999). The minor, 2-fold

differences in the k_{cat} and K_m^{OPHS} values of AtTS1, compared to those reported by Laber and colleagues (k_{cat} = 0.86 s^{-1}, K_m^{OPHS} = 30 μM), may be due to differences in assay conditions, as Laber *et al* used the end-point malachite green assay while we employed the recently developed continuous assay, described in Chapter 3 (Laber *et al.* 1999; Morneau *et al.* 2012). The use of a continuous assay ensures that kinetic parameters are measured under steady-state conditions (Shepherd and Dailey, 2005). The assumption of linearity over the course of the assay period and the potential of product, which builds up in an end point assay, to compete with substrate for binding to the active site can lead to underestimation of k_{cat} when employing an end-point assay. The discrepancies in the observed kinetic parameters of AtTS1 may also be the result of variation in the estimation of OPHS or protein concentrations, which would affect K_m^{OPHS} and k_{cat}, respectively.

The k_{cat} and K_m^{OPHS} values of CaTS (1.00 ± 0.04 s^{-1} and 70 ± 20 μM) and LcTS (1.50 ± 0.04 s^{-1} and 100 ± 15 μM) are similar to the measured parameters for AtTS1 (1.7 ± 0.1 s^{-1} and 70 ± 10 μM), suggesting the L-Asp metabolic model could be used to inform the rational metabolic engineering of the pulse species (Curien *et al.* 2009). However, the effect of SAM on the k_{cat} of AtTS1 (8.5-fold increase), CaTS (2.5-fold increase) and LcTS (4-fold increase) is distinct. The k_{cat} and K_m values of both enzymes in the presence and absence of SAM were analyzed using the equations 4.1 and 4.2, respectively (Curien *et al.* 2003), in order to determine the apparent kinetic parameters as a function of SAM concentration to measure the flux of OPHS at the branch-point.

$$k_{cat}^{app} = \frac{k_{cat}^{no\,SAM} + k_{cat}^{SAM} x \frac{[SAM]^2}{K_1 K_2}}{\frac{(1+[SAM]^2)}{K_1 K_2}} \quad (4.1)$$

$$K_m^{app} = \left(\frac{K_m^{no\,SAM}\, x \frac{1+\frac{[SAM]}{0.5}}{1+\frac{[SAM]}{1.1}}}{1+\frac{[SAM]^2}{K_m^{SAM}}} \right) \quad (4.2)$$

With K_1K_2 representing the binding constants for the association of SAM (73 μM^2) with AtTS1 (Curien *et al.* 2003). These equations take into account SAM concentration as a factor in the k_{cat} and K_m value of plant TS, allowing for the calculation of the parameters at varying SAM concentrations. Setting the SAM concentration to physiological levels (20 μM), the k_{cat}^{app} and K_m^{app} of AtTS1 were calculated as 1.5 s^{-1} and 230 μM, respectively. The k_{cat}^{app} and K_m^{app} of AtTS2, CaTS, and LcTS were calculated as 0.6 s^{-1} and 650 μM, 0.9 s^{-1} and 260 μM, and 1.3 s^{-1} and 220 μM, respectively. The flux of OPHS (J_{OPHS}) is equal to the sum of the flux of L-cystathionine (J_{Cyst}) and the flux of L-Thr (J_{Thr}), which are defined as the Michaelis-Menten equation using $k_{cat}^{app}$and $K_m^{app}$of TS and CGS. The calculation of J_{Thr} was completed using equation 4.3.

$$J_{Thr} = \frac{k_{cat}^{app}[TS][OPHS]}{K_m^{app} + [OPHS]} \quad (4.3)$$

With [OPHS] and [TS] set to the physiological concentration estimates used in the construction of the *A. thaliana* OPHS branch-point (80 μM and 5 μM, respectively) (Curien *et al.* 2003), the J_{Thr} of CaTS and LcTS was calculated as 1.1 μM s^{-1} and 1.7

μM s^{-1}, respectively, compared to the J_{Thr} of 1.9 μM s^{-1} of AtTS1 and 0.3 μM s^{-1} of AtTS2. In comparison, J_{Cyst} in *A. thaliana* was calculated as 0.1 μM s^{-1} based on k_{cat} and K_m^{OPHS} and K_m^{Cys} values measured previously (Ravanel *et al.* 1998a; Curien *et al.* 2003). These values indicate that in *A. thaliana*, under physiological conditions and including the two forms of TS, J_{OPHS} = 2.4 μM s^{-1}. AtTS1 was calculated to account for 80% of OPHS flux, however, the addition of AtTS2, which was calculated to be responsible for 14% of OPHS flux, decreases J_{Cyst} to approximately 6% of the flux of OPHS, compared to the 20-30% it was previously attributed (Curien *et al.* 2003). Since the kinetic parameters of CGS from the pulse species are lacking, an estimation of J_{OPHS} can be made using J_{Cyst} from *A. thaliana*, where J_{OPHS} in *C. arietinum* and *L. culinaris* are equal to 1.2 μM s^{-1} and 1.8 μM s^{-1}, respectively. With this assumption, CaTS and LcTS account for 91% and 94% of OPHS flux, respectively. The role of CaTS and LcTS in OPHS flux partitioning is subject to change with the determination of the kinetic parameters of pulse CGS. According to these calculations, the branch-point model from *A. thaliana* cannot be used to study OPHS flux in the pulse species because the magnitude of flux partitioning of AtTS1 differs from that of CaTS and LcTS.

The k_{cat}/K_m^{OPHS} of AtTS2 is 14-fold lower than that of AtTS1 in the presence of 100 μM SAM. The presence of SAM has negligible effect on the K_m^{OPHS} of AtTS2 (600 ± 300 μM in the presence of 100 μM SAM versus 400 ± 30 μM in the absence of SAM). In contrast, the allosteric effector resulted in similar increases of 8.5-fold and 7-fold in the k_{cat} of AtTS1 and AtTS2, respectively. These results demonstrate that while AtTS2 is allosterically activated by SAM, the mechanism is likely different

from that of AtTS1 (Table 4.1). *A. thaliana* gene expression array tools revealed ubiquitous mRNA expression of *AtTS1* and *AtTS2* in *A. thaliana*, with similar expression levels between the two homologues, although the expression of AtTS1 is approximately 30-fold higher in select tissues than that of AtTS2 (Figure 4.5). Peak expression of *AtTS1* is observed in the late-stage development of seeds, and peak *AtTS2* transcript expression is found in the apical meristem, floral organs, and the hypocotyl of *A. thaliana* (Figure 4.5) (Schmid *et al.* 2005; Winter *et al.* 2007). The systemic expression of both forms of AtTS indicates that the biosynthesis of L-Thr occurs in all plant tissues; however, the concentration of both *AtTS1* and *AtTS2* in rapidly developing tissues such as seeds, flowers, and meristemic tissue, suggests high levels of amino acid biosynthesis are required for developing tissues. This is similar to the transcript expression patterns of *A. thaliana* aspartate kinase (AK), which has distinct peak transcript expression in rapidly developing tissues for its various homologues, such as the rosette (*AK1*), first node (*AK2* and *AK3*), and shoot apex (bifunctional *AK-HSDH*) (Winter *et al.* 2007). The expression pattern of *AtTS2* suggests that the second form of TS in *A. thaliana* may have evolved to support amino acid biosynthesis in developing tissues in order to meet the amino acid requirements for development.

When creating a kinetic model of a metabolic pathway, all active forms of the enzyme(s) in the pathway must be included in order to develop an accurate model, since the different homologues of each enzyme in the pathway may contribute uniquely to the flux of metabolites. The use of an incomplete kinetic model in metabolic engineering design may lead to ineffective alterations to flux due to the

Figure 4.5. Expression patterns of AtTS1 (A) and AtTS2 (B) in various tissues of *A. thaliana*. The fold-change (C) of the expression of AtTS1 relative to AtTS2 is also shown. Data obtained from the *Arabidopsis* electron fluorescent pictograph (eFP) browser provided by the Bio-Analytic Resource (BAR) at the University of Toronto (Winter *et al.* 2007).

A

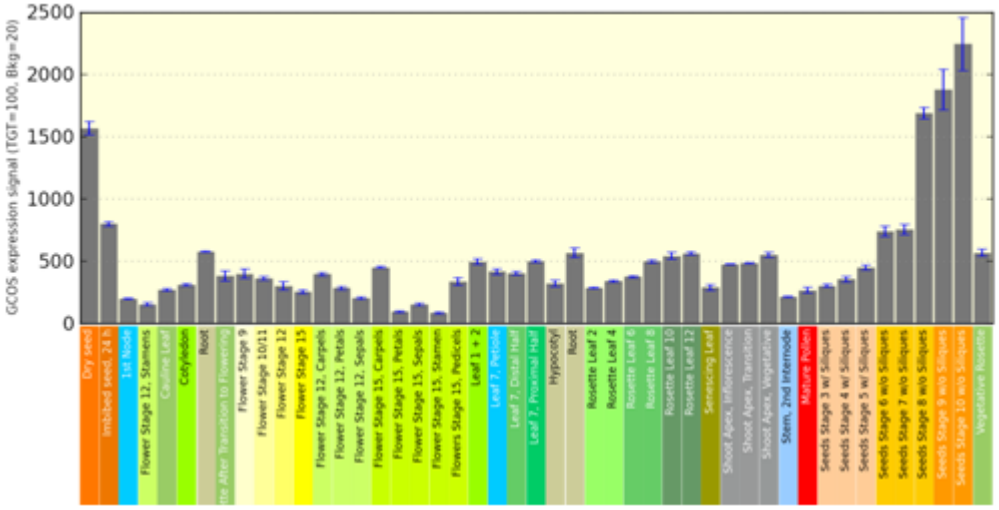
GCOS expression signal (TGT=100, Bkg=20)
2500
2000
1500
1000
500
0

B

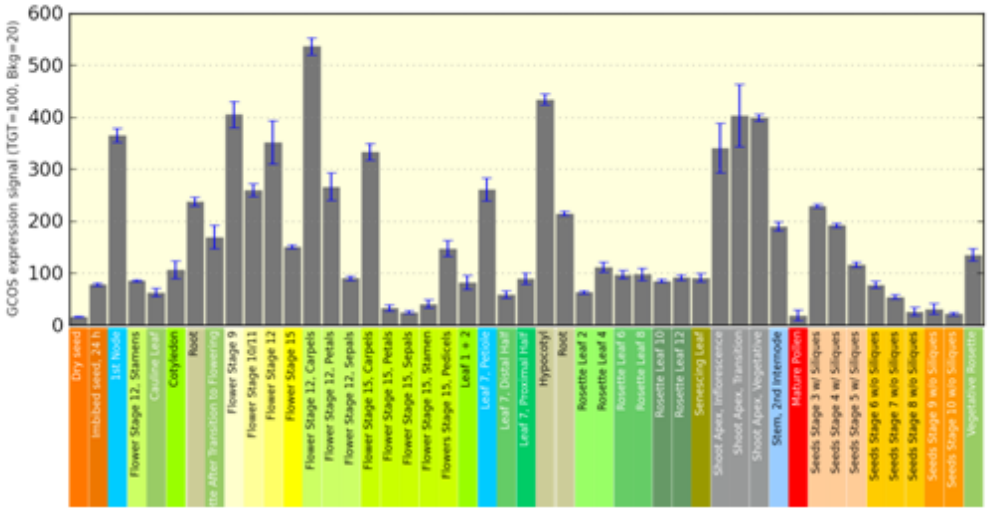
GCOS expression signal (TGT=100, Bkg=20)
600
500
400
300
200
100
0

C

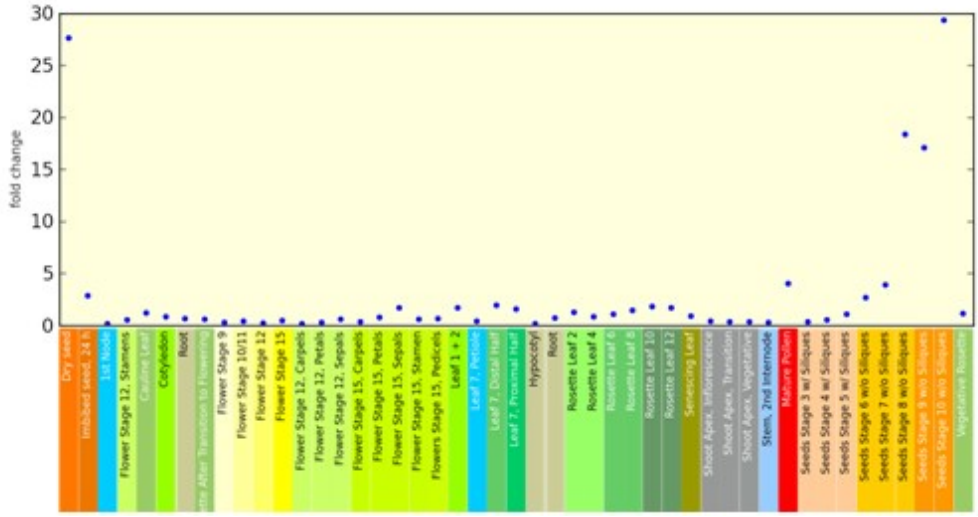
fold change
30
25
20
15
10
5
0

unforeseen contribution of the omitted isoforms of the enzyme. For example, a kinetic model of the L-Asp metabolic pathway that were to use only one homologue of AK to represent the flux of L-Asp, rather than the four forms of AK found in *A. thaliana*, would result in that particular homologue being attributed 100% of the control over metabolic flux, leading to an overestimation of its influence (Curien *et al.* 2007). In the case of AtTS1, the calculations of J_{Thr} indicate that while AtTS1 may account for 80% of the flux, only approximately 6% of the remaining flux of OPHS goes to L-Met synthesis. Any attempts at altering the regulation or expression of AtTS1 in order to reduce the flux would not have accounted for the 14% of OPHS flux diverted to AtTS2, thus leading to the potential overestimation of the effect of metabolic engineering strategies.

A C-terminal 6-His tag was added to CaTS to enable affinity chromatography in an attempt to expedite purification and increase enzyme purity. The addition of the affinity tag to CaTS results in a 3-fold increase in k_{cat} and a 4-fold increase in K_m^{OPHS}, compared to wild-type CaTS, in the presence and absence of 100 μM SAM. The shift in the kinetic parameters indicates that the addition of a C-terminal affinity tag should not be employed for plant TS. The C-terminus of the protein is situated in proximity to the SAM-binding domain at the dimer interface, such that the 6-His tag may influence communication between the 2 sites, thereby shifting the kinetic parameters compared to the wild-type version of the enzyme (Mas-Droux *et al.* 2006). In *A. thaliana*, the two solvent-exposed SAM molecules (SAM2 and SAM4) form stacking interactions between their adenosine rings and W101 (W139 in CaTS) of each monomer, triggering a 150° rotation of the PLP molecule (Mas-Droux *et al.* 2006).

This shift results in the catalytically competent form of the active site and facilitates the binding of substrate (Mas-Droux *et al.* 2006). In the absence of SAM, the imidazole rings of the 6-His tag may interact with these tryptophan residues in a similar manner, causing a partial shift in the PLP co-factor, accounting for the 4-fold increase in k_{cat}, and the subsequent 5-fold increase in k_{cat}/K_m^{OPHS} when compared to CaTS in the absence of SAM.

4.6. Conclusion

In plants, the concentration of many amino acids may be altered by perturbations in the metabolic flux of neighboring pathways, as many amino acid biosynthetic pathways, like those derived from L-Asp, rely on common metabolite pools. Previous attempts to increase L-Met biosynthesis, that modified the regulation or expression of TS or CGS, resulted in unintended changes in the partitioning of metabolites in the L-Asp pathway, often associated with undesirable phenotypic effects (Inaba *et al.* 1994; Bartlem *et al.* 2000; Zeh *et al.* 2001; Gakiere *et al.* 2002; Avraham and Amir, 2005). A kinetic model recreating the OPHS branch-point in the target species will be useful in informing metabolic engineering by providing a tool to predict potential alterations to the flux of adjoining pathways (Rohwer, 2012). Since the flux of OPHS depends exclusively on TS and CGS activity, branch-point kinetics can be modelled with the rate equations of both enzymes and the physiological concentrations of OPHS, L-Cys, and SAM (Curien *et al.* 2003). The kinetic parameters of TS from *C. arietinum* and *L. culinaris* are now known, and can be combined with those of CGS from the pulse species, when they become available, to

create the branch-point model. Following the mathematical reconstruction of the OPHS branch-point, the model must be validated by reconstitution *in vitro*, using enzymes and metabolites at physiological concentrations, and making any necessary adjustments to variables of the model based on experimental data (Curien *et al.* 2003; Curien *et al.* 2009). The data presented in this chapter can be used to inform future metabolic engineering projects in pulse species to successfully increase L-Met production to levels that meet human daily intake requirements.

5. GENERAL CONCLUSION

Legumes such as *C. arietinum* and *L. culinaris* are rich in carbohydrates, proteins, fiber, and minerals, and so are considered to be among the most nutritional sources of plant protein (Singh, 1985; Dixon and Hosking, 1992). However, they are not balanced sources of amino acids, as they are deficient in the essential amino acid methionine (L-Met) from the perspective of human dietary requirements. Supplementing a legume-rich diet with a balanced intake of cereals and animal sources can provide adequate amounts of essential amino acids. However, up to 90% of the consumption of legumes occurs in developing countries where vegetarianism is predominant and particularly in rural areas where poverty prevents access to a varied diet (Muntz *et al.* 1998; Agriculture and Agri-Food Canada, 2011). A sub-optimal intake of essential amino acids can lead to protein energy malnutrition (PEM), which manifests itself in lowered disease resistance, decreased blood proteins, as well as mental and physical developmental retardation in children (Hoorweg and Stanfield, 1976). It is estimated that one third of the children in developing countries suffer from PEM (de Onis, 1993; World Health Organization, 2006). The demand to improve the nutritional quality of staple crops such as *C. arietinum* and *L. culinaris* has grown in recent years (Acharjee and Sarmah, 2013). Enhancement of the nutritional quality of grain legumes has been attempted through seed-specific expression of L-Met-rich seed storage proteins, or the expression of SAM-insensitive *AtCGS* under seed-specific promoters (Chiaiese *et al.* 2004; Hanafy *et al.* 2013; Song *et al.* 2013). These projects had limited success in increasing protein-bound L-Met to levels that meet human dietary requirements, either due to the concurrent decrease in

endogenous sulfur-rich seed proteins (Chiaiese *et al.* 2004), or the limited incorporation of the accumulated L-Met into seed storage proteins and its subsequent degradation (Hanafy *et al.* 2013; Song *et al.* 2013).

L-Met belongs to the L-Asp family of amino acids, along with L-Thr, L-Lys, and L-Ile (Jander and Joshi, 2010). In plants, the enzymes CGS and TS, involved in L-Met and L-Thr biosynthesis, respectively, compete for the OPHS substrate. The flux of OPHS between these two pathways is regulated by the L-Met-derivative SAM, through the allosteric activation of TS and the post-transcriptional modulation of *CGS* transcript stability (Curien *et al.* 1998; Chiba *et al.* 2003). Given the competition for a common substrate by CGS and TS, manipulations of the OPHS branch-point for the purpose of increasing L-Met biosynthesis must consider the effects on both metabolic pathways. A kinetic model of the OPHS branch-point in the target species can be used to inform the *in vivo* engineering of the branch-point by predicting the effects of alterations on flux distribution in both L-Met and L-Thr metabolism (Rohwer, 2012). The work presented in this thesis provides an important step in building a kinetic model of the OPHS branch-point in *C. arietinum* and *L. culinaris*.

The characterization of plant TS for informing future genetic engineering projects requires a suitable kinetic assay and a reliable method for synthesizing the OPHS substrate. In Chapter 2, I described the development of these procedures. Unlike many previous OPHS synthetic protocols, I opted for the use of purified homoserine kinase (HSK) over crude protein extracts and the addition of limited amounts of ATP and recycling of the ADP by-product using phospho(enol) pyruvate (PEP) and pyruvate kinase (PK) (Laber *et al.* 1994a; Laber *et al.* 1994b). Newly

formed OPHS must be separated from residual ADP for accurate quantification using the phosphate-detecting malachite green assay, yet the separation process is difficult, thus potentially confounding the results of kinetic assays. I modified the synthetic method described by Laber and colleagues, by further reducing the concentration of ATP from 5 mM to 1 mM to limit residual phosphates in the reaction mixture, thereby avoiding the mis-estimation of OPHS concentration (Laber *et al.*1994a; Laber *et al.* 1994b). However, the use of PEP introduced the potential for an increased background rate of the reaction caused by residual pyruvate. Separation of OPHS from pyruvate was completed *via* anion exchange chromatography, and any contaminating pyruvate was measured using HO-HxoDH, so as to detect OPHS fractions containing sufficient pyruvate levels to affect the background rate. The measurement of TS kinetic parameters was completed using a range of OPHS up to enzyme saturation (0.2-5 mM). Typically, kinetic assays use substrate concentrations at 10x K_m in order to simulate saturation conditions. In the case of TS, 1.2 mM OPHS was identified as the requisite maximum OPHS concentration in the assay (Laber *et al.* 1999). Ultimately, the maximum concentration required for plant TS was experimentally determined to be 3-5 mM (Chapter 4). Recovered OPHS was concentrated to 15-30 mM.

The development of a continuous, coupled-coupled assay used to study the activity of plant TS was necessary for accurately measuring the steady-state kinetic parameters reported in this thesis. Previous studies have employed discontinuous assays quantifying the L-Thr or phosphate products of TS *via* HPLC or reaction with malachite green, respectively (Laber *et al.* 1994a; Curien *et al.* 1998). A continuous

method, coupling the reaction of AtTS1 with threonine deaminase (TD) and lactate dehydrogenase (LDH) was reported for the *in vitro* measurement of flux at the OPHS branch-point, but had not been optimized for determination of the steady-state parameters of TS (Curien *et al.* 2003). The *A. thaliana* OPHS branch-point model was constructed with kinetic parameters determined using an end-point assay, and so the model may have utilized non-steady state kinetic parameters in its construction, potentially leading to the miscalculation of flux distribution (Curien *et al.* 2003). The TD/LDH system was not used for the subsequent measurement of the kinetic parameters of TS from other species (Lee *et al.* 2005; Covarrubias *et al.* 2008; Murakawa *et al.* 2011). LDH and TD are not optimal coupling enzymes for measuring TS activity, due to the preference of the former for pyruvate rather than the α-ketobutyrate product of TD, and the dependence of the latter on allosteric activation by L-valine (Eisenstein, 1991; Aitken *et al.* 2003). In contrast, the use of hydroxyisocaproate dehydrogenase (HO-HxoDH) and the non-allosteric variant of TD from *E. coli* (eTD_{L447F}) as coupling enzymes provides optimal conditions for the measurement of the activity of TS from both plants and microorganisms by relieving the L-valine requirement of TD, and due to the higher catalytic efficiency for pyruvate of HO-HxoDH compared to LDH (Chapter 2). This assay is suitable for the construction of future kinetic models of both the OPHS branch-point, and the L-Asp metabolic pathway.

The construction of a kinetic model requires a detailed understanding of the regulation, compartmentalization, and activity of the component enzymes, such as the information described in this thesis for TS from *C. arietinum* (CaTS) and *L. culinaris*

(LcTS). CaTS and LcTS share 77-82% identity with TS from *G. max*, with the residues key to cofactor and SAM-binding being conserved (Chapter 3). TS function *in vivo* was verified through the complementation of a L-Thr-auxotrophic *E. coli* strain, lacking the coding sequence for TS, with the full-length and mature (lacking the transit peptide) constructs of *CaTS, LcTS,* and *AtTS2* (Baba *et al.* 2006). Fusing of the N-terminal region of the *CaTS* and *LcTS* coding sequences in frame with GFP, and subsequent transformation into *A. tumefaciens* and transient expression in *N. tabacum* leaves, showed that these regions encode a functional chloroplast transit peptide (Chapter 3). This indicates that L-Thr biosynthesis occurs in the chloroplast in these two pulse species, as was expected from the localization of the pathway in *A. thaliana* and *S. tuberosum* (Curien *et al.* 1996; Casazza *et al.* 2000). The kinetic parameters of CaTS (k_{cat} = 1.00 ± 0.04 s^{-1}, K_m^{OPHS} = 70 ± 20 μM) and LcTS (k_{cat} = 1.50 ± 0.04 s^{-1}, K_m^{OPHS} = 100 ± 15 μM) in the presence of 100 μM SAM are consistent with those of AtTS1 (k_{cat} = 1.7 ± 0.1 s^{-1}, K_m^{OPHS} = 70 ± 10 μM) (Chapter 4). However, the recently constructed mathematical model of the *A. thaliana* L-Asp metabolic pathway (Curien *et al.* 2009) may not be suitable to describe the flux distribution in the pulse species due to the disparate number of TS homologues between *A. thaliana*, *C. arietinum*, and *G. max* (Arabidopsis Genome Initiative, 2000; Schmutz *et al.* 2010; Jain *et al.* 2013). Furthermore, the degree of OPHS flux control of AtTS1 (80%) differs from that of CaTS (estimated at 91%) and LcTS (estimated at 94%). Successfully increasing L-Met production in the *C. arietinum* and *L. culinaris* will require the creation of a species-specific kinetic model of the OPHS metabolic branch-point. The information presented in this thesis provides a starting point for

the development of the mathematical model of OPHS flux toward L-Thr synthesis. When combined with similar data from CGS, this model will be a powerful tool for informing future metabolic engineering of pulse species. One such kinetic model, which recreated the pathway of sucrose metabolism, has been used to inform strategies for the improvement of sucrose accumulation by predicting the effects of altered expression of one of the enzymes involved in futile sucrose cycling (Rossouw *et al.* 2007; Rohwer, 2012). Similar predictions of flux in relation to increased or decreased expression and regulation of CGS and TS in the pulse species will facilitate the identification of metabolic engineering strategies with high chances of success prior to integrating these strategies *in vivo*.

AtTS2 was studied in this work in an attempt to elucidate its role in OPHS flux partitioning. Prior to the discovery of AtTS2, it was believed that AtTS1 was unique in *A. thaliana* chloroplasts (Curien *et al.* 1996). The construction of the L-Asp pathway model omitted AtTS2, since it was found to have 120-fold lower activity than AtTS1 at physiological SAM concentrations (Curien *et al.* 2009). In this thesis, I reported the finding that the coding sequence of AtTS2 encodes a functional protein, able to complement L-Thr auxotrophy (Chapter 3). The coding sequence of AtTS2 also contains a functional chloroplast transit peptide, indicating that the enzyme is likely found in the plastid, along with the other L-Asp metabolic enzymes (Chapter 3). In Chapter 4, I reported that AtTS2 is allosterically regulated, displaying an 8.5-fold higher k_{cat}/K_m^{OPHS} in the presence of 100 μM SAM. The k_{cat}/K_m^{OPHS} of AtTS2 is one order of magnitude lower than that of AtTS1 in the presence of SAM, confirming the reported lower activity of the enzyme (Curien *et al.* 2009). The distinct kinetic

parameters of AtTS2, the finding that this enzyme may account for 28% of OPHS flux partitioning, along with the similar transcript expression levels of both forms of TS in most *A. thaliana* tissues, indicate that this enzyme is likely involved in the partitioning of OPHS flux, and that it should be considered in future branch-point modelling in *A. thaliana*.

5.1. Future Directions

The creation of a kinetic model of the OPHS branch-point will facilitate future attempts to increase the synthesis of L-Met in the pulse species. TS is a promising target for metabolic engineering, since it accounts for approximately 70% of OPHS flux (Curien *et al.* 2003; Chapter 4). To date, no evidence exists of the OPHS branch-point model or the L-Asp metabolic model having informed subsequent metabolic engineering projects. I propose first that the kinetic parameters of the *mto2* variant of AtTS1, with an Arg substitution at Leu204, should be measured and integrated into the branch-point model to examine the effect of impaired AtTS1 activity on metabolic flux, as a baseline for determining levels of TS activity that would be useful in increasing flux toward L-Met synthesis (Bartlem *et al.* 2000; Curien *et al.* 2003). Since no kinetic studies were done on this TS variant, there is a lack of understanding about the mechanism for impaired TS activity, whether it is K_m^{OPHS}, k_{cat}, or both values that are primarily affected by the substitution of the large, basic, polar amino acid, adjacent to the active site lysine (Bartlem *et al.* 2000). In these plants, L-Thr concentration is decreased to 6% of wild-type levels, however it is not clear if this is due to a low level of activity of AtTS1, or if it is a result of a basal level of AtTS2

activity (Bartlem *et al.* 2000). Understanding the mechanism of impaired TS activity in the *mto2* line, as well as the ability of AtTS2 to compensate for impaired AtTS1 activity, may provide a starting point for future alterations to the TS active site to manipulate activity and increase L-Met synthesis.

Given the large changes in k_{cat}/K_m^{OPHS} of plant TS in the presence of SAM, ranging from 20-fold in LcTS to 80-fold in AtTS1, the residues involved in SAM-binding have the potential to be manipulated, thus resulting in alterations of the allosteric activation of the enzyme. Probing the allosteric site of AtTS1 has the potential to identify key residues that can be mutated to alter SAM binding and modify the activation of AtTS1, thus lessening its effect on OPHS flux distribution between L-Met and L-Thr biosynthesis (Mas-Droux *et al.* 2006). However, to date, no such studies have been reported. The topography of the AtTS1 SAM-binding sites, as well as the orientation of the bound SAM molecules, is different from those observed in other SAM-binding proteins, including methyltransferases and SAM-radical dependent enzymes such as biotin synthase, representing a plant-specific SAM-binding mechanism (Martin and McMillian, 2002; Berkovitch *et al.* 2004; Mas-Droux *et al.* 2006). As such, mutagenesis studies in other SAM-binding enzymes will not be useful in informing the selection of target residues for altering the allosteric activation of plant TS. Nevertheless, several residues conserved only in plant TS that play key roles in SAM-binding are potential targets for the exploration of the allosteric site, such as P102, Y103, and G104, residues that form polar interactions with the adenosyl group of SAM, and W101 which forms a stacking interaction with the adenine ring (Figure 1.4) (Mas-Droux *et al.* 2006). After identification of these

residues and kinetic characterization of TS mutant proteins, the effect of these mutants on the OPHS branch-point can be measured *in silico* through the kinetic model and *in vitro* using the continuous, coupled-coupled assay, prior to engaging in *in vivo* genetic modifications.

TS is an attractive target for the metabolic engineering of important crop plants aimed at increasing L-Met levels, due to its key role in the partitioning of OPHS flux. Altering the effect of TS on flux distribution would permit the increased biosynthesis of L-Met by lessening the competition between TS and CGS, resulting in an increase in free L-Met. Historically, the use of constitutive or seed-specific promoters to increase the expression of SAM-insensitive CGS in plants has improved the pool of free L-Met, with little or no effect on the levels of protein-bound L-Met, thus failing to meet the human daily L-Met requirements (Gakiere *et al.* 2002; Hanafy *et al.* 2013; Song *et al.* 2013). For example, the expression of the *mto1* variant of *AtCGS* in the seeds of *G. max* was met with a 9-fold increase in total seed L-Met levels, with no increase in protein-bound L-Met, and excess L-Met likely being degraded or converted into SAM, rather than being integrated into seed proteins (Hanafy *et al.* 2013). This indicates that increasing the pool of free L-Met alone through manipulations in OPHS flux is not a suitable strategy for increasing the nutritional significance of important crop species (Hesse *et al.* 2004). The expression of L-Met-rich proteins in legume seeds, in combination with alterations in OPHS flux to meet the increased demand for L-Met, is more likely to be successful in the creation of pulse species that meet the amino acid requirements for adequate human nutrition. Through the use of a kinetic model of the OPHS branch-point, informed by the results

described in this thesis, future metabolic engineering endeavours in the important pulse species *C. arietinum* and *L. culinaris* have a greater chance of successfully enhancing L-Met production to meet global nutritional needs.

REFERENCES

Acharjee, S., and Sarmah, B.K. 2013. Biotechnologically generating "super chickpea" for food and nutritional security. Plant Science 207: 108-116.

Agriculture and Agri-Food Canada. 2011. Canadian Pulse Industry: Situation and Outlook. Market Outlook Report 3(2). Accessed online at http://www5.agr.gc.ca/resources/prod/doc/misb/mag-gam/mor-rmar/pdf/rmar_03_02_2011-06-08_eng.pdf (accessed on January 9, 2014).

Aitken, S.M., Kim, D.H., and Kirsch, J.F. 2003. *Escherichia coli* cystathionine -synthase does not obey ping-pong kinetics: novel continuous assays for the elimination and substitution reactions. Biochemistry 42: 11297-11306.

Alliance grain traders. 2011. History of pulse [online]. Available from http://www.alliancegrain.com/about-pulses/history-of-pulse.htm (accessed on October 7, 2012)

Amir, R., Han, T., and Ma, F. 2012. Bioengineering approaches to improve the nutritional values of seeds by increasing their methionine content. Molecular Breeding 29: 915-924.

Arabidopsis Genome Initiative. 2000. Analysis of the genome sequence of the flowering plant *Arabidopsis thaliana*. Nature 408: 796-815.

Avraham, T., and Amir, R. 2005. The expression level of threonine synthase and cystathionine -synthase is influenced by the level of both threonine and methionine in *Arabidopsis* plants. Transgenic Research 14: 299-311.

Azavedo, RA., Arruda, P., Turner, W., and Lea, P. 1997. The biosynthesis and metabolism of the aspartate derived amino acids in higher plants. Phytochemistry 46: 395-419.

Azavedo, RA., Lancien, M., Lea, PJ. 2006. The aspartic acid metabolic pathway, and exciting and essential pathway in plants. Amino Acids 30: 143-162.

Baba, T., Ara, T., Hasegawa, M., Takai, Y., Okumura, Y., Baba, M., Datsenko, K.A., Tomita, M., Wanner, B.L., Mori, H. 2006. Construction of *Escherichia coli* K-12 in-frame, single-gene knockout mutants: the Keio collection. Mol Syst Biol **2**:1-11.

Bartlem, D., Lambein, I., Okamoto, T., Itaya, A., Uda, Y., Kijima, F., Tamaki, Y., Nambara, E., and Naito, S. 2000. Mutation in the threonine synthase gene results in overaccumulation of soluble methionine in *Arabidopsis*. Plant Physiology 123: 101-110.

Berkovitch, F., Nicolet, Y., Wan, J.T., Jarrett, J.T., and Drennan, C.L. 2004. Crystal structure of biotin synthase, an *S*-adenosylmethionine-dependent radical enzyme. Science: 303(5654): 76-79.

Bernard, N., Johnsen, K., Ferain, T., Garmyn, D., Hols, P., Holbrook, J.J., and Delcour, J. 1994. NAD^+-dependent D-2-hydroxyisocaproate dehydrogenase of *Lactobacillus delbrueckii* subsp. *Bulgaricus* – gene cloning and enzyme characterization, Eur. J. Biochem. 224: 439-446.

Bockelmann, W., Beuck, H.P., Lick, S., and Heller, K. 1995. Purification and characterization of a new tripeptidase from *Lactobacillus delbrueckii* ssp *Bulgaricus* B14, Int. Dairy J. 5: 493-502.

Bourniquel, A.A., and Mollet, B. 2002. Purification and characterization of the 3-phosphoglycerate kinase from the thermophile *Lactobacillus delbrueckii* subsp *lactis*, Int. Dairy J. 12: 723-728.

Bradford, M.M. 1976. A rapid and sensitive method for the quantification of microgram quantities of protein utilizing the principle of protein-dye binding. Anal. Biochem. 72: 248-254.

Burr, B., Walker, J., Truffa-Bachi, P., and Cohen, G.N. 1976. Homoserine kinase from *Escherichia coli* K12. European Journal or Biochemistry 62: 519-526.

Casazza, AP., Basner, A., Hofgen, R., and Hesse, H. 2000. Expression of a threonine synthase from *Solanum tuberosum* L. is not metabolically regulated by photosynthesis related signals or by nitrogenous compounds. Plant Science 157: 43-50.

Chassagnole, C., Rais, B., Quentin, E., Fell, D.A., and Mazat, J-P. 2001. An integrated study of threonine-pathway enzyme kinetics in *Escherichia coli*, Biochem. J. 356: 415-423.

Chiaiese, P., Ohkama-Ohtsu, N., Molvig, L., Godfree, R., Dove, H., Hocart, C., Fujiwara, T., Higgins, T.J.V., and Tabe, L.M. 2004. Sulphur and nitrogen nutrition influence the response of chickpea seeds to an added, transgenic sink for organic sulphur. Journal of Experimental Botany 55(404): 1889-1901.

Chiba, Y., Ishikawa, M., Kijima, F., Tyson, RH., Kim, J., Yamamoto, A., Nambara, E., Leustek, T., Wallsgrove, R., and Naito, S. 1999. Evidence for autoregulation of cystathionine -synthase mRNA stability in *Arabidopsis*. Science 286: 1371-1374.

Chiba, Y., Sakurai, R., Yoshino, M., Ominato, K., Ishikawa, M., Onouchi, H., and Naito, S. 2003. *S*-adenosyl-L-methionine is an effector in the posttranscriptional autoregulation of the cystathionine -synthase gene in *Arabidopsis*. Proceedings of the National Academy of Sciences 100: 10225-10230.

Clausen, T., Huber, R., Prade, L., Wahl, M.C., and Messerschmidt. 1998. Crystal structure of *Escherichia coli* cystathionine γ-synthase at 1.5Å resolution. The EMBO Journal **17**(23): 6827-6838.

Covarrubias, A.S., Hogbom, M., Bergfors, T., Carroll, P., Mannerstedt, K., Oscarson, S., Parish, T., Jones, T.A., and Mowbray, S.L. 2008. Structural, biochemical, and *in vivo* investigations of the threonine synthase from *Mycobacterium tuberculosis*, J. Mol. Biol. 381: 622-633.

Curien, G., Dumas, R., Ravanel, S., Douce, R. 1996. Characterization of an *Arabidopsis thaliana* cDNA encoding an *S*-adenosylmethionine-sensitive threonine synthase. Federation of European Biochemical Societies 390: 85-90.

Curien, G., Job, D., Douce, R., and Dumas, R. 1998. Allosteric activation of *Arabidopsis thaliana* threonine synthase by *S*-adenosylmethionine, Biochemistry 37: 13212-13221.

Curien, G., Ravanel, S., Dumas, R. 2003. A kinetic model of the branchpoint between the methionine and threonine biosynthetic pathways in *Arabidopsis thaliana*. European Journal of Biochemistry 270: 4615-4627.

Curien, G., Laurencin, M., Robert-Genthon, M., and Dumas, R. 2007. Allosteric monofunctional aspartate kinases from *Arabidopsis*. FEBS Journal 274(1): 164-176.

Curien, G., Bastien, O., Robert-Genthon, M., Cornish-Bowden, A., Cardenas, M.L., and Dumas, R. 2009. Understanding the regulation of aspartate metabolism using a model based on measured kinetic parameters. Molecular Systems Biology **5**: 1-14.

Datko, A.H., Giovanelli, J., and Mudd S.H. 1974. Homocysteine biosynthesis in green plants, J. Biol. Chem. 249: 1139-1155.

Dixon, R.M., and Hosking, B.J. 1992. Nutritional value of grain legumes for ruminants. Nutritional Research Reviews 5: 19-43.

Dizigan, M.A., Kelly, R.A., Voyles, D.A., Leuthy, M.H., Malvar, T.M., and Malloy, K.P. 2007. High lysine maize compositions and event LY038 maize plants. United States Patent No, 7157281.

Eichel, J., González, J.C., Hotze, M., Matthews, R.G. and Schröder, J. 1995. Vitamin B12-independent methionine synthase from a higher plant (*Catharanthus roseus*). European Journal of Biochemistry 230: 1053–1058.

Eisenstein, E. 1991. Cloning, expression, purification, and characterization of biosynthetic threonine deaminase from *Escherichia coli*, J. Biol. Chem. 266: 5801-5807.

Eisenstein, E., Yu, H.D., Fisher, K.E., Iacuzio, D.A., Ducote, K.R., and Schwarz, F.P. 1995. An expanded two-state model accounts for homotropic cooperativity in biosynthetic threonine deaminase from *Escherichia coli*, Biochem. 34: 9403-9412.

Eliot, A.C., and Kirsch, J.F. 2004. Pyridoxal phosphate enzymes: mechanistic, structural, and evolutionary considerations. Annual Review of Biochemistry 73: 383-415.

Farrington, G.K., Kumar, A., Shames, S.L., Ewaskiewicz, J.I., Ash, D.E., and Wedler F.C. 1993. Threonine synthase of *Escherichia coli*: inhibition by classical and slow-binding analogues of homoserine phosphate, Arch. Biochem. Biophys. 307: 165-174.

Farsi, A., Lodha, P., Skanes, J.E., Los, H., Kalidindi, N., and Aitken, S.M. 2009. Interconversion of a pair of active-site residues in *Escherichia coli* cystathionine γ-synthase, *E. coli* cystathionine β-lyase, and *Saccharomyces cerevisiae* cystathionine γ-lyase and development of tools for the investigation of their mechanisms and reaction specificity. Biochemistry and Cell Biology **87**: 445-457.

Flavin, M., and Slaughter, C. 1960. Threonine synthetase mechanism: studies using isotopic hydrogen, J. Biol. Chem. 235: 1112-1118.

Gakiere, B., Denis, L., Droux, M., and Job, D. 2002. Over-expression of cystathionine γ-synthase in *Arabidopsis thaliana* leads to increased levels of methionine and *S*methylmethionine. Plant Physiology and Biochemistry 40: 119-126.

Galili, G., and Amir, R. 2012. Fortifying plants with the essential amino acids lysine and methionine to improve nutritional quality. Plant Biotechnology Journal 11: 211-222.

Galili, G., and Hofgen, R. 2002. Metabolic engineering of amino acids and storage proteins in plants. Metabolic Engineering 4: 3-11.

Garrido-Franco, M., Ehlert, S., Messerschmidt, A., Marinkovic, S., Huber, R., Laber, B., Bourenkov, GP., and Clausen, T. 2002. Structure and function of threonine synthase from yeast. The Journal of Biological Chemistry 277: 12396-12405.

Giovanelli, J., Veluthambi, K., Thompson, G., Mudd, SH., and Datko, A. 1984. Threonine synthase of *Lemna paucicostata*. Plant Physiology 76: 285-292.

Hacham, Y., Avraham, T., and Amir, R. 2002. The N-terminal region of *Arabidopsis* cystathionine -synthase plays in important regulatory role in methionine metabolism. Plant Physiology 128: 454-462.

Hanafy, M.S., Rahman, S.M., Nakamoto, Y., Fujiwara, T., Naito, S., Wakasa, K., and Ishimoto, M. 2013. Differential response of methionine metabolism in two grain

legumes, soybean and azuki bean, expressing a mutated form of *Arabidopsis* cystathionine γ-synthase. Journal of Plant Physiology 170: 338-345.

Hesse H., Kreft, O., Maimann, S., Zeh, M., Willmitzer, L., and Hofgen, R. 2001. Approaches toward understanding methionine biosynthesis in higher plants. Amino Acids 20: 281-289.

Hesse, H., Kreft, O., Maimann, S., Zeh, M., and Hoefgen, R. 2004. Current understanding of the regulation of methionine biosynthesis in plants. Journal of Experimental Botany 55: 1799-1808.

Hoffman, LM., Donaldson, DD., and Heman, EM. 1988. A modified storage protein is synthesized, processed, and degraded in the seeds of transgenic plants. Plant Molecular Biology 11: 717-729

Hoorweg, J., and Stanfield, J.P. 1976. The effects of protein energy malnutrition in early childhood on intellectual and motor abilities in later childhood and adolescence. Developmental Medicine & Child Neurology 18: 330-350.

Hughes, C., Gebhardt, J., Reuss, A., and Matthews, B. 1999. Identification and expression of a cDNA encoding cystathionine -synthase in soybean. Plant Science 146: 69-79.

Inaba, K., Fujiwara, T., Hayashi, H., Chino, M., Komeda, Y., and Naito, S. 1994. Isolation of an *Arabidopsis thaliana* mutant, *mto1*, that overaccumulates soluble methionine. Plant Physiology 104: 881-887.

Jain, M., Misra, G., Patel, R.K., Priya, P., Jhanwar, S., Khan, A.W., Shah, N., Singh, V.K., Garg, R., Jeena, G., Yadav, M., Kant, C., Sharma, P., Yadav, G., Bhatia, S., Tyagi, A.K., and Chattopadhyay, D. 2013. A draft genome sequence of the pulse crop chickpea (*Cicer arietinum* L.). The Plant Journal 74: 715-729.

Jander G., and Joshi, V. 2010. Recent progress in deciphering the biosynthesis of aspartate-derived amino acids in plants. Molecular Plant 3(1): 54-65.

Jaworski, A. F., Lodha, P. H., Manders, A. L., and Aitken, S. M. Exploration of the Active Site of *Escherichia coli* Cystathionine γ-Synthase. *Protein Science* 21(11): 1662-1671.

Kim, J., Lee, M., Chalam, R., Martin, M.N., Leustek, T., and Boerjan, W. 2002. Constitutive overexpression of cystathionine γ-synthase in *Arabidopsis* leads to accumulation of soluble methionine and *S*-methylmethionine. Plant Physiology **128**: 95-107.

Kingsbury, J.M., and McCusker, J.H. 2008. Threonine biosynthetic genes are essential in *Cryptococcus neoformans*, Microbiology 154: 2767-2775.

Knoke, B., Textor, S., Gershenzon, J., and Schuster, S. 2009. Mathematical modelling of aliphatic glucosinolate chain length distribution in *Arabidopsis thaliana* leaves. Phytochemistry Reviews 8: 39-51.

Kusano, M., Fukushima, A., Redestig, H., Kobayashi, M., Otsuki, H., Onouchi, H., Naito, S., Hirai, M.Y., Saito, K. 2010. Comparative metabolomics charts the impact of genotype-dependent methionine accumulation in *Arabidopsis thaliana*. Amino Acids 39: 1013-1021.

Kreft, B., Townsend, A., Pohlenz, HD., Laber, B. 1994. Purification and properties of cystathoinine -synthase from wheat (*Triticum aestivum* L.). Plant Physiology 104: 1215-1220.

Kreft, O., Hoefgen, R., and Hesse, H. 2003. Functional analysis of cystathionine γ-synthase in genetically engineered potato plants. Plant Physiology 131: 1843-1854.

Laber, B., Gerbling, K-P., Harde, C., Neff, K-H., Nordhoff, E., and Pohlenz, H-D. 1994a. Mechanisms of interaction of *Escherichia coli* threonine synthase with substrates and inhibitors, Biochem. 33: 3413-3423.

Laber, B., Lindell, S.D., and Pohlenz, H-D. 1994b. Inactivation of *Escherichia coli* threonine synthase by DL-*Z*-2-amino-5-phosphono-3-pentoic acid, Arch. Microbiol. 161 : 400-403.

Laber, B., Maurer, W., Hanke, C., Grafe, S., Ehlert, S., Messerschmidt, A., and Clausen, T. 1999. Characterization of recombinant *Arabidopsis thaliana* threonine synthase. European Journal of Biochemistry 263: 212-221.

Laloi, P., Atlan, D., Blanc, B., Gilbert, C., and Portalier, R. 1991. Cell-wall-associated proteinase of *Lactobacillus delbrueckii* subsp *blugaricus* CNRZ 397 – Differential extraction, purification and properties of the enzyme, Appl. Microbiol. Biot. 36: 196-204.

Lanzetta, P.A., Alvarez, L.J., Reinach, P.S., and Candia, O.A. 1979. An improved assay for nanomole amounts of inorganic phosphate, Anal. Biochem. 100: 95-97.

Lee, S.I., Kim, H.U., Lee, Y.-H., Suh, S.-C., Lim, Y.P., Lee, H.-Y., and Kim, H.-I. 2001. Constitutive and seed-specific expression of a maize lysine-feedback-insensitive dihydrodipicolinate synthase gene leads to increased free lysine levels in rice seeds. Molecular Breeding 8: 75-84.

Lee, M., Martin, M.N., Hudson, A.O., Lee, J., Muhitch, M.J., and Leustek, T. 2005. Methionine and threonine synthesis are limited by homoserine kinase availability and not the activity of homoserine kinase in *Arabidopsis thaliana*. Plant J. 41: 685-696.

Madison, JT., and Thompson, JF. 1976. Threonine synthetase from higher plants: stimulation by *S*-adenosylmethionine and inhibition by cysteine. Biochemical and Biophysical Research Communications 71: 684-691.

Maimann, S., Wagner, C., Kreft, O., Zeh, M., Willmitzer, L., Hofgen, R., Hesse, H. 2000. Transgenic potato plants reveal the indispensable role of cystathionine ß-lyase in plant growth and development. The Plant Journal 23: 747-758.

Maimann, S., Hoefgen, R., Hesse, H. 2001. Enhanced cystathionine β-lyase activity in transgenic potato does not force metabolite flow towards methionine. Planta 214: 163-170.

Mandal S., and Mandal R.K. 2000. Seed storage proteins and approaches for improvement of their nutritional quality by genetic engineering. Current Science 79(5): 576-589.

Martin, J.L., and McMillan, F.M. 2002. SAM (dependent) I am: the *S*-adenosylmethionine-dependent methyltransferase fold. Current Opinion in Structural Biology 12(6): 783-793.

Mas-Droux, C., Biou, V., and Dumas, R. 2006. Allosteric threonine synthase: reorganization of the pyridoxal phosphate site upon asymmetric activation through *S*-adenosylmethionine binding to a novel site. The Journal of Biological Chemistry 281: 5188-5196.

Mato, JM., Martinez-Chantar, ML., and Lu, SC. 2008. Methionine metabolism and liver disease. Annual Review of Nutrition 28: 273-293.

Morneau, D.J.K., Abouassaf, E., Skanes, J.E., and Aitken, S.M. 2012. Development of a continuous assay and steady-state characterization of *Escherichia coli* threonine synthase. Analytical Biochemistry 423: 78-85.

Morneau, D.J.K., Jaworski, A.F., and Aitken, S.M. 2013. Identification of cystathionine γ-synthase and threonine synthase from *Cicer arietinum* and *Lens culinaris*. Biochemistry and Cell Biology 95: 95-101.

Muntz, K., Christov, V., Saalbach, G., Saalbach, I., Waddell, D., Pickardt, T., Schieder, O., and Wustenhagen, T. 1998. Genetic engineering for high methionine grain legumes. Nahrung 42: S125-S127.

Murakawa, T., Machida, Y., and Hayashi, H. 2011. Product-assisted catalysis as the basis of the reaction specificity of threonine synthase, J. Biol. Chem. 286: 2774-2784.
Cohen, G.N., and Hirsch, M.-L. 1954. Threonine synthase, a system for synthesizing L-threonine from L-homoserine, J. Bacteriol. 67: 182-190.

Nikiforova, V., Kempa, S., Zeh, M., Maimann, S., Kreft, O., Casazza, AP., Riedel, K., Tauberger, E., Hofgen, R., and Hesse, H. 2002. Engineering of cysteine and methionine biosynthesis in potato. Amino Acids 22: 259-278.

Nordlee, J.A., Taylor, S.L., Townsend, J.A., Thomas, L.A., and Bush, R.K. 1996. Identification of Brazil-nut allergen in transgenic soybeans. New England Journal of Medicine 334(11): 688-692.

Ominato, K., Akita, H., Suzuki, A., Kijima, F., Yoshino, T., Yoshino, M., Chiba, Y., Onuchi, H., and Naito, S. 2002. Identification of a short highly conserved amino acid sequence as the functional region required for posttranscriptional autoregulation of the cystathionine γ-synthase gene in *Arabidopsis*. The Journal of Biological Chemistry **277**(39): 36380-36386.

de Onis, M., Monteiro, C., Akré, J., Clugston, G. 1993. The worldwide magnitude of protein-energy malnutrition: an overview from the WHO Global Database on Child Growth. Bulletin of the World Health Organization 71: 703-712.

Parsot, C., Cossart, P., Saint-Girons, I., and Cohen, G.N. 1983. Nucleotide sequence of *thrC* and of the transcription termination region of the threonine operon in *Escherichia coli* K12. Nucleic Acids Research 11: 7331-7345.

Perrachi, A., Bettati, S., Mozzarelli, A., Rossi, G.L., Miles, E.W., and Dunn, M.F. 1996. Allosteric regulation of tryptophan synthase: effects of pH, temperature, and α-subunit ligands on the equilibrium distribution of pyridoxal 5'-phosphate-L-homoserine intermediates. Biochemistry 35: 1872-1880.

Rais, B., Chassagnole, C., Letellier, T., Fell, D.A., and Mazat, J-P. 2001. Threonine synthesis from aspartate in *Escherichia coli* cell-free extracts: pathway dynamics, Biochem. J. 356: 425-432.

Ramos, C., and Calderon, I.L. 1994. Biochemical evidence that the *Saccharomyces cerevisiae THR*4 gene encodes threonine synthetase, FEBS Lett. 351: 357-359.

Ravanel, S., Droux, M., and Douce, R. 1995. Methionine biosynthesis in higher plants. I. Purication and characterization of cystathionine γ-synthase from spinach chloroplasts. Archives of Biochemistry and Biophysics 316: 572-584.

Ravanel, S. 1997. Methionine biosynthesis in higher plants: biochemical and molecular characterization of the transsulfuration pathway enzymes. Comptes Rendus de l'Academie des Sciences Series III: Sciences de la vie 320: 497-504.

Ravanel, S., Gakiere, B., Job, D., and Douce, R. 1998a. Cystathionine -synthase from *Arabidopsis thaliana*: purification and biochemical characterization of the recombinant enzyme over-expressed in *Escherichia coli*. Biochemical Journal 331: 639-648.

Ravanel, S., Gakiere, B., Job, D., Douce, R. 1998b. The specific features of methionine biosynthesis and metabolism in plants. Proceedings of the National Academy of Sciences 95: 7805-7812.

Rohwer, J.M. 2012. Kinetic modelling of plant metabolic pathways. Journal of Experimental Botany 63(6): 2275-2292.

Roje, S. 2006. *S*-adenosyl-L-methionine: beyond the universal methyl group donor. Phytochemistry 67: 1686-1698.

Rossouw, D., Bosch, S., Kossmann, J., Botha, F.C., and Groenewald, J.H. 2007. Downregulation of neutral invertase activity in sugarcane cell suspension cultures leads to a reduction in respiration and growth and an increase in sucrose accumulation. Functional Plant Biology 34(6): 490-498.

Schallau, K., and Junker, B.H. 2010. Simulating plant metabolic pathways with enzyme-kinetic models. Plant Physiology 152: 1763-1771.

Schildkraut I., and Greer, S.B. 1973. Threonine synthetase-catalyzed conversion of phosphohomoserine to α-ketobutyrate in *Bacillus subtilis*, J. Bacteriol 115: 777-785

Schmid, M., Davison, T.S., Henz, S.R., Pape, U.J., Demar, M., Vingron, M., Scholkopf, B., Weigel, D., and Lohmann, J.U. 2005. A gene expression map of *Arabidopsis thaliana* development. Nature Genetics 37: 501-506.

Schmutz, J., Cannon, S.B., Schlueter, J., Ma, J., Mitros, T., Neslson, W., Hyten, D.L., Song, Q., Thelen, J.J., Cheng, J., Xu, D., Hellsten, U., May, G.D., Yu, Y., Sakurai, T., Umezawa, T., Bhattacharyya, M.K., Sandhu, D., Valliyodan, B., Lindquist, E., Peto, M., Grant, D., Shu, S., Goodstein, D., Barry, K., Futrell-Griggs, M., Abernathy, B., Du, J., Tian, Z., Zhu, L., Gill, N., Joshi, T., Libault, M., Sethuraman, A., Zhang, X.-C., Shinozaki, K., Nguyen, H.T., Wing, R.A., Cregan, P., Specht, J., Grimwood, J., Rokhsar, D., Stacey, G., Shoemaker, R.C., and Jackson, S.A. 2010. Genome sequence of the palaeopolyploid soybean. Nature 463: 178-183.

Schnyder, J., and Rottenberg, M. 1975. Improved synthesis of *O*-phosphohomoserine, Helv. Chim. Acta 58: 518-521.

Shames, S.L., and Wedler, F.C. 1984. Homoserine kinase of *Escherichia coli*: kinetic mechanism and inhibition by L-aspartate semialdehyde, Arch. Biochem. Biophys. 235: 359-370.

Shaver, J.M., Bittel, D.C., Sellner, J.M., Frisch, D.A., Somers, D.A., and Gengenbach, B.G. 1996. Single-amino acid substitutions eliminate lysine inhibition of maize dihydrodipicolinate synthase. Proceedings of the National Academy of Sciences 93(5): 1962-1966.

Shen, B., Li, C., Tarczynski, M. 2002. High free-methionine and decreased lignin content result from a mutation in the *Arabidopsis S*-adenosyl-L-methionine synthetase 3 gene. The Plant Journal 29: 371-380.

Shepherd, M., and Dailey, H.A. 2005. A continuous fluorimetric assay for protoporphyrinogen oxidase by monitoring porphyrin accumulation. *Analytical Biochemistry* 344(1): 115-121.

Singh, U. 1985. Nutritional quality of chickpea (*Cicer arietinum* L.): current status and future research needs. Plant Foods for Human Nutrition 35: 339-351.

Skarstedt, M.T., and Greer, S.B. 1973. Threonine synthetase of *Bacillus subtilis*, J. Biol. Chem. 248: 1032-1044.

Song, S., Hou, W., Godo, I., Wu, C., Yu, Y., Matityahu, I., Hacham, Y., Sun, S., Han, T., and Amir, R. 2013. Soybean seeds expressing feedback-insensitive cystathionine γ-synthase exhibit a higher content of methionine. Journal of Experimental Botany 64(7): 1917-1926.

Sparkes, I.A., Runions, J., Kearns, A., and Hawes, C. 2006. Rapid, transient expression of fluorescent fusion proteins in tobacco plants and generation of stably transformed plants. Nature Protocols **1**(4): 2019-2025.

Steegborn, C., Messerschmidt, A., Laber, B., Streber, W., Huber, R., and Clausen, T. 1999. The crystal structure of cystathionine γ-synthase from *Nicotiana tabacum* reveals its stubstrate and reaction specificity. Journal of Molecular Biology 290: 983-996.

Stitt, M., Sulpice, R., and Keurentjes, J. 2010. Metabolic networks: how to indentify key components in the regulation of metabolism and growth. Plant Physiology 152: 428-444.

Sun, S., and Liu, Q. 2004. Transgenic approaches to improve the nutritional quality of plant proteins. In Vitro Cellular Developmental Biology 40: 155-162.

Szczesiul, M., and Wampler, DE. 1976. Regulation of a metabolic system in vitro: synthesis of threonine from aspartic acid. Biochemistry 15: 2236-2244.

Tabe, L., and Higgins, TJV. 1998. Engineering plant protein composition for improved nutrition. Trends in Plant Science 3(7): 282-286.

Theze, J., Kleidman, L., and Saint Girons, I. 1974. Homoserine kinase from *Escherichia coli* K-12: properties, inhibition by L-threonine, and regulation of biosynthesis, J. Bacteriol. 118: 577-581.

Thoen, A., Rognes, S., Aarnes, H. 1978. Biosynthesis of threonine from homoserine in pea seedlings: 2. Threonine synthase. Plant Physiology and Biochemistry 13: 113-119.

Thomazeau, K., Curien, G., Dumas, R., and Biou, V. 2001. Crystal structure of threonine synthase from *Arabidopsis thaliana*. Protein Science 10: 638-648.

Uys, L., Botha, F.C., Hofmeyr J.-H.S., and Rohwer, J.M. 2007. Kinetic model of sucrose accumulation in maturing sugarcane culm tissue. Phytochemistry 68: 2375-2392.

Van Veldhoven, P.P., and Mannaerts, G.P. 1987. Inorganic and organic phosphate measurements in the nanomolar range, Anal. Biochem. 161: 45-48.

Watanabe, Y., and Shimura, K. 1955. Biosynthesis of threonine from homoserine, J. Biochem. 42: 181-192.

Winter, D., Vinegar, B., Nahal, H., Ammar, R., Wilson G.V., and Provart, N.J. 2007. An "electronic fluorescence pictograph" browser for exploring and analyzing large-scale biological data sets. PLoS One 8: e718.

World Health Organization (WHO). 2006. Global burden of protein-energy malnutrition in the year 2000. Global Burden of Disease 2000. Accessed online at http://www.who.int/healthinfo/statistics/bod_malnutrition.pdf (January 16, 2014).

Wormser, E., and Pardee, A. 1958. Regulation of threonine biosythesis in *Escherichia coli*. Archives of Biochemistry and Biophysics 78: 416-432.

Zeh, M., Casazza, AP., Kreft, O., Roessner, U., Bieberich, K., Willmitzer, L., Hoefgen, R., and Hesse, H. 2001. Antisense inhibition of threonine synthase leads to high methionine content in transgenic potato plants. Plant Physiology 127: 792-802.